Optic flow processing in premotor descending neurons of the fly

Adrian Wertz

München 2009

Optic flow processing in premotor descending neurons of the fly

Adrian Wertz

Dissertation
an der Fakultät für Biologie
der Ludwig-Maximilians-Universität
München

vorgelegt von

Adrian Wertz
aus Leonberg

München, Januar 2009

Erstgutachter:	Prof. Dr. Alexander Borst
Zweitgutachter:	Prof. Dr. Andreas Herz
Tag der mündl. Prüfung:	09.03.2009

Table of Contents

Table of figures

Abbreviations

CC	Cross Correlation
DCMD	Descending Contralateral Movement Detector
DI	Difference Index
DNIV	Descending Neuron IV
DNOVS	Descending Neurons of the Ocellar and Vertical System
FNMN	Frontal Nerve Motor Neuron
HSE	Horizontal System Equatorial
HSN	Horizontal System Northern
HSS	Horizontal System Southern
LGMD	Lobula Giant Motion Detector
LPTC	Lobula Plate Tangential Cell
MI	Matching Index
V2	Vertical Two
VS	Vertical Systems

Summary

Sensory-motor integration requires sensory information to be transformed into appropriate motor commands. Visually guided behavior in the blowfly *Calliphora* is a tractable model for sensory-motor integration, which provides the opportunity to apply electrophysiological and neuroanatomical methods to investigate the underlying neural network. The lobula plate tangential cells are major players with respect to sensory processing of optic flow and have been described in the literature in detail. However, little is known about premotor descending neurons. The objective of this thesis is to gain insights into the physiology and functioning of premotor descending neurons. Specifically, intra- and extracellular recordings were used to investigate how the representation of optic flow information is transformed from motion sensitive tangential cells of the lobula plate onto two premotor descending neurons, namely DNOVS1 and DNOVS2. With dual recordings and dye coupling, it was possible to describe the electrical connectivity between the presynaptic lobula plate tangential cells and the postsynaptic DNOVS cells.

The first paper (Haag, Wertz and Borst, 2007) presented in this thesis describes the physiology and the connectivity of the prominent descending neuron called DNOVS1. DNOVS1 responds to motion stimuli with a graded shift in membrane potential and receives synaptic input from a subset of lobula plate tangential cells, i.e. the so-called VS-cells. This specific wiring leads to a linear integration of the VS cell output signals and

results in a preference of DNOVS1 for rotational flow-fields around a particular body axis.

The second paper (Wertz, Haag and Borst, 2008) assesses the motion sensitivity and connectivity of another descending neuron, DNOVS2. This cell responds to motion stimuli with a change of firing frequency. Experiments involving stimulation of the ipsi- and the contralateral eye indicate that ipsilateral computation of motion information is modified non-linearly by motion information from the contralateral eye. Performing double recordings of DNOVS2 and lobula plate tangential cells, these experiments reveal that DNOVS2 is connected ipsilaterally to a subset of vertical sensitive cells. From the contralateral eye, DNOVS2 receives input most likely from V2, a heterolateral spiking neuron. This specific neural circuit is responsible for the non-linear tuning of DNOVS2 to rotation around the longitudinal body axis.

The third manuscript (Wertz, Plett, Haag and Borst, submitted to J Neurosci) analyzes how optic flow information is processed from VS cells onto DNOVS cells, given the wiring described in the previous publications. To this end, a custom built LED arena subtending 240° of azimuth and 95° of elevation was applied for two measurements. First the receptive fields of DNOVS1 and DNOVS2 as well as those of their presynaptic elements, i.e. VS-cells 1-10 and V2, were mapped by measuring locally the cell's motion sensitivity and preferred direction in different parts of the fly's visual field. In the second type of experiments the preferred movement according to the six degrees of freedom as well as the preferred axis of rotation within the horizontal plane using full-field, i.e. global stimuli were determined. By comparing the results with the expectation given by the known connectivity of DNOVS with VS cells, the transformation of motion information from VS onto DNOVS cells was analyzed. The receptive field structures of both DNOVS cells can be predicted in detail from the

receptive field structure of VS-cells and the V2-cell and the coupling strength of DNOVS with them. They turn out to have different preferred axes of rotation compatible with their different receptive field structure. Their preferred axes of rotation result from a match of the optic flow caused by the respective type of ego-motion with their specific receptive field structures.

In conclusion, the results presented in this thesis analyzes the processing of optic flow information at the network level by describing (i) the coupling of the premotor neurons DNOVS1 and DNOVS2 to different subsets of lobula plate tangential cells and (ii) the integration of the signals leading to a tuning of DNOVS cells to rotations around different body axes. Optic flow information appears to be mixed down from the lobula plate onto descending neurons providing the motor centers in the thoracic ganglion with behaviorally relevant information.

1 General introduction

A central objective of neurobiology is to understand how the sensory world is represented in a neural system and transformed into appropriate motor commands. Sensory neurons process and convey information about our surroundings and provide thus the physiological basis for how we interact with the external world. However, before this information can be used to guide behavior; it has to be transformed into a form that is appropriate for the motor system. Such sensory-motor transformation is a general problem that is faced by all animals, including humans. Yet beyond simple reflexes, little is known about how such sensory-motor transformations take place. Visually guided behavior in the blowfly *Calliphora* represents a tractable model to study sensory motor transformation and provides us with the opportunity to apply an integrated system approach (anatomy, electrophysiology and computational modeling) to investigate the underlying neural network.

1.1 Visually guided behavior

The ability of animals to navigate in the world relies heavily on the processing of visual information. Whenever an animal moves through its environment or an object moves past it, the visual system is confronted with motion. The speed and sophistication of visually guided behavior in insects can be illustrated by two examples that involve pursuit maneuvers: first, when in pursuit of flying conspecifics, a fly only needs 30 ms to execute a corrective turn once its target has changed course (Collett and Land, 1975). Second, dragonflies actively use motion camouflage to disguise themselves during aerial pursuit (Mizutani et al., 2003). To get an initial understanding of how flies respond to different optic flow patterns, behavioral experiments have concentrated on compensatory optomotor behavior in response to the movement of large vertically or horizontally striped backgrounds. When the background is oscillated, a tethered flying fly attempts to turn, both its body and head, in order to follow the background (Fermi and Reichardt, 1963; Götz 1964; Reichardt, 1969; Poggio and Reichardt, 1976; Reichardt and Poggio, 1976; Hengstenberg, 1984; Hengstenberg et al., 1986; Egelhaaf and Borst, 1993). During flight and walking, the classical optomotor reflex is assumed to minimize retinal image slip and therefore help maintain stability in the face of external perturbations such as wind or internal perturbations such as bilaterally asymmetric motor output. Investigations of this optomotor response have unraveled some of the characteristics of motion perception by the fly's visual system (Reichardt, 1969).

1.2 Elementary motion detection

The first models about how motion information might be calculated in nervous systems were obtained from behavioral studies on various types of insect. A formal algorithm to compute the direction of motion from time varying brightness patterns was developed by Hassenstein and Reichardt (1956) after observing the optomotor behavior in the *Chlorophanus* beetle using a delay and compare approach (Exner, 1868). This model has become known as the 'correlation type motion detector' (for review see: Borst and Egelhaaf, 1993; Clifford and Ibbotsen, 2003). The essential operation of this model is a comparison of the brightness level in one input channel delayed with a low-pass filter with the signals of the neighboring input channel in a multiplication step. When an object passes the detector from left to right, bright features in the pattern activate the left input channel before the right input channel (Fig. 1.1). The time interval between activation depends both on the velocity of the object and the distance between the two input channels. If the left input signal is delayed by the low pass filter correctly, both signals will arrive simultaneously at the multiplication stage of the left subunit, resulting in a large response. The mirrored subunit performs just the opposite; it separates the two signals from each other, which then become smaller through the multiplication. After subtracting the output signals of both subunits, the final output response is obtained. The average of an array of such detectors results in a directionally selective motion signal across the visual field. A separate array of Reichardt detectors will then be required for computing motion in each direction.

One consequence of such a computation is that the response of the animal to a drifting sine grating is expected to show a velocity optimum. For a moving grating, the response amplitude of the motion detector is a function of the contrast frequency of the

visual pattern and not the absolute velocity. This means that the maximum amplitude depends on the ratio of the spatial wavelength of the brightness pattern to its velocity. This was found to hold true in behavioral experiments on the beetle *Chlorophanus* (Hassenstein and Reichardt, 1956), the honeybee *Apis* (Kunze, 1961), the housefly *Musca* (Eckert, 1973; Fermi and Reichardt, 1963) and the fruitfly *Drosophila* (Götz, 1964; Heisenberg, 1972; Buchner et al., 1978). Subsequent research on the blowflies *Phaenicia* and *Calliphora* confirmed the Reichardt model (Egelhaaf et al., 1989; Single and Borst, 1998), and that this response feature is also fully retained in large-field motion-sensitive interneurons in the brain of the fly (Eckert, 1980; Haag et al., 2004; Joesch et al, 2008).

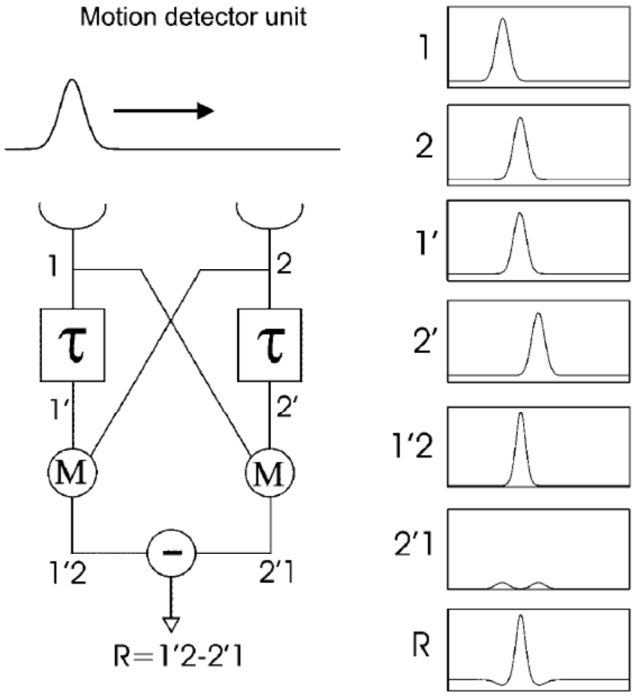

Figure 1.1 The Reichardt and Hassenstein model for directionally selective motion.
Basic scheme of a correlation-type motion detector together with the signals in the various processing lines. A Gaussian luminance distribution is shown moving to the right. The input lines 1 and 2 reflect this luminance change as the stimulus passes by (note the delay between the signals in line 1 and 2). The delay line shifts these signals to the right (1' and 2'). Thus, the signals coincide at the left multiplication stage but are displaced at the right multiplication stage. This leads to strong output signals for the left detector subunit (1'2) but to only small signals in the right one (2'1). After subtraction of these signals, the final output shows strong direction selectivity. Picture is taken from Borst and Haag (2002)

1.3 Motion vision in the fly brain

The processing of optic flow starts in the eye with the sensation of brightness felt by light sensitive cells in the eye (Fig. 1.2). In blowflies, the eye is constructed from a vast array of ~5000 hexagonal ommatidia (Hardie, 1984). The spatial resolution of light detected by the retina is about 100 times poorer than in humans (Land and Eckert, 1985). In addition visual acuity is not uniform across the whole retina. In the female blowfly *Calliphora* the spatial resolution is about twice as high in the frontal visual field as in the lateral part (Petrowitz et al., 2000). Each ommatidium possesses its own lens and set of photoreceptors, R1-R8. The photoreceptors R1-R6 are arranged around the outside of the ommatidia, while R7 and R8 lay centrally one above the other. The different photoreceptors in one ommatidium have different optical axes. However, groups of photoreceptors within neighboring ommatidia having parallel optical axes project onto the same postsynaptic cell. This organization is called neural superposition and increases the sensitivity without sacrificing acuity (Kirschfeld, 1967). The photoreceptors send their axons to a set of brain structures, the 'visual ganglia', devoted exclusively to visual processing. The different neuropile are called the *lamina*, *medulla* and *lobula* complex and are organized into columns that retinotopically represent positions in the world. Thus, in each neural layer the neighborhood relationships between image points are conserved (Fig. 1.2b). The lobula complex can be divided into the lobula and the lobula plate. The output of photoreceptors R1-6 project to the lamina, while photoreceptor cells R7 and R8 project to the medulla (layers M6 and M3 respectively).

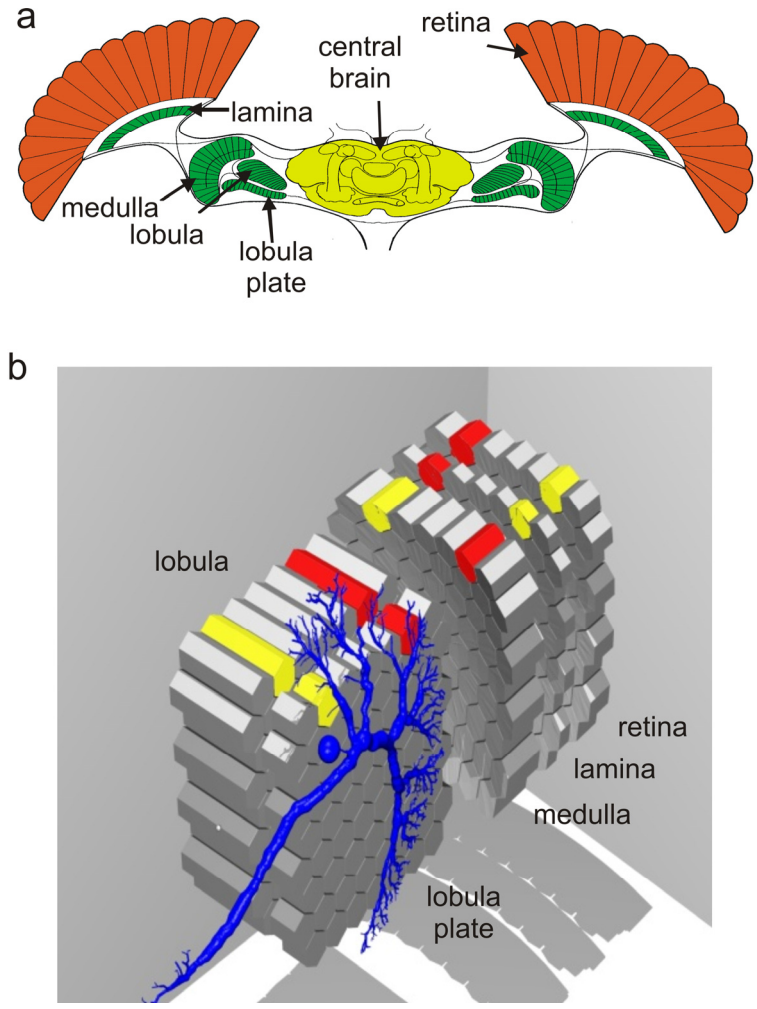

Figure 1.2: Visual system of the fly

a) Schematic horizontal cross-section through the y head. The three layers of the optic ganglia are indicated in green. b) 3D scheme of the visual ganglia together with a LPTC are displayed in blue. The columns in each layer can be seen to represent the facets of the retina in a one-to-one fashion leading to a retinotopic projection of the visual surrounding onto the dendrites of LPTCs. Picture taken from Borst and Haag (2002).

1.3.1 Lamina

The lamina is a very regularly structured neuropile. For each point in the visual world there is one column comprising 5 laminar monopolar cells (L1-L5). Each column is encapsulated by glia cells, and each group is termed a 'cartridge'. Photoreceptor cells from different ommatidia that respond to the same angle of light send their axonal processes through a complex crossover arrangement to the same synaptic cartridge in the

lamina. Three lamina monopolar cells (L1 to L3) receive input from photoreceptors R1-R6. L1 and L2 have narrow and peaked receptive fields similar to those of the photoreceptors (Järvilehto and Zettler, 1973; Dubs, 1982) and have been shown to amplify signals arriving from photoreceptors (Laughlin, 1981). Research on the fly *Drosophila* revealed that lamina cells ramify in different layers of the medulla suggesting that the photoreceptors split into parallel pathways there (Takemura et al., 2008). The L1-cell projects to both layers M1 and M5 of the medulla, while the L2-cell projects to layer M2 (Bausenwein et al., 1992). By first blocking the synaptic transmission in L1 and L2, and afterwards restoring the pathway, Rister et al. (2007) found that L1 and L2 together are necessary and sufficient for motion detection, thus excluding L3 and another pathway (amacrine cell – T1) for providing input to motion detection.

1.3.2 Medulla

The medulla is organized into retinotopic columns with the same number of columns as the lamina has cartridges. Each column is divided into ten layers. Using the 2-Deoxy-Glucose (2-DG) method it could be shown that specific layers are labeled during motion stimulation (Bausenwein et al., 1992; Bausenwein and Fischbach, 1992). Generally, the pathways carrying motion information can be divided into two: one initiated by input from L1-cells and another by L2-cells. The input to the medulla from L1 monopolar cells synapses on the intrinsic medulla neurons Mi1, in layer M1 and M5. This in turn synapses on medullary output T4-cells in layer M10 that project directly to the lobula plate. The second important pathway passing through the medulla arrives in layer M2 from L2-cells. Here, the L2-cells connect to the trans-medulla Tm1-cell that connects to the most posterior stratum of the lobula.

1.3.3 Lobula Complex

The lobula complex consists of two structures, the lobula and the lobula plate. The lobula is organized in retinotopic columns, but with fewer columns than the previous neuropile structures and has therefore a coarser visual resolution (Strausfeld, 1989). The lobula is divided into six layers, as opposed to the ten layers in the medulla. During motion stimuli three layers within the lobula are labeled using the 2-DG method (Buchner et al., 1984). The most posterior layer of the lobula contains the axonal arborizations of the Tm1 cells from the medulla as well as the T5 dendritic arborizations which are all part of the second pathway for motion vision.

The lobula plate is similar in structure to the lobula. Using the 2-DG method, four separate layers can be distinguished depending on the direction of motion presented to the fly (Buchner et al., 1984; Bausenwein et al., 1992; Bausenwein and Fischbach, 1992). The four different layers are innervated by four distinct types of both T5-cells and T4-cells. Each cell type project to a different layer (Strausfeld and Lee, 1991). Large neurons are found in the lobula plate covering many hundreds of columns with their dendrites. These so called lobula plate tangential cells (LPTCs) extend their dendrites to the four different strata of the lobula plate according to their preferred direction (Eckert, 1982; Hengstenberg, 1982; Hausen et al., 1980; 1982; 1984; Krapp et al., 1998). On the basis of ablation experiments as well as the similarities between the LPTC response properties and different types of motion-driven behaviors of flies (Heisenberg et al., 1978; Geiger and Nässel, 1981 ;1982; Hausen and Wehrhahn, 1983; 1990; Borst and Bahde, 1988; Borst, 1991), it was concluded that LPTCs are involved in the fly's visual course control. However, the most significant response characteristic of all LPTCs is their directionally selective response to visual motion. LPTCs can be grouped by 1) whether they respond to horizontal or vertical motion 2) the shape of their response, 3) where the neurons

send their axonal projections, and 4) whether they respond to large or small field motion. LPTCs, sensitive to large field motion and their response properties, are introduced in the following chapter.

1.3.4 Lobula Plate Tangential Cells

The lobula plate contains approximately 60 tangential cells per brain hemisphere that extend their dendrites across many columns. LPTCs receive feed-forward input from the retinotopically organized cells that come from the lamina, medulla and lobula and provide the main output from the lobula plate. They are relatively large cells with invariant anatomy, making them ideal for electrophysiological studies.

There are two centrifugal horizontal cells (CH-cells) per hemisphere, named the dorsal (dCH) and ventral (vCH) cells for their respective receptive field locations (Fig. 1.3). These cells do not connect directly to columnar elements of the lobula plate, but instead receive motion information from other LPTCs (Cuntz et al., 2003; Haag and Borst, 2002; Farrow et al., 2006). CH-cells have two types of synaptic specializations in their dendritic branches: electrical synapses that provide ipsilateral visual input from the horizontal **s**ensitive cells (HS cells), and pre-synaptic GABAergic specializations that send information to small field LPTCs such as the figure detection cell (Gauck et al., 1997; Warzecha et al., 1993). CH-cells are activated by front-to-back motion presented in front of the ipsilateral eye that elicits a graded depolarization of the membrane potential. Back-to-front motion presented in front of the contralateral eye elicits via the heterolateral neuron H2 an increase of EPSP.

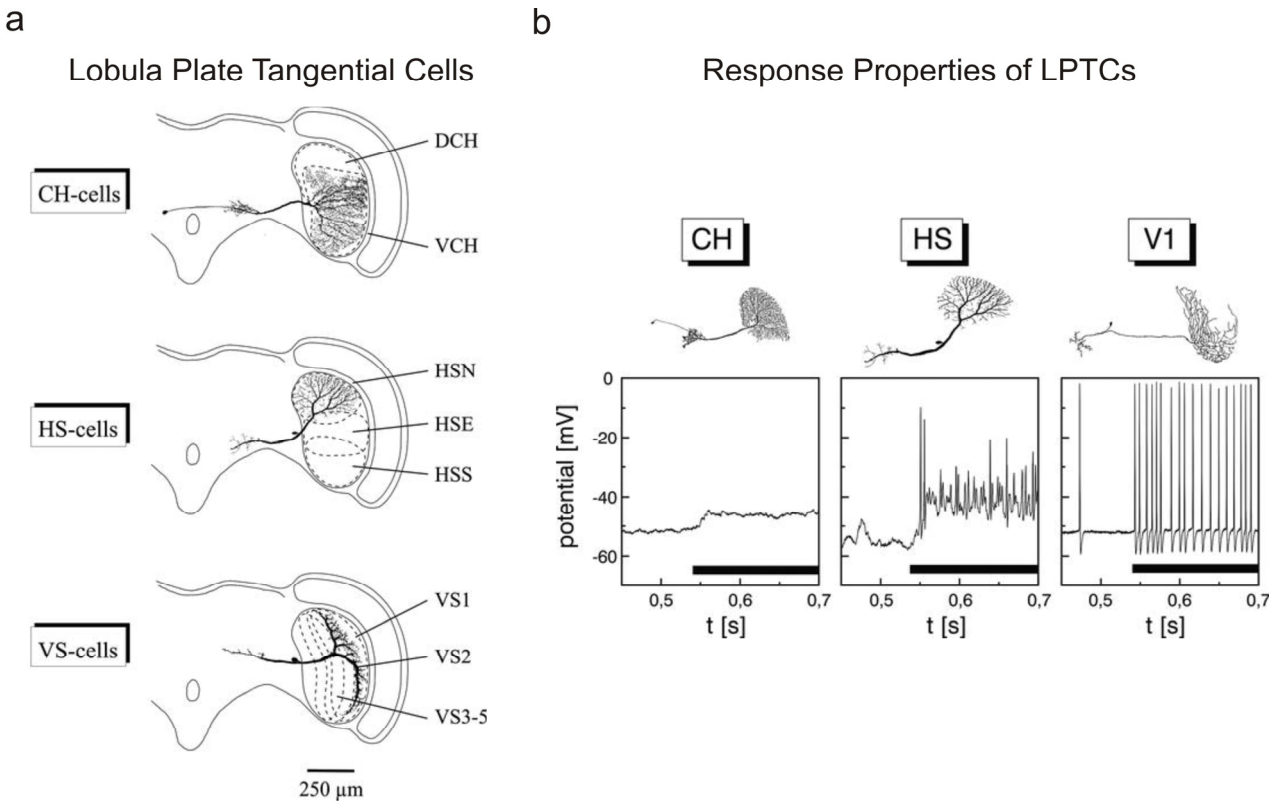

Figure 1.3: Lobula Plate Tangential Cells and their response properties.

a) Enlarged frontal view of fly brain highlighting the position of different LPTCs within the lobula plate. The dotted lines indicate the dendritic extent of the different LPTCs. Figure modified from Borst and Haag (1996). b) LPTCs respond to motion stimuli presented in the ipsilateral visual field in three distinct modes: pure graded depolarization (CH-cells), a mixed depolarization superimposed with spikelets (HS- and VS-cells) or with an increase in spiking frequency (V1-, H1-, H2- and the FD-cells). Picture is taken from Borst and Haag (2002).

In each lobula plate there are three horizontal system (HS) cells (Hausen, 1982), the northern (HSN), equatorial (HSE) and southern (HSS) cells (Fig. 1.3). These three cells view the upper, middle and lower parts of the visual field respectively. The dendritic tree of each cell covers approximately one third of the lobula plate, such that the HSN covers the dorsal third, the HSE the middle third and the HSS the ventral third. HS-cells respond to their preferred direction, which is front-to-back motion, with a graded potential depolarization and spikelets that are irregular in size. Additionally, back-to-front motion presented in front of the contralateral eye causes an increase in the EPSP activity recorded in the HSN- and HSE-cells but not the HSS-cell. During spatially restricted

motion stimulation presented in front of the ipsilateral eye, local calcium accumulation occurs in their dendritic trees (Borst and Egelhaaf, 1992; Egelhaaf et al., 1993; Dürr and Egelhaaf, 1999; Haag and Borst, 2002).

The cellular organization of the vertically responsive LPTCs is slightly different. There are ten vertical system cells (VS-cells) per brain hemisphere (Hengstenberg et al., 1982; Krapp et al., 1998). Each VS-cell is characterized by its bifurcating axon resulting in a dorsal and ventral main dendrite (Fig. 1.3 and Fig. 1.4). They all respond maximally to downward motion, presented at a particular frontal-posterior position, with a graded depolarization of the membrane potential (Hengstenberg, 1982; Haag et al., 1997; Krapp et al., 1998). VS-cells with more medial dendritic trees respond also weakly to upward motion in the frontal part of the visual world.

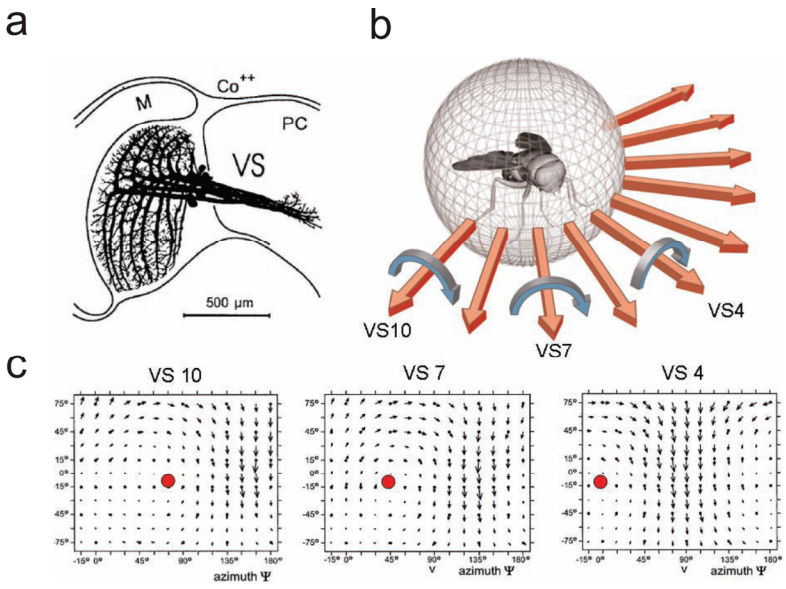

Fig. 1.4 VS cells as rotation detectors.
a) Anatomy of VS cells as obtained from Co fills. b) Schematic fly with various axes of rotation. c) Receptive fields of three example VS cells. Note that receptive fields match different axes of rotation around different poles (*red* dot). Picture is taken from Borst and Haag (2007).

Krapp and colleagues (Krapp and Hengstenberg, 1996; Krapp et al., 1998) characterized the VS cells' receptive fields by determining local sensitivity to motion as well as local preferred directions. Drawing an arrow at each location in the visual field

with the length corresponding to the sensitivity and the direction indicating the preferred direction resulted in three examples of the plots shown in Figure 1.4c. The receptive fields closely resemble a flow field generated by rotation of the fly around a specific axis within the horizontal plane of the eye. Each of the VS cells seems to be tuned to respond optimally to a rotation around a particular body axis, with the optimal axis changing gradually along the azimuth with increasing number of VS cell (Fig. 1.4).

Whereas previously the various LPTCs had been assumed to process their dendritic signal more or less in parallel, independent from each other, a series of double recording studies revealed a pronounced inter- and intrahemispheric connectivity between almost all LPTCs investigated so far (Farrow et al., 2006, Hausen 1984; Haag and Borst 2001, 2002, 2003, 2004, 2005, 2007 and 2008). There are a number of LPTCs that connect the two lobula plates. These cells respond to motion with changes in their firing rate. There are cells that respond to horizontal motion (H1, H2 and Hu) and cells that respond to vertical motion (V1-V2) (Hausen, 1984). An example for an interhemispheric connection is the preference of H2 for rotational stimuli over translating ones by an electrical coupling of H2 with HSE from the opposite lobula plate (Farrow et al., 2006). An example for an intrahemispheric connection is the VS cell network. With double recordings (Haag and Borst, 2004), dye coupling (Haag and Borst, 2005), ablation experiments (Farrow et al., 2005) and calcium imaging (Elyada et al., submitted) it was shown, that VS cells are electrically coupled in a chain like manner. The benefit of coupling the signals from neighboring VS cells after dendritic integration came from compartmental model studies (Cuntz et al., 2007; Weber et al., 2008). Through the coupling, the VS cell network is able to interpolate linearly between the output signals of VS cells, leading to a robust representation of the axis of rotation even in the presence of textureless patches of the visual surround (Cuntz et al., 2007).

In sum many of the connections found between different LPTCs turned out to be electrical in nature. Some of the connections are located between the axon terminals of the neurons, whereas others are located between the dendrites of neighboring cells. While our knowledge about the neural network of LPTCs in the brain has increased tremendously within the last couple of years, far less is known about neurons postsynaptic to LPTCs supplying motor neurons in the thoracic ganglion.

1.4 Motion information in descending neurons

Many of the tangential cells of the blowfly lobula plate are well described with respect to their visual response properties and the connectivity amongst them. Much less is known about how optic flow information is represented in postsynaptic descending neurons supplying motor circuits in the thoracic ganglion. One reason for that is that research on descending neurons is challenged by the huge numbers of neurons connecting the brain with the thoracic ganglion (Coggshall et al., 1973). In the blowfly *Calliphora*, there are more than 8000 fibers in the cervical connective. An unknown part of these fibers is descending, the other part ascending. Thus besides the anatomy of descending neurons little is known about their physiology (but see Gronenberg and Strausfeld, 1990; Strausfeld and Gronenberg, 1990; Gilbert et al., 1995; Gronenberg et al., 1995; Chan et al., 1998).

Descending neurons that are directionally sensitive to wide-field motion have been reported in a number of other insects, for example moths (Collett and Blest, 1966; Rind, 1983), locusts (Kien, 1974; Rowell and Reichert, 1986), dragonflies (Olberg, 1981a,b) and bees (Ibbotson and Goodman, 1990; Ibbotson, 1991). One intensively studied example in locusts is the DCMD (Descending Contralateral Movement Detector), which is

connected to the LGMD (Lobula Giant Motion Detector) and might play an important role in collision avoidance (Hatsopoulos et al., 1995; Judge and Rind, 1997; for review see Rind and Simmons, 1999).

In the fruitfly *Drosophila*, the giant descending neuron involved in the escape jump has been described (Tanouye and Wyman, 1980). This large descending neuron receives visual input and is electrically coupled to the tergo-trochanter motor neuron in the thorax. This motor neuron initiates the jump by an extension of the mesothoracic legs. In addition three pairs of wing muscles become activated. A recent study showed that, in response of a looming stimulus, the escape response is directional, away from the threat (Card and Dickinson, 2008). Whereas the giant fiber pathway in the thoracic ganglion has been studied so far, the connectivity to LPTCs in the brain is not yet clear.

In the blowfly *Calliphora*, the anatomy of descending neurons has been investigated mainly by cobalt backfills in which either the cervical connective was bathed in a cobalt solution or the cobalt solution was iontophoretically injected into the cervical connective (Strausfeld and Bassemir, 1985a; 1985b; Strausfeld and Seyan, 1984; Milde and Strausfeld, 1986; Strausfeld et al., 1987; Strausfeld and Gronenberg, 1990; Gronenberg and Strausfeld, 1991). Descending neurons send their axons down the ventral nerve cord to branch segmentally into motor neuropils (Fig.1.5; Gronenberg et al., 1995). Generally, the organization of descending neurons in the thoracic ganglion reflects their arrangement in the brain. Posterior descending neurons send their axons dorsally to neck motor neuropils and to neuropils involved in flight control. Thus the same descending can contribute to two motor systems, head movements and fight control.

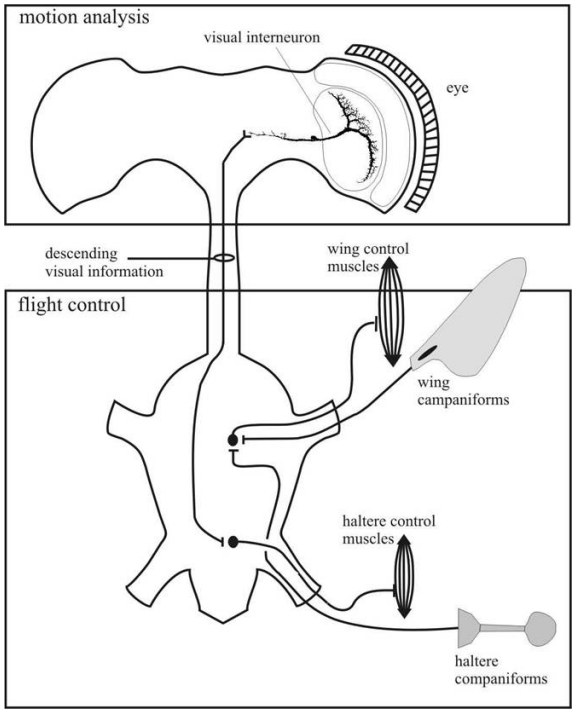

Figure 1.5 Schematic representation of the fly nervous system with the brain containing the visual ganglia (top) and the thoracic ganglion containing the motor control centers (bottom)

One of the large motion-sensitive tangential cells is shown to contact a descending neuron which runs through the cervical connective. In the thorax, such descending neurons are thought to contact motor neurons controlling the wings and halteres. Haltere mechanosensory sensillae synapse on wing control muscles, thus providing a means by which visual information can directly influence mechanosensory feedback to steering muscles. Picture is taken from Borst and Dickinson (2003).

Cobalt backfills led, besides many other descending neurons, to the staining of a prominent group of three Y-shaped cells termed DNOVS (Descending Neurons of the Ocellar and Vertical System, Strausfeld and Bassemir, 1985). Ocelli are light-sensitive organs on the dorsal surface of the head and appear to be suited for detecting changes in overall brightness (Schuppe and Hengstenberg, 1993). In a pioneering study, Gronenberg et al. (1995) showed that these neurons respond to light ON, to antennal air currents, and to visual motion. In addtion, these cells are biocytin-coupled to neck motor neurons, which mediate head rotation (Strausfeld et al., 1987; Gilbert et al., 1995).

1.5 Goals

For visual orientation and course-stabilization, flies rely heavily on the optic flow information perceived during flight (chapter 1.1). Whereas a lot is known about the algorithm for motion detection (chapter 1.2) and the processing of optic flow by interneurons of the fly brain (chapter 1.3), little is known about the further processing in postsynaptic premotor neurons (chapter 1.4). The aim of this thesis is to analyze with electrophysiological methods how optic flow information is represented in two premotor descending neurons of the fly, namely DNOVS1 and DNOVS2.

Chapter 2 assesses the physiology and connectivity of the descending neuron DNOVS1 while chapter 3 focuses on the descending neuron DNOVS2. Chapter 4 analyzes the processing of optic flow information from VS cells onto DNOVS cells. Using a custom built LED arena covering a huge part of the visual field local as well as global motion sensitivity in VS cells and both DNOVS cells are compared.

2 Integration of lobula plate output signals by DNOVS1, an identified premotor descending neuron

This chapter was published in 2007 by Juergen Haag, Adrian Wertz and Alexander Borst in the Journal of Neuroscience (Vol. 27(8) pp.1992-2000)

Juergen Haag performed and analyzed the experiments concerning the physiology and anatomy of DNOVS1 in the fly brain. Adrian Wertz measured and analyzed the sensitivity for vertical motion along the azimuth of all VS cells as well as of DNOVS1 in the thoracic ganglion. The manuscript was written by Juergen Haag and Alexander Borst.

Many motion sensitive tangential cells of the lobula-plate in blowflies are well described with respect to their visual response properties and the connectivity amongst them. They have large and complex receptive fields with different preferred directions in different part of their receptive fields matching the optic flow that occurs during various flight maneuvers. However, much less is known about how tangential cells connect to postsynaptic neurons descending to the motor circuits in the thoracic ganglion, and how optic flow is represented in these downstream neurons. Here we describe the physiology and the connectivity of a prominent descending neuron called DNOVS1. We find that DNOVS1 is electrically coupled to a subset of VS-cells. The specific wiring leads to a preference of DNOVS1 for rotational flow-fields around a particular body axis. In addition, DNOVS1 receives input from interneurons connected to the ocelli.

2.1 Introduction

For visual course control, flies rely on a set of motion-sensitive neurons called lobula plate tangential cells or LPTCs. LPTCs represent about 60 large neurons per brain hemisphere each of which can be identified individually due to its invariant anatomy and characteristic visual response properties (Pierantoni, 1976; Hausen, 1977; Hausen, 1982; Hengstenberg et al., 1982; Borst and Haag, 1996). Amongst them, cells are found responding preferentially to vertical motion like the VS-cells (*V*ertical *S*ystem) as well as cells, which are best, activated by horizontal motion like the HS-cells (*H*orizontal *S*ystem). Per hemisphere, there exist three HS-cells (the northern HSN, the equatorial HSE and the southern HSS-cell) and 10 VS-cells (VS1-VS10) together covering almost completely the visual space surrounding the animal. LPTCs often have complex receptive fields with different preferred direction in different parts of the visual field matching the optic flow that occurs during specific flight maneuvers of the fly (Krapp and Hengstenberg, 1996; Krapp et al., 1998; Franz and Krapp, 2000; Karmeier et al., 2003). HS- and VS-cells are the major output elements of the lobula plate. They convey flow-field information onto descending neurons which ultimately control motor neurons for locomotion or head movements.

Over the last decades LPTCs have been studied extensively with respect to their visual response properties (Hausen, 1977, 1981; Hengstenberg, 1977; Hengstenberg et al., 1982; Eckert and Dvorak, 1983; Haag, 1994; Haag et al., 1999; for review see Hausen, 1984; Borst and Haag, 2002) and the connectivity amongst them (Hausen, 1981, 1984; Haag and Borst, 2001, 2002, 2003, 2004, 2005; Horstmann et al., 2000; Farrow et al., 2003, 2006). However less is known about the neurons where LPTCs project to. These descending neurons have been mainly described anatomically (Strausfeld and Bassemir,

1985a, b; Strausfeld and Seyan, 1985; Milde and Strausfeld, 1986; Strausfeld et al., 1987;) but little is known about their physiology (but see Gronenberg and Strausfeld, 1990; Strausfeld and Gronenberg, 1990; Gronenberg et al., 1995; Gilbert et al., 1995; Chan et al., 1998; Huston and Krapp, 2003) and their specific connectivity to LPTCs.

The anatomy of descending neurons has been investigated mainly by cobalt backfills where either the cervical connective was bathed in a cobalt solution or the cobalt solution was iontophoretically injected into the cervical connective. This led, besides many other descending neurons, to the staining of a prominent group of three Y-shaped cells termed DNOVS (Descending Neurons of the Ocellar and Vertical System, Strausfeld and Bassemir, 1985). Ocelli are light-sensitive organs on the dorsal surface of the head. The three ocelli form a triangle and each one has a single wide-angle lens. With the photoreceptor array being out-of-focus, they appear to be suited for detecting changes in overall brightness (Schuppe and Hengstenberg, 1993). The DNOVS project with their axons through the cervical connective into the prothoracic ganglion. The cobalt fill revealed dye coupling between a subset of VS-cells (VS4-VS9) and DNOVS1. In their study, Strausfeld and Bassemir (1985) found that most of the contacts between VS-cells and DNOVS1 are mediated by chemical synapses. In addition however, also gap-junction like appositions were found in close vicinity to chemical synapses. Besides the input from VS-cells, additional input to DNOVS1 from ocellar interneurons, so called L-neurons (Simmons et al., 1994), was suggested.

In this article we present electrophysiological data on a specific descending neuron, the DNOVS1 (also called DNDC 1-1 in Gronenberg et al., 1995). Given the described connectivity to VS-cells, we studied how the signals of a subset of VS-cells and ocellar input are integrated on the dendrite of DNOVS1.

2.2 Materials and Methods

2.2.1 Preparation and Set-up

Female blowflies (*Calliphora vicina*) were briefly anesthesized with CO_2 and mounted ventral side up with wax on a small preparation platform. The head capsule was opened from behind; the trachea and airsacs, which cover the lobula plate, were removed. To eliminate movements of the brain caused by peristaltic contractions of the esophagus the proboscis of the animal was cut away and the gut was pulled out. This allowed stable intracellular recordings of up to 45 minutes. The fly was then mounted on a heavy recording table looking down onto the stimulus monitors. The fly brain was viewed from behind through a fluorescence microscope (Axiotech Vario 100 HD, Zeiss).

2.2.2 Stimulation

Stimuli were generated on Tektronix 608 monitors by an image synthesizer (Picasso, Innisfree) and consisted of a one-dimensional grating of 16.7° spatial wavelength and 87% contrast displayed at a frame rate of 200 Hz. The mean luminosity of the screen was 11.2 cd/m^2. The intensity of the pattern was square-wave modulated along its vertical axis. For measuring the sensitivity along the azimuth (Fig. 2.1) we used three Tektronix monitors: monitor 1 was placed contralateral and extended from -90 to -30° in the horizontal direction and from +40 to -30 ° in the vertical direction; monitor 2 was placed at position -15 to +40°, monitor 3 was at position 55 to 120°. Each monitor screen was divided into five stripes each with a horizontal extent of 11 for monitor 2 and 13° for monitor 3. The pattern inside these stripes could be moved independently. For all other experiments (Figs. 2.2 and 2.8) we used two Tektronix monitors. The stimulus

field extended from 16 to 42° and from 95 to 133° along the azimuth and from -30 to+30° in elevation of the fly.

For stimulating the ocelli, we used a blue (λ=466 nm, 72 Cd/m^2) LED (LB3336, Osram) placed in front of the ocelli at a distance of 2 mm. Shielding the LED ensured that the facet eyes did not become stimulated by the LED. This was also confirmed by experiments were we occluded the ocelli. Switching on the LED did not elicit a response in DNOVS1.

2.2.3 Electrical recording

For intracellular recordings of the cells, electrodes were pulled on a Brown-Flaming micropipette puller (P-97) using thin-wall glass capillaries with an outer diameter of 1 mm (Clark, GC100TF-10). The tip of the electrode was filled with 10 mM Alexa 488 (Molecular Probes). The shaft of the electrode was filled with a 2 M KAc solution. Electrodes had resistances of about 15 MΩ. For dual intracellular recordings, one electrode was filled with the green fluorescent dye Alexa 488, the other electrode filled with the red fluorescent dye Alexa 568 (Molecular Probes). For the Neurobiotin staining the tip of the electrode was filled with a mixture of 3 % Neurobiotin (vectorlabs, Burlingame) and 3 % Fluorescein. A SEL10-amplifier (npi-electronics) operated in the bridge mode was used throughout the experiments. In the experiments with dual intracellular recordings we used an additional SEL10-amplifier. For data analysis the output signals of the amplifiers were fed to a PIII PC via an 12 bit A/D converter (DAS-1602/12, Computerboards, Middleboro, MA) at a sampling rate of 5 kHz and stored to hard disc. The signals were evaluated off line by a program written in Delphi (Borland).

The responses to motion stimuli were calculated by averaging the membrane potential from 200 msec after the onset of the motion stimulus over 800 msec. The

membrane potential averaged over 500 msec before the onset of the motion stimulus was then subtracted from this value.

Normalized cross-correlograms (Figs. 2.5b, c) were calculated from the first 800 milliseconds of the membrane potentials according to Kimpo et al. (2003). Defining the cross-correlation CC(τ) between two responses r_A and r_B as

$$CC(\tau) = \left\langle \frac{1}{T} \int_0^T dt \cdot r_A(t) \cdot r_B(t+\tau) \right\rangle$$

and the total power σ_X^2 of $r_X(t)$ as

$$\sigma_X^2 = \left\langle \frac{1}{T} \int_0^T dt \cdot r_X^2(t) \right\rangle,$$

the normalized cross-correlation $h(\tau)$ then is:

$$h(\tau) = \frac{CC(\tau)}{\sqrt{\sigma_A^2 \cdot \sigma_B^2}}$$

For recording from DNOVS1, a VS-cell was filled with Alexa 488 and visualized under fluorescence light. The VS-cell then served as a landmark for finding the DNOVS1 neuron. All the recordings were made from the dendritic region of DNOVS1 and from the axons of the VS-cells. VS-cells were identified using a method described by Farrow (2005). There, not only the specific anatomy of the cell was taken into account, but also the relative position of their ventral dendrite within the lobula-plate.

2.2.4 Two photon microscopy

For registering the anatomy of DNOVS1, we used a custom-built 2-Photon microscope (Denk et al, 1990, Haag et al, 2004) consisting of the following components: a 5 W-pumped Ti:Sapphire laser (MaiTai, Spectra Physics), a pockels cell (Conoptics),

scan mirrors incl. drivers (Cambridge Technology), a scan lens (4401-302, Rodenstock), a tube lens (MXA 22018, Nikon), a dichroic mirror (DCSPR 25.5x36, AHF Tuebingen), and a 40x water immersion lens (Zeiss). The lens can move along all three axes by a step-motor driven micromanipulator (MP285-3Z, Sutter Instruments). Emitted light is filtered in parallel by two bandpass filters (HQ 535/50M and HQ 610/75M, Chroma) and collected by multialkali photomultipliers (R6357, Hamamatsu). The whole system is controlled by custom-written software (CfNT V1.569, Michael Mueller, MPI for medical Research, Heidelberg, Germany). 3D reconstruction of the cells was performed with the software package AMIRA V4.0 (Mercury Computer Systems, Berlin, Germany).

2.2.5 Histology

After filling a cell with the Neurobiotin and Fluorescein mixture, it was identified under the fluorescence microscope. The fly was then kept at +4° Celsius for at least 60 minutes to allow for diffusion of Neurobiotin to coupled cells. The head of the fly was then cut off and fixed for 24 -48 hours at 4° Celsius in 4% Paraformol and 0.2 % Picric acid mixture in 0.15 M phosphate buffer. The head was washed in PBS buffer and the brain was taken out. The brain was then frozen in liquid nitrogen for 20 seconds. After several rinses with phosphate buffered saline (PBS), the brain was incubated with Vectastain ABC Kit (Vector Labs) overnight. Before incubation in a 0.025 % $CoCl_2$ and 0.02 % $NiCl_2$ mixture in PBS buffer for 30 minutes the brain was rinsed several times in PBS buffer. The diaminobenzidine (DAB) reaction was started by transferring the tissue in a solution containing 0.05 % $CoCl_2$, 0.02 % $NiCl_2$ and 0.01 % H_2O_2 for 10 minutes at room temperature. The brain was then washed again in PBS buffer and dehydrated in alcohol before embedding it in mixture of distyrene, tricresyl phosphate and xylene

(DPX). The stained cells were identified under a dissection microscope (MZFLIII, Leica). Pictures were taken with a CCD-camera (Leica DC 320).

2.3 Results

In a first set of experiments, we measured the responses of DNOVS1 to up- and downward motion at different azimuth positions. Figure 2.1a shows a schematic drawing of the setup we used. As VS-cells, DNOVS1 responds to motion stimuli with a graded shift in membrane potential. As an example, the response to a vertical pattern movement at 120° azimuth is shown (Fig. 2.1b). Downward motion of the pattern leads to a depolarization, upward motion to a hyperpolarization of the cell. Although the responses of DNOVS1 look similar to the responses of VS-cells, there are some differences. In contrast to VS-cells, no indications for active membrane properties can be found in the response to motion (but see Fig. 2.7). In none of the recordings, action potentials in response to visual motion stimuli could be detected. In addition, without any motion stimuli, there seems to be massive input from presynaptic neurons leading to a rather unstable resting potential. The response to upward and downward motion at different azimuth positions is shown in Figure 2.1c. DNOVS1 did not respond to motion in front of the contralateral eye (position -90 to -30°). The strongest response was found for lateral to caudal stimulus positions. Due to technical limitations it was not possible to measure the response to monitor positions more caudal than 120°. Besides the response to stimuli in the lateral-caudal field, there was a significant response to upward motion in the frontal part of the receptive field. At this frontal position, the response to upward and downward motion was not symmetrical (see also Fig 2.2, third and fourth column).

In general, the responses to visual motion stimuli at the positions tested were rather small compared to the responses found in VS-cells.

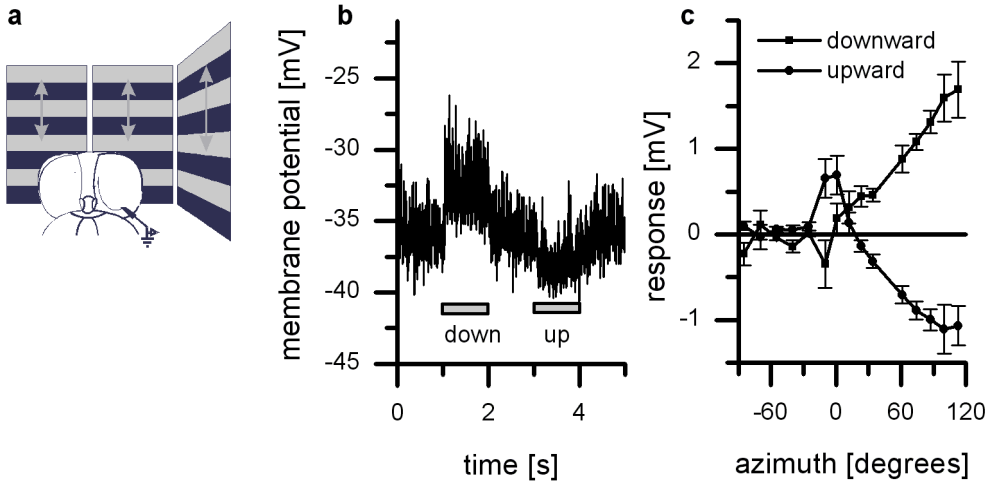

Figure 2.1: Intracellular recording from DNOVS1.

a) Schematic drawing of the stimulation. b) Example response of DNOVS1 to vertical motion at an azimuth position of 120°. The cell responds to downward motion with a depolarization, to upward motion with a hyperpolarization of the membrane potential. The response is superimposed by massive synaptic background. **c**) Responses of DNOVS1 to vertical motion as a function of the azimuth position. The highest response to vertical motion is elicited at lateral stimulus positions where downward motion depolarizes and upward motion hyperpolarizes the cell. In addition, DNOVS1 responds to motion in the frontal part with an inverse preferred direction. DNOVS1 does not respond to motion in front of the contralateral eye. Data represent the mean value recorded from n=5 flies. Error bars represent the standard error of the mean.

The measured sensitivity profile with an upward sensitivity in the frontal region and a downward sensitivity in the lateral-caudal region points towards a rotation selective flow-field. In order to test this, we recorded the response of DNOVS1 to simultaneous motion stimuli shown at different locations in the receptive field. To do so we used two stimulus monitors: one placed in front of the fly and a second one in the lateral visual field (Fig. 2.2a). Figure 2.2b shows the response of DNOVS1 to different combinations of motion stimuli. The four left columns show the responses to single stimuli, the four

right columns to combinations of motion stimuli. As already shown in Fig 2.1c, DNOVS1 responds with a depolarization to downward motion in the lateral monitor (dark grey, first column) and to upward motion in the frontal monitor (fourth column). The combined motion stimulus (frontal upward and lateral downward) elicited the strongest depolarization (Fig. 2.2b, rightmost column). This indicates that DNOVS1 is tuned more to a rotational flow-field than to a translatory one. The comparison between the measured responses to the combined stimuli (right columns) and the arithmetic sum of the responses to single stimuli (light grey columns) indicate a nearly linear summation of the individual responses.

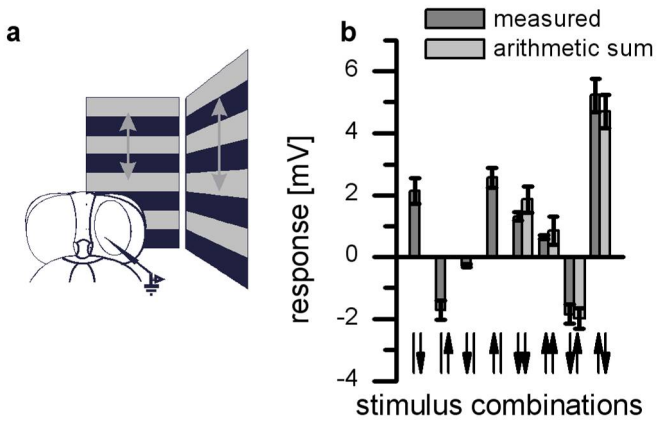

Figure 2.2: Responses of DNOVS1 to simultaneous motion in two sectors of the receptive field.

a) Schematic drawing of the stimulus situation. b) Averaged responses of DNOVS1 to simultaneous motion stimuli in both monitors (dark grey columns). The neuron responds best to a rotatory motion stimuli consisting of upward motion in the frontal and downward motion in the lateral eye field (rightmost stimulus configuration). Light grey columns show the arithmetic sum of the responses to single stimuli. The measured and the calculated responses to combined stimuli are almost identical. Data represent the mean ± s.e.m recorded from n=4 flies.

In order to investigate the connectivity between VS-cells and DNOVS1 we performed dual intracellular recordings from different VS-cells and DNOVS1, injecting current into one cell and recording the potential response in the other. As an example,

Figure 2.3a shows the membrane potential of DNOVS1 in response to current injection into a VS7-cell. Negative current injection led to a hyperpolarization, positive current to a depolarization of DNOVS1. Thus, current of both polarities is transmitted from VS7 onto DNOVS1. The next experiment demonstrates that the connection works both ways: when the current was injected into DNOVS1, VS7 became de- or hyperpolarized, respectively, depending on the sign of current injection (Fig. 2.3b). This bi-directional coupling of the two cells speaks in favor of electrical synapses between them.

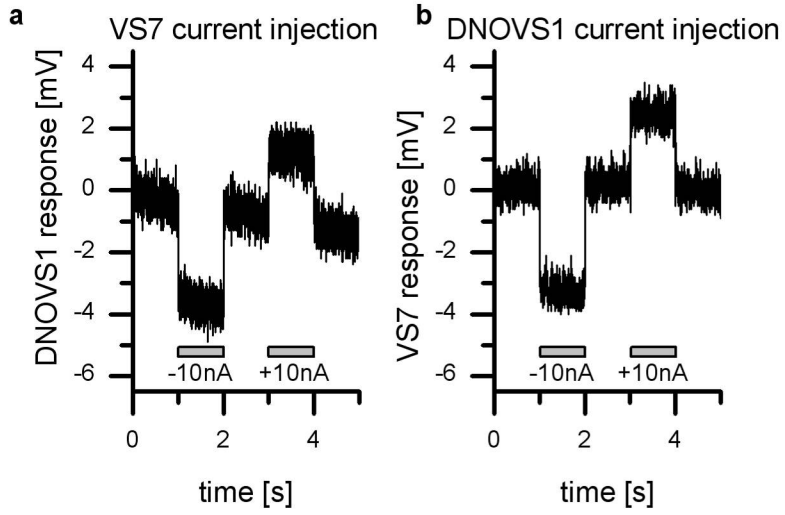

Figure 2.3: Dual intracellular recording from DNOVS1 and VS7.
a) Current injection of -10 nA and +10 nA into VS7 led to a hyper- and depolarization of DNOVS1, respectively. b) Same as a, but current was injected into DNOVS1

In a series of experiments, we investigated the connectivity between all VS-cells (except VS10) and DNOVS1 within one brain hemisphere. In general, current injection into VS-cells led to a change of the membrane potential of DNOVS1 and vice versa. However, the coupling strength between the different VS-cells and DNOVS1 varied considerably. Current injection into VS1-VS3 elicited only weak responses in DNOVS1. The strongest coupling could be found between VS6/VS7 and DNOVS1 (Fig. 2.4).

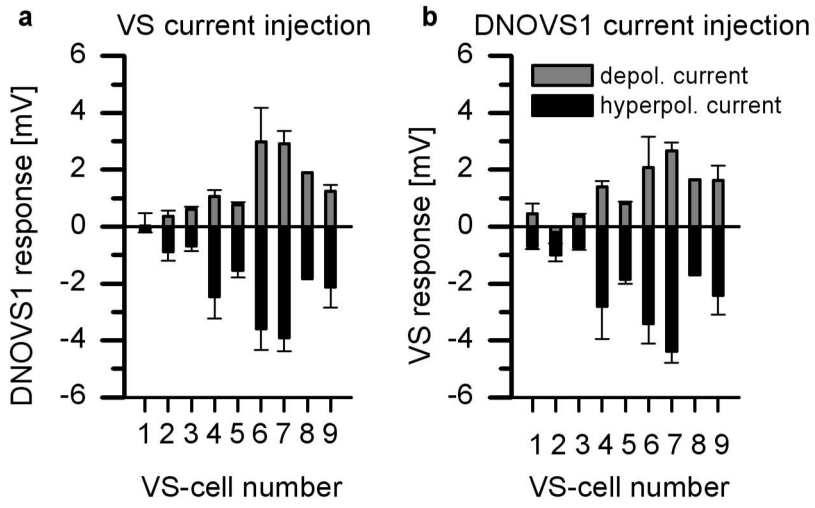

Figure 2.4: Double intracellular recording from DNOVS1 and different VS-cells.
a) Current injection of -10 nA (black bars) and +10 nA (grey bars) in different VS-cells elicited different levels of hyper- and depolarization DNOVS1. Whereas DNOVS1 showed only weak responses to the current injection in VS1-VS3, it responded more strongly when current was injected into VS4-VS9. The strongest response was found for current injection into VS6 and VS7. b) Same as a, but current was injected into DNOVS1 and the response was measured in different VS-cells. As before, the strongest response could be found in VS6 and VS7. These experiments demonstrate that not only current of both polarities is transmitted between DNOVS1 and VS-cells, but that the connection also works in both directions. Data represent the mean ± s.e.m of VS1 (n=2), VS2 (n=2), VS3 (n=6), VS4 (n=2), VS5 (n=2), VS6 (n=2), VS7 (n=5), VS8 (n=1), VS9 (n=3).

The similarity between the voltage traces of both cell types when no stimulus was provided suggested in addition the coupling between VS-cells and DNOVS1. Figure 2.5a shows a double recording of the membrane potentials of DNOVS1 and VS7. We quantified the similarity by calculating the cross correlation function between the signals from both cells (Fig. 2.5b). We found a strong positive correlation between the two signals which peaks at zero time lag. The peak is almost symmetrical around zero and has a half-width of only 3.2 ms. The plot of the correlation peaks for the different VS-cells and DNOVS1 (Fig. 2.5c) revealed a pattern similar to the one obtained from current injection experiments (compare with Fig. 2.4): whereas the membrane potential of VS1-

VS3 and DNOVS1 showed only a weak correlation, the signals of VS6-VS8 and DNOVS1 turned out to be strongly correlated.

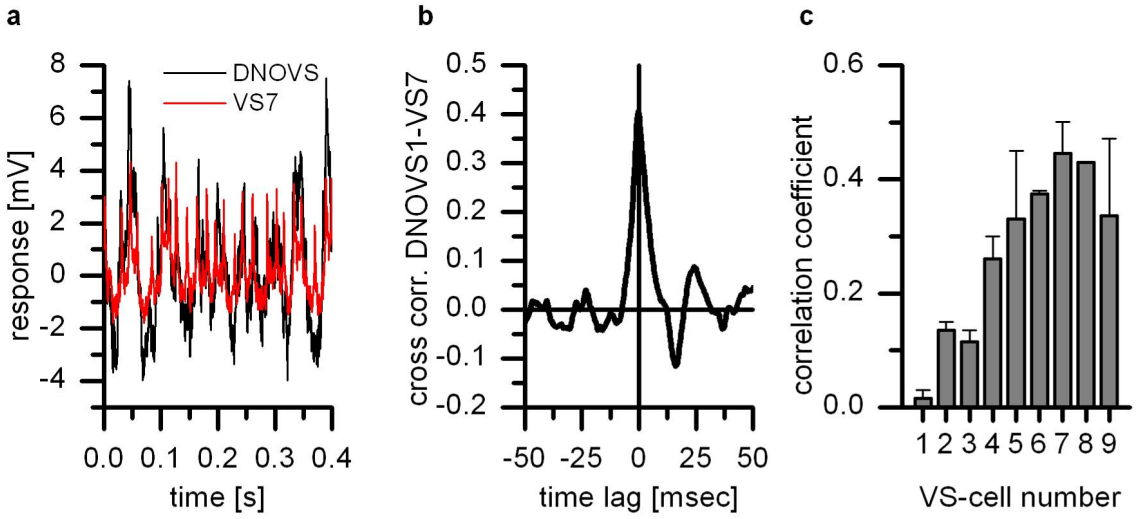

Figure 2.5: Cross correlation between VS-cells and DNOVS1 membrane potential.
a) Time course of the membrane fluctuations without any motion stimulus of DNOVS1 (black) and a simultaneously recorded VS7 (red). Note that the signals are similar. b) Normalized cross correlogram (see Materials & Methods) of the signals shown in a. The peak of the cross correlogram occurs at zero time lag. c) Average of the cross correlogram peak amplitudes of different VS-cells and DNOVS1. The peak amplitudes of the cross correlation follow a distribution reminiscent on the one of coupling coefficients revealed by current injection (compare to Fig. 2.4). Same data set as Fig. 2.4.

Knowing the connectivity and coupling strength between the various VS-cells and DNOVS1, we asked the question how the input from VS-cells is integrated on DNOVS1. We therefore measured the response of VS-cells to the exact same set of stimuli we used before to characterize DNOVS1 (Fig. 2.1a). Figure 2.6a shows the sensitivity of the VS-cell responses to downward, figure 2.6b to upward motion along the azimuth in a false color code. Since none of the VS-cell showed a response to contralateral azimuth positions (-90 to -30°), we did not plot the data for these azimuth positions. The peak of the sensitivity to downward and upward motion shifts from frontally to caudally for VS1 to VS9, respectively. In addition, VS7-VS9 showed a sign

reversal in their response to motion in the frontal visual field. The measured responses of the VS-cells are in agreement with the results of Krapp et al. (1998) who used small dots to map the preferred orientation.

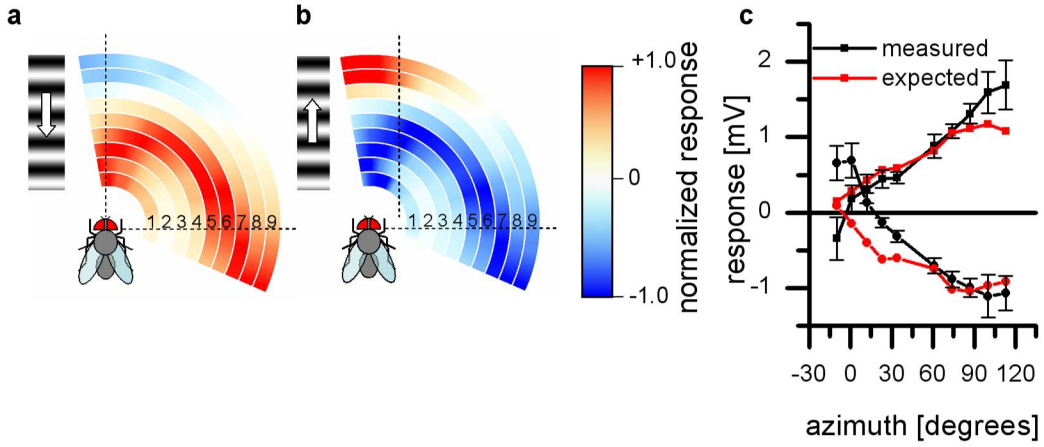

Figure 2.6: Sensitivity of VS-cells to vertical grating motion as a function of the azimuth position.

a) Responses of VS-cells to downward motion. b) Responses of VS-cells to upward motion. Responses were normalized with respect to the maximum response amplitude (positive response maximum for downward motion and negative response maximum for upward motion) and are shown color coded with blue representing hyperpolarization and red representing depolarization. The peak sensitivity for the different VS-cells shifts along the azimuth according to the location of the cells dendrite in the lobula plate. VS1-VS3 had the highest responses in the frontal area and VS9 responded best to lateral-caudal stimuli. Data represent the mean recorded from VS1 (n=2), VS2 (n=3), VS3 (n=8), VS4 (n=7), VS5 (n=5), VS6 (n=5), VS7 (n=6), VS8 (n=3), VS9 (n=2). c) Responses of DNOVS1 (black) to upward and downward motion at different azimuth positions (same data as in Fig. 2.1c) together with the average responses of VS1-VS9 (red) weighted by their connection strength to DNOVS1 as determined by current injection (Fig. 2.4).

The response profile for a given VS-cell was then multiplied with the measured coupling strength to DNOVS1 (see Fig. 2.4) and integrated over all VS-cells. This gave an estimate of the sensitivity for a neuron that integrates linearly the output of VS-cells. The comparison between this estimated sensitivity and the measured sensitivity for vertical pattern motion of DNOVS1 along the azimuth is shown in Figure 2.6c. For

stimuli moving downward, the expected sensitivity matches quite well the measured sensitivity of DNOVS1. As for DNOVS1, the responses are almost zero for frontal stimulus positions and are biggest for lateral-caudal stimuli. In contrast, the expected responses for upward motion differ especially for frontal stimuli (-10 to +1° azimuth): whereas DNOVS1 responded with a depolarization to frontal upward motion, the calculated responses were almost zero at these azimuth positions.

Based on anatomical findings, Strausfeld and Bassemir (1985) suggested that in addition to input from VS-cells, DNOVS1 also receives input from the ocelli via L-neurons. For measuring the responses to the ocellar input, we used an LED to illuminate the ocelli. Figure 2.7a shows the response of DNOVS1 to a 500 msec light pulse emitted by the LED. DNOVS1 responds to the onset of this stimulus with a transient hyperpolarization followed by fast depolarizing deflections of the membrane potential. Switching off the LED leads to a characteristic off response. It consists of a fast depolarization followed by a slow decay back to the resting membrane potential. In order to test whether the fast depolarizing off-response is due to the activation of intrinsic voltage-gated currents or simply reflects a passive postsynaptic potential, we hyper- and depolarized the membrane of DNOVS1 by injecting steady-state negative or positive current and measured the off-response to the ocellar stimulation under these different conditions. In the case that voltage-dependent currents contribute to the fast depolarization in the off-response, strong hyperpolarizing current injection should prevent their activation. Depolarizing current injection should lead to an inactivation of the voltage-dependent currents. If the response is solely due to synaptic input without any active amplification, the amplitude of the fast transient should depend linearly on the injected current. Figure 2.7b shows the result of such an experiment. Plotted is the amplitude of the fast deflection after switching off the light stimulus as a function of the steady current injection. For steady current injections between -10 nA and +5 nA the

amplitude of the fast depolarization followed almost linearly the amount of injected current. For current injections more negative than -15 nA, however, the amplitude of the peak decreased. This non-linear dependence of the off-response peak amplitude on the amount of injected current suggests a contribution of active conductances. Further support for this comes from analyzing the kinetics of the off-response: its falling phase could be fitted best by a double exponential decay (R^2=0.93 for double exponential decay and R^2=0.78 for single exponential decay) consisting of a fast (τ=2msec) and a slow component (τ=40-80 msec). Figure 2.7b shows the amplitude for the two components as a function of the injected current. While the slow component showed only a weak dependence on the injected current with a slight increasing trend towards hyperpolarizing currents, the amplitude of the fast component increased for current injections from +5 to -10 nA, decreased for more negative currents and became almost zero for injections of -30 nA. The fast component might be driven by active conductances whereas the slow component might reflect the passive EPSP. This finding is further supported by voltage clamp experiments (Fig. 2.7c). Here the membrane was clamped to -40 mV and the response to the light stimulus was measured. The recorded current trace showed that the light off response consists only of the slow component (τ=59 msec).

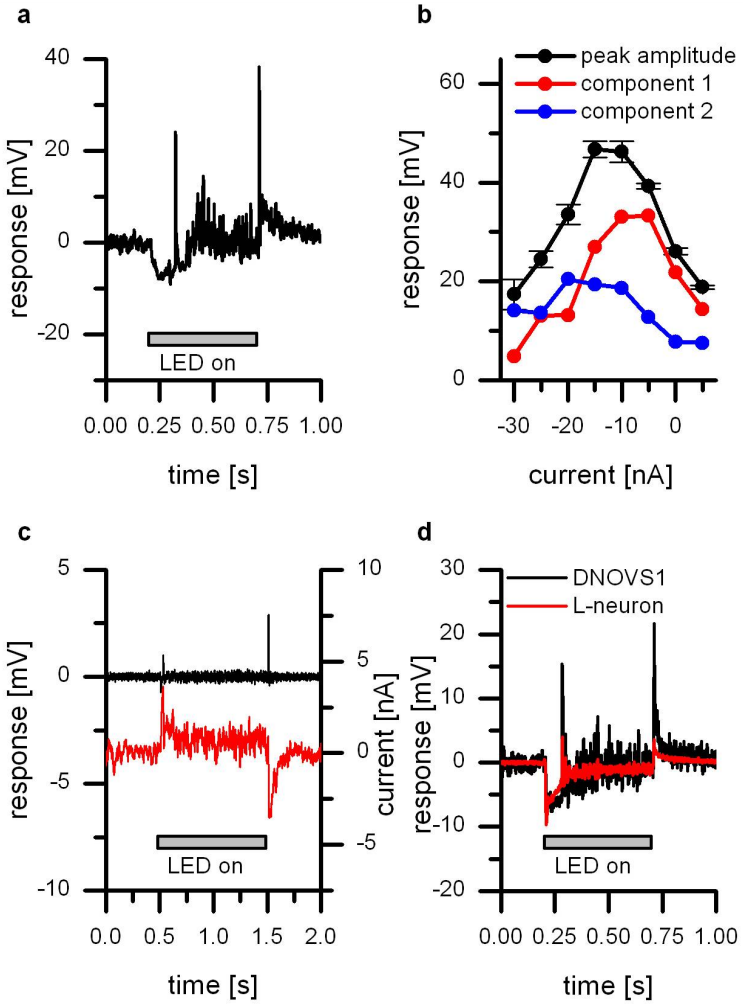

Figure 2.7: Responses of DNOVS1 to a stimulation of the ocelli.

a) Single response trace of DNOVS1. During the time indicated by the grey bar the ocelli were stimulated by an LED. The response to light-on consists of a transient hyperpolarization followed by spike-like fluctuations of the membrane potential. Switching off the light induces a fast depolarizing peak that returns to zero with two different time constants. b) Dependence of the amplitude of the transient off-response on the amount of steady-state current injected into DNOVS1 (black line). The peak amplitude showed a nearly linear dependence for current injection between -15 nA - +5 nA. For more negative currents the amplitude became reduced. Off-responses could be fitted best by a double exponential decay, with a fast (τ=1.5-2.7 ms) and a slow component (τ=40-80 ms). The amplitude of the fast component (red line) reached the maximum for current injection of -10 nA - 5 nA and became almost zero for current injection of -30 nA. The amplitude of the slow component (blue line) reached the maximum for injection of -20 nA. c) Voltage clamp experiment of DNOVS1. The membrane potential (black line) was clamped to -40 mV. The off response consists of an inward current and can be fitted with a single exponential decay with a time constant of 62 ms and amplitude of -3.7 nA. d) Response of an L-neuron (red line) and response of a simultaneously recorded DNOVS1 (black line) to the stimulation of the ocelli. The L-neuron responded to light on with a fast transient hyperpolarization followed by a plateau. Switching off the LED elicited a small depolarization. Data represent the mean from five sweeps recorded in a single fly.

Ocellar input does not arrive directly at DNOVS1, but rather via a group of interneurons, called L-neurons (Strausfeld and Bassemir, 1985). To measure the synaptic input of L-neurons to DNOVS1 directly, we recorded simultaneously from DNOVS1 and one L-Neuron (Fig. 2.7d). As DNOVS1, the L-Neuron also responds to the light on stimulus with a transient hyperpolarization followed by a hyperpolarized plateau during light stimulation and a weak transient depolarization in response to switching off the LED.

The quantitative difference between the response of DNOVS1 and the simultaneously recorded L-neuron is most likely due to additional input from other L-neurons onto DNOVS1. It has been shown (Toh and Kuwabara, 1975) that the nerve projecting from the ocelli into the dorsal deuterocerebrum consist of twelve large interneurons (L-neurons) and a much higher number of thin neurons (S-neurons). Forwardfills of neurons of the ocellar nerve have suggested that at least four of the L-neurons might be presynaptic to DNOVS1 (Strausfeld and Bassemir, 1985), but their visual response properties have not been investigated. In different insect species it has been found that the L-neurons respond to stimulation of the ocelli with a graded and a spiking response (blowfly: Simmons et al., 1994; honeybee: Milde, 1984; Milde and Homberg, 1984). The common response of the L-neurons to light on is an inhibition and a depolarization as the light off response. The L-neuron shown here did not exhibit a pronounced light off response that could explain the amplitude of the slow component in the off-response of DNOVS1. This synaptically driven depolarization is most likely mediated by other L-neurons synapsing onto DNOVS1 in addition.

The experiments described so far demonstrate that DNOVS1 receives input from two separate sources: from the photoreceptors of the compound eye via the VS-cells and from photoreceptors of the ocelli via L-neurons. In order to test how the input signals

from the two different sources (VS-cells and L-neurons) are integrated, we combined these two stimuli and measured the response of DNOVS1. Figure 2.8a shows the response to visual motion displayed in front of the compound eye and Figure 2.8b the response to the light on-off stimulus delivered to the ocelli. The delay between stimulus onset and response is much shorter (12.9 ± 1.8 msec) than it is for the motion response (42.4 ± 1.7 msec, n=7). The measured delay in the response of DNOVS1 to stimulation of the ocelli was in the range of delays reported by Parsons et al. (1993) for the response of the LPTC V1 after stimulation of the ocelli. This short delay indicates that the response of DNOVS1 to light pulses is mediated by a different pathway than the motion response. When we combined the two stimuli, DNOVS1 showed a response (Fig. 2.8c, black line) that is almost the linear sum of the responses to the single stimuli (Fig. 2.8c, red line). There is only a small deviation at the beginning of the stimulus where the calculated response is stronger than the measured response.

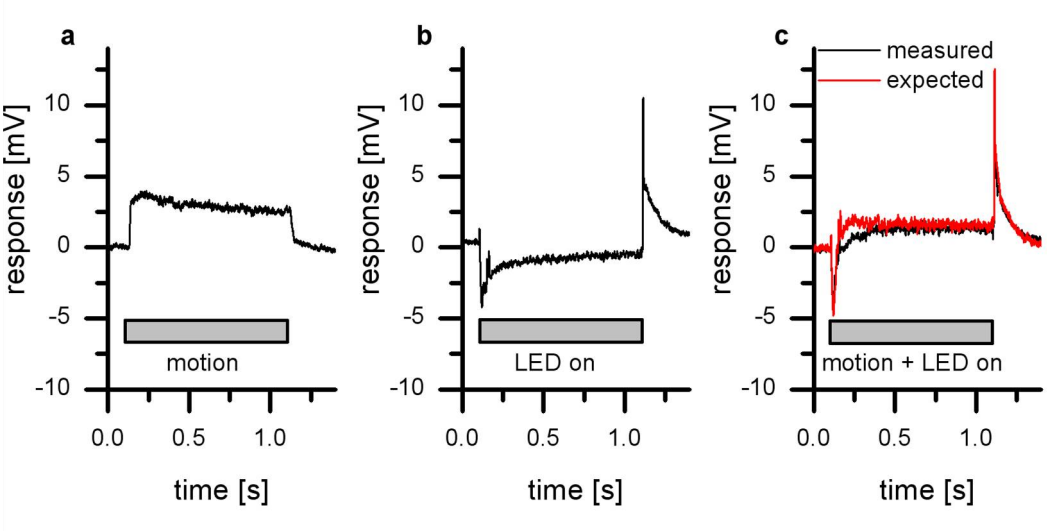

Figure 2.8: Response of DNOVS1 to stimulation of the facet eye and the ocelli.

a) Response of DNOVS1 to upward motion in the frontal part and simultaneous downward motion in the lateral part of the receptive field. b) Response of DNOVS1 to stimulation of the ocelli. c) Response of DNOVS1 to a combination of a motion stimulus displayed to the facet eye and a light on-off stimulus delivered to the ocelli (black line). The response to the combined stimulus is nearly the linear sum of the responses to the individual stimuli (red line). Data represent the mean recorded from n=8 flies.

The double recording of VS-cells and DNOVS1 indicated electrical synapses between VS4-VS9 and DNOVS1. To provide additional evidence for the proposed connectivity between VS-cells and DNOVS1, we injected the Fluorescein-Neurobiotin dyes either into a VS-cell (Fig. 2.9a, data from Haag and Borst, 2005) or into DNOVS1 (Fig. 2.9b). The labeled cell was identified under the fluorescence microscope and a picture was taken. For the further histological investigation, only those brains were taken where only a single cell was visible under the fluorescence light. If the dye was injected into a VS-cell (in the example shown, a VS6) the DNOVS1 was co-stained, dye injection into DNOVS1 led to a co-staining of VS5 – VS9. These results are in accordance with an electrical coupling of VS4 - VS9 and DNOVS1.

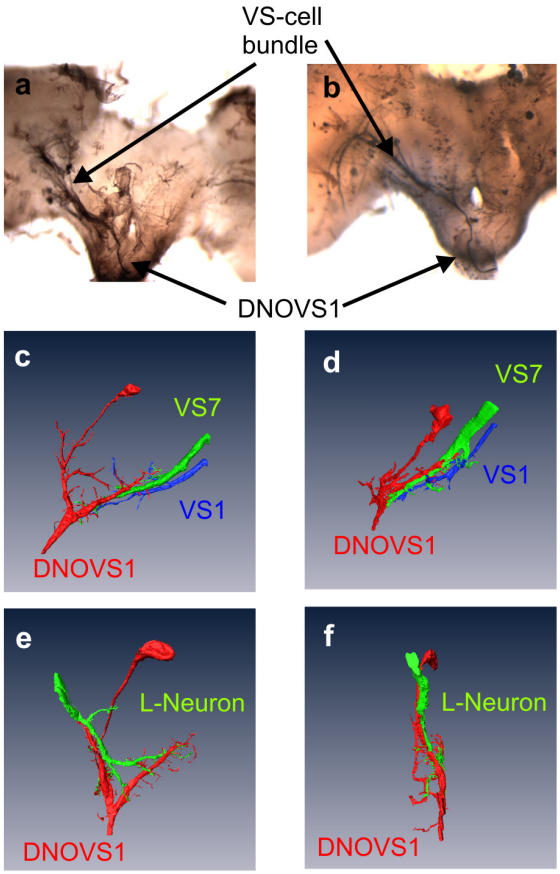

Figure 2.9: Anatomy & dye coupling.
a) Neurobiotin staining of a VS6. Besides the co-staining of adjacent VS-cells, DNOVS1 was found to be labeled, too (data from Haag and Borst, 2005). b) Injection of Neurobiotin into DNOVS1 led to a specific co-staining of VS-cells. VS6 and VS7 showed the strongest staining and VS5, VS8 and VS9 were stained weakly. This confirms the results about the coupling strength between DNOVS1 and the VS-cells (see Fig. 2.2c). c) Two photon imaging of DNOVS1 and VS-cells. DNOVS1 (red) was filled with the red fluorescent dye Alexa568, VS1 (blue) and VS7 (green) were filled with the green fluorescent Alexa488. Shown is a XY-projection. The side view (d) shows that the axon terminal of VS7 and the dendrite are in close vicinity. e) XY projection of DNOVS1 (red) and an L-neuron (green). f) same as e, but in a side view. Two-photon image stacks are subject to iso-surface rendering by Amira software package (see Material & Methods)

Figures 2.9c-f show the anatomy of VS-cells, DNOVS1 and an L-neuron obtained from two photon image stacks after filling the cells with Alexa 488 and Alexa 568. In Figure 2.9c,d three neurons are stained: a DNOVS1 (filled with Alexa 568) in red, a VS7 in green and a VS1 in blue (both cells were filled with Alexa 488). While the endings of VS7 and the dendritic branches of DNOVS1 are in close vicinity, the endings of VS1 and DNOVS1 are in different depth (d). The gap between the two cells makes it rather unlikely that there are synaptic contacts between VS1 and DNOVS1. Figure 2.9e and 2.9f show a stained DNOVS1 (filled with Alexa 568) and an L-neuron (filled with Alexa 488). The axon terminals of the L-neuron contact the lateral dendritic branch of DNOVS1.

2.4 Discussion

The results presented above demonstrate that DNOVS1 receives synaptic input from at least two different sources, from a subset of large-field motion sensitive VS-cells as well as from the ocelli via ocellar interneurons. We also found that DNOVS1 is specifically tuned to rotational flow-fields such as generated by rotation of the fly around a particular body axis. In contrast to locusts where ocelli have been shown to play a role in optomotor behavior of the animal (Taylor, 1981b) it has been shown in the blowfly that the ocellar dorsal light response has only little influence on the optomotor response (Hengstenberg, 1993; Schuppe and Hengstenberg, 1993). Therefore, any discussion about the possible interplay between ocellar and motion input would be highly speculative. We therefore will concentrate the following discussion on the motion sensitive response features of DNOVS1. In particular, we will discuss three issues raised in this context by the above findings: Can the small graded responses of DNOVS1 to motion stimuli be reliably transmitted through the cervical connective to the motor

neurons in the thoracic ganglion? Can the tuning of the receptive field to rotational flow-fields be explained by the described coupling to VS-cells? And finally: In what respect does the representation of image motion at the level of DNOVS1 differ from the one in lobula plate cells?

2.4.1 Small response amplitudes to motion stimuli

We found that DNOVS1 responds to motion stimuli with a graded shift in membrane potential. However, compared to the signals of other graded potential neurons like their presynaptic VS-cells, the responses measured in the DNOVS dendrite were rather weak. Although it is possible to elicit action potentials by current injection (data not shown), and although the off-response to ocellar stimulation showed a clear indication of active membrane conductance (Fig. 2.7), we did not find any evidence for a contribution of active processes to the motion response. This poses the problem of how well such small graded responses can be transmitted passively over a rather long distance of roughly 2 mm along the axon into the thoracic ganglion. To address this question, instead of recording from the dendrite we placed the electrodes in the axon close to the thoracic ganglion and recorded the response of DNOVS1 to motion stimuli. The responses of DNOVS1 recorded close to the thoracic ganglion were on average only 40 % smaller than responses recorded in the dendrite (n=2, data not shown). It, thus, seems that the specific membrane conductance of the DNOVS axon is small enough to ensure signal transmission with little amplitude loss to its postsynaptic partner cells in the thoracic ganglion, even without amplification by voltage-dependent membrane processes.

2.4.2 Rotational tuning and specific connectivity to VS-cells

Our statements about the connectivity of DNOVS1 to the VS-cells are based on two findings: first we measured the potential response to current injection of both polarities and in both directions (Fig. 2.4), next we measured the correlation strength of the signals in both cells without stimulation (Fig. 2.5). Both types of experiments revealed that DNOVS1 is substantially connected to VS-cells 4-9, with maximum coupling to VS7 and VS8, and only residual coupling to the frontal cells VS1-3. The measured weak coupling between VS1-3 and DNOVS1 might be due to the coupling of the VS-cells to each other (Haag and Borst, 2004). Current injection into VS3 leads to a response in VS4 which is then transmitted to DNOVS1, and consequently would not indicate a direct coupling between VS3 and DNOVS1.

In order to see whether the coupling coefficients determined this way are in accordance with the azimuthal sensitivity distribution of DNOVS1 (Fig. 2.1), we determined the corresponding sensitivity profile of all VS-cells except VS10 using the exact same stimulus device (Fig. 2.6). To avoid any ambiguities in identifying VS-cells, we also took precise measurements of the location of the ventral dendrite along the medial-lateral axis within the lobula plate (Farrow, 2005). Summing up the sensitivities of the VS-cells weighted according to the coupling strengths led to a linear prediction of the azimuth sensitivity of DNOVS1 that is shown next to the measured one in Fig. 2.6. Both profiles can be seen to match quite well, with peak sensitivity for lateral positions decreasing towards frontal positions. If DNOVS1 were to integrate over all VS-cells with equal strength, a rather homogeneous sensitivity for downward motion at all azimuth positions would result (data not shown). In the frontal part, however, a significant deviation of the measured DNOVS1 sensitivity from the expected one can be observed: Whereas the measured sensitivity exhibits a zero crossing at about 15 degree and inverts

its sign at frontal positions, the expected sensitivity for upward motion is approximately zero at frontal positions. This means that from the connectivity pattern DNOVS1 is expected to respond to vertical motion at lateral positions irrespective to motion displayed in front of the fly. The neuron would, thus, not discriminate between a translational flow-field originating by an upward motion of the fly ('lift') and a rotational flow-field originating by rotation of the fly around its longitudinal axis ('roll'). Quite in contrast, it responds most strongly to lateral downward motion and frontal upward motion, resulting in a specific tuning to rotational flow-fields, where the pole of the rotation is located at 15° azimuth (Fig. 2.2). Mechanistically, this might be explained by reciprocal inhibitory connections between the most frontal and most lateral VS-cells postulated in a recent study on current injection experiments from pairs of VS-cells (Haag and Borst, 2004). Such an inhibitory loop can explain the slight preference for upward motion of lateral VS-cells in frontal positions of the visual field. If such connections are located at the axon terminal regions of VS-cells, as has been found for electrical connections (Cuntz et al, submitted), the effect of this reciprocal inhibition and the resulting sign inversion would be underestimated in recordings from mid-axonal positions of the cells, but would show up much more pronounced in the dendrite of a postsynaptic cell such as DNOVS1. Another possibility to explain the above phenomenon is the existence of chemical synapses between VS-cells and DNOVS1: whereas our experiments have revealed no positive evidence for such connections, chemical synapses have been anatomically described by Strausfeld and Bassemir (1985). While nothing is known about the strength and nature of these synapses, there effects might combine with the electrical coupling and become visible during visual motion stimulation leading to a rotational tuning of DNOVS1 as found in this study. A third possibility, which cannot be excluded at present, is the connection of DNOVS1 to other neurons of the fly optic lobes, which have escaped our notice so far. A final decision

between the above alternatives will have to wait until a complete description of the circuitry will be available from serial block face scanning electron microscopy technology (Denk and Horstmann, 2004).

2.4.3 Functional significance of rotational tuning

Aside from the problem discussed above of how to explain the observed receptive field properties of DNOVS1 given the observed connectivity to VS-cells, another interesting question is how the representation of image flow at the level of DNOVS1 differs from the one in the presynaptic set of VS-cells. Although our stimulation device did not allow displaying rotational stimuli, we approximated such stimuli by showing vertical image motion going up- and downward at different positions simultaneously, and compared the responses of DNOVS1 to combined stimuli to the sum of responses to the individual stimulus components. As was observed with ocellar stimulation, the outcome of these experiments revealed a perfectly linear response behavior of DNOVS1 (Fig. 2.2). While such a linear superposition of individual response components might not sound as an indication for a high degree of specificity, it is indeed much different from the strongly sublinear response summation observed in the vertical cells of the lobula plate. There, the responses of VS-cells tend to saturate with increasing size of stimulated area (Haag et al, 1992). Furthermore, stimulation of V1, a heterolateral neuron postsynaptic to VS1-3 (Kalb et al, 2006) revealed that, unlike DNOVS1, V1 responds almost as strongly to large-field downward motion as to rotational flow-fields that perfectly match its receptive field (Karmeier et al, 2003). Thus, a linear response summation in DNOVS1 increases its response selectivity compared to the one of lobula plate cells substantially. A quantitative analysis of this effect requires stimulation of all VS-cells with rotational flow-fields as well as with translational ones, and comparing the

resulting flow-field selectivity with the one observed at the level of descending neurons such as DNOVS1. Such an analysis will further elucidate how the neural representation of flow-fields changes at the various processing levels from lobula plate through descending down to motor neurons in the neck and thorax of the fly (for first results on flow-fields of neck motoneurons see Huston and Krapp, 2003 and Krapp and Huston, 2005).

2.5 Acknowledgements

We are grateful to Renate Gleich, Marianne Braun and Dietmute Bueringer for excellent technical assistance. This work was supported by the Max-Planck-Society, a grant of the BMBF to the Bernstein center Munich to J.H. and by a grant of the DFG (GRK 1091) to A.W.

3 Nonlinear integration of binocular optic flow by DNOVS2, a descending neuron of the fly

This chapter was published in 2008 by Adrian Wertz, Alexander Borst and Juergen Haag in the Journal of Neuroscience (Vol. 28(12) pp. 3131-3140)

For visual orientation and course-stabilization, flies rely heavily on the optic flow perceived by the animal during flight. The processing of optic flow is performed in motion-sensitive tangential cells of the lobula plate which are well described with respect to their visual response properties and the connectivity amongst them. However, little is known about the postsynaptic descending neurons which convey motion information to the motor circuits in the thoracic ganglion. Here we investigate the physiology and connectivity of an identified premotor descending neuron, called DNOVS2 (for descending neuron of the ocellar and vertical system). We find that DNOVS2 is tuned in a supra-linear way to rotation around the longitudinal body axis. Experiments involving stimulation of the ipsi- and the contralateral eye indicate that ipsilateral computation of motion information is modified non-linearly by motion information from the contralateral eye. Performing double recordings of DNOVS2 and lobula plate tangential cells, we find that DNOVS2 is connected ipsilaterally to a subset of vertical sensitive cells. From the contralateral eye, DNOVS2 receives input most likely from V2, a heterolateral spiking neuron. This specific neural circuit is sufficient for the tuning of DNOVS2, making it probably an important element in optomotor roll movements of the head and body around the fly's longitudinal axis.

3.1 Introduction

Flying animals rely heavily on visual cues in order to control chasing, cruising and landing behavior (Borst and Bahde, 1988; Frye and Dickinson, 2001; Srinivasan and Zhang, 2004). In the blowfly, panoramic and small-field visual stimuli elicit optomotor movements of the head and body which attempt to stabilize the visual input on the retina (Hengstenberg, 1984; 1988; 1991). The processing of optic flow is performed in the third visual neuropil, the lobula plate. There, approximately 60 lobula plate tangential cells (LPTCs) per brain hemisphere selectively integrate motion signals provided by local, columnar elements arranged in a retinotopic fashion (Borst and Egelhaaf, 1992; Haag et al., 1992; Single and Borst, 1998). LPTCs can be identified individually due to their invariant anatomy and characteristic visual response properties (Hausen, 1982; Hengstenberg et al., 1982; Borst and Haag, 2002). Amongst them, cells of the vertical system (VS-cells) respond preferentially to vertical motion while cells of the horizontal system (HS-cells) are best excited by horizontal motion. In addition to the columnar input, many tangential cells receive input from other tangential cells (Farrow et al., 2003; 2005; 2006; Haag and Borst, 2001; 2002; 2003; 2004; 2005; 2007; Hausen, 1984; Horstmann et al., 2000; Kalb et al., 2006). Together with the directionally selective input from columnar elements, these lobula plate network interactions are responsible for the tangential cell tuning to specific flow fields (Cuntz et al., 2007; Franz and Krapp, 2000; Krapp and Hengstenberg, 1996; Krapp et al., 1998; Karmeier et al., 2003). While LPTCs have been studied extensively, much less is known about the descending neurons postsynaptic to LPTCs, which project via the cervical connective into the thoracic ganglion.

The anatomy of descending neurons has been investigated mainly by cobalt backfills from the cervical connective (Strausfeld and Seyan, 1985; Strausfeld and Bassemir, 1985; Gronenberg and Strausfeld, 1991). Three descending neurons, belonging to a group of Y-shaped descending neurons called DNOVS (for Descending Neurons of the Ocellar and Vertical System), were found that showed cobalt coupling to neck motor neurons of the frontal nerve and to LPTCs. Ocelli are light sensitive organs on the dorsal surface of the head and appear to be suited for detecting changes in overall brightness (Schuppe and Hengstenberg, 1993). The physiology and connectivity of DNOVS1 was described recently (Haag et al., 2007).

In the following, we present the physiological response characteristics of DNOVS2 (also called DNDC1-2 by Gronenberg et al., 1995). Gronenberg et al. (1995) showed that the neuron responds to light ON, to antennal air currents and to visual motion and is biocytin-coupled to neck motor neurons, which mediate head rotation (Strausfeld et al., 1987; Gilbert et al., 1995). Here we demonstrate that DNOVS2 is specifically connected to LPTCs and tuned in a supra-linear way to rotation around the longitudinal body axis.

3.2 Materials and Methods

3.2.1 Preparation and Setup

Three – to ten days old female blowflies (*Calliphora vicina*) were briefly anesthetized with CO_2 and mounted ventral side up with wax on a small preparation platform. The thorax was opened from behind to get access to the connective. The fly muscles and intestinal organs were pulled out. To minimize movements of the connective, the legs

were cut away and the abdominal region was waxed. After alignment of the fly with reference to their deep pseudopupil, it was mounted on a heavy recording table facing three stimulus monitors. To stabilize the intracellular recordings, the connective was lifted up by a hook. For double recordings, the head capsule was opened from behind, the trachea and airsacs which normally cover the lobula plate were removed. The connective was viewed from behind through a fluorescence stereo microscope (MZ FLIII; Leica, Bensheim, Germany).

3.2.2 Visual stimulation

Visual stimuli were presented on three Tektronix (Wilsonville, OR) cathode ray tube monitors (width, 10 cm; height, 13 cm). With 0º azimuth in front of the fly, monitor 1 was placed in front of the left eye and extended from -90º to -30º in azimuth and from +40º to -30º in elevation; monitor 2 was placed in front of the right eye at an azimuth position of -15º to +40º, monitor 3 at azimuth position 55º to 120º (see Fig. 3.2 a, b). As seen by the fly, the three monitors together covered an azimuth of 210°. For measuring the sensitivity along the azimuth (Fig. 3.2), each monitor screen was divided into five stripes each with a horizontal extent of 11º to 13º. The same stripe width was used for measuring the stimulus combinations shown in Figure 3.7. For all other experiments we presented motion over the full monitor screen. The positions of the monitors were fixed at the positions indicated in Fig. 3.2 and we recorded either from the right or the left DNOVS2. For the stimulus combinations in Figure 3.3 and Figure 3.4 we presented vertical motion in two monitors, first individually and then simultaneous combinations of vertical motion in both. The asymmetric monitor positions resulted in different azimuth positions of the stimulus for the right and left DNOVS2. To avoid confusion, we mirrored all responses of the left DNOVS2. Thus, the responses for different

stimulus situation are presented below as if they had been obtained from the right DNOVS2. Accordingly, we refer to the right brain hemisphere as the ipsilateral side and to the left hemisphere as the contralateral side. With this asymmetric monitor configuration we received 6 axis of rotation (Fig. 3.4) with poles of rotation at -42°, -22°, -12°, 12°, 22°, 42°. To mimic a rotation around a longitudinal body axis (pole of rotation at 0°), we placed one monitor in front of the ipsilateral eye and one in front of the contralateral eye with mirror symmetric azimuth position from 20°-75°. Stimulus pattern was moved for one second followed by one second of rest. The pattern consisted of a square wave grating with a spatial wavelength of 25°, produced by an image synthesizer (Picasso; Innisfree, Cambridge, MA) at a frame rate of 200 Hz. The image synthesizer was controlled by a Pentium III PC via a DDA06 board (ComputerBoards, Middleboro, MA). The pattern moved at a speed of 42°/s, corresponding to a temporal frequency of 1.7 Hz. The pattern contrast was 95%. The mean luminance was 12 cd m^{-2}. The stimulation and acquisition software was written in Delphi (Borland, Buffalo, NY).

3.2.3 Electrical Recordings

For intracellular recordings, glass electrodes were pulled on a Flaming/Brown micropipette puller (model P-97; Sutter Instrument, Novato, CA), using thin-walled glass capillaries with an outer diameter of 1 mm (GC100TF-10; Clark Electromedical Instruments, Pangbourne, UK). The tip of the electrode was filled with either 10 mM Alexa Fluor 488 hydrazide (Alexa 488) or 10 mM Alexa Fluor 568 hydrazide (Alexa 568) (both Molecular Probes, Eugene, OR). Alexa 488 and Alexa 568 fluoresce as green and red, respectively, allowing us to identify more than one cell at a time. For Neurobiotin staining the tip of the electrode was filled with a mixture of 3 % Neurobiotin (Vectorlabs, Burlingame) and 3 % Fluorescein (Molecular Probes). The shaft of the

electrode was filled with 2 M KAc plus 0.5 M KCl. The electrodes had resistances between 15 and 35 MΩ. Recorded signals were amplified using an SEL10 amplifier (NPI Electronic, Tamm, Germany). The output signals of the amplifier were fed to a Pentium III personal computer (PC) via a 12-bit analog-to-digital converter (DAS-1602; ComputerBoards, Middleboro, MA) at a sampling rate of 5 kHz. Recordings of DNOVS2 were made in the connective near the thoracic ganglion. DNOVS2 was identified based on its anatomy compared to the other DNOVS cells (Fig. 3.1 and Strausfeld and Bassemir, 1985). VS cells were recorded from the axon and were identified using a method described by Farrow (2005). There, not only the characteristic anatomy of the cell was taken into account, but also the relative position of their ventral dendrite within the lobula-plate. V2 was recorded in its axonal arborization and could be identified due to its invariant anatomy (Hausen, 1976; 1981; Hausen and Egelhaaf, 1989).

Standard tungsten electrodes with an impedance of about 1 MΩ were used for extracellular recordings of DNOVS2 and V2 cells. Extracellular signals were amplified, band-pass filtered and subsequently processed by a threshold device delivering a 100-mV pulse of 1 ms duration each time a spike was detected (workshop of Max-Planck-Institute for Biological Cybernetics, Tübingen, Germany). The output signals of the threshold device were fed to the same Pentium III PC at a sampling rate of 1 kHz. Electrodes were positioned in the connective near the axon of a DNOVS2 cell or near the axonal arborization of V2 cells.

3.2.4 Calculating neural responses

Data analysis was performed offline using custom-built software written in either Delphi (Borland, Buffalo, NY) or Matlab (The MathWorks, Natick, MA). Graded neural responses were calculated by averaging the membrane potential during the stimulus,

which was either motion of a one-dimensional grating or current injection, minus the baseline membrane potential. The spiking response of DNOVS2 to stimuli of constant velocity was calculated by counting the number of spikes during the last 800 ms of stimulus presentation minus the spike frequency of 200 ms before stimulus onset.

3.2.5 Two photon microscopy

For registering the anatomy of DNOVS2 and V2, we used a custom-built 2-Photon microscope (Denk et al., 1990; Haag et al., 2004) consisting of the following components: a 5 W-pumped Ti:Sapphire laser (MaiTai, Spectra Physics, San Jose. CA), a pockels cell (Conoptics, Danbury, CT), scan mirrors incl. drivers (Cambridge Technology, Lexington, MA), a scan lens (4401-302, Rodenstock, Columbus, OH), a tube lens (MXA 22018; Nikon, Tokyo, Japan), a dichroic mirror (DCSPR 25.5x36; AHF, Tuebingen, Germany), and a 40x water immersion lens (Zeiss, Oberkochen, Germany). The lens can move along all three axes by a step-motor driven micromanipulator (MP285-3Z; Sutter Instruments, Novato, CA). Emitted light is filtered in parallel by two bandpass filters (HQ 535/50M and HQ 610/75M; Chroma Technology, Brattleboro, VT) and collected by multialkali photomultipliers (R6357; Hamamatsu, Bridgewater, NJ). The whole system is controlled by custom-written software (CfNT V1.569, Michael Mueller, MPI for medical Research, Heidelberg, Germany). 3D reconstruction of the cells was performed with the software package AMIRA V4.1 (Mercury Computer Systems, Berlin, Germany).

3.2.6 Histology

After filling a cell with the mixture of Neurobiotin and Fluorescein, the neuron was identified under the fluorescence microscope. The fly was then kept at +4° Celsius

for at least 60 minutes to allow for diffusion of Neurobiotin to coupled cells. The brain and the thoracic ganglion were taken out of the body and fixed overnight at 4° Celsius in 4 % Paraformol and 0.2 % Glutaraldehyd mixture in 0.15 M phosphate buffer. After several rinses with phosphate buffered saline (PBS), the brain was incubated with Vectastain ABC Kit (Vector Labs) overnight. Before incubation in a 0.02 % $CoCl_2$ and 0.025 % $NiCl_2$ mixture in PBS buffer for 30 minutes the brain was rinsed several times in PBS buffer. The diaminobenzidine (DAB) reaction was started by transferring the tissue in a solution containing 0.02 % $CoCl_2$, 0.025 % $NiCl_2$ and 0.01 % H_2O_2 for 10 minutes at room temperature. The brain was then washed again in PBS buffer and dehydrated in alcohol before embedding it in a mixture of distyrene, tricresyl phosphate and xylene (DPX). The stained cells were identified under a dissection microscope (MZFLIII, Leica). Pictures were taken with a CCD-camera (Leica DC 320).

3.3 Results

In the first series of experiments we measured the responses of DNOVS2 cells to visual stimuli using intracellular recording electrodes. This allowed us to fill the cell with a fluorescent dye. The characteristic dendritic anatomy of DNOVS2 together with DNOVS1, DNOVS3 or LPTCs, obtained from two-photon image stacks, is shown in Figure 3.1. DNOVS2 (red) was filled with the fluorescent dye Alexa 568 together with either DNOVS1 (blue) or DNOVS3 (green), filled with Alexa 488. Both preparations were reconstructed in AMIRA. The superposition of the reconstructions is shown in Figure 3.1c. The superposition was achieved by a maximum alignment of the DNOVS2 cells. All DNOVS cells have a characteristic Y-shape, with a medial and lateral dendritic branch (Strausfeld and Bassemir, 1985).

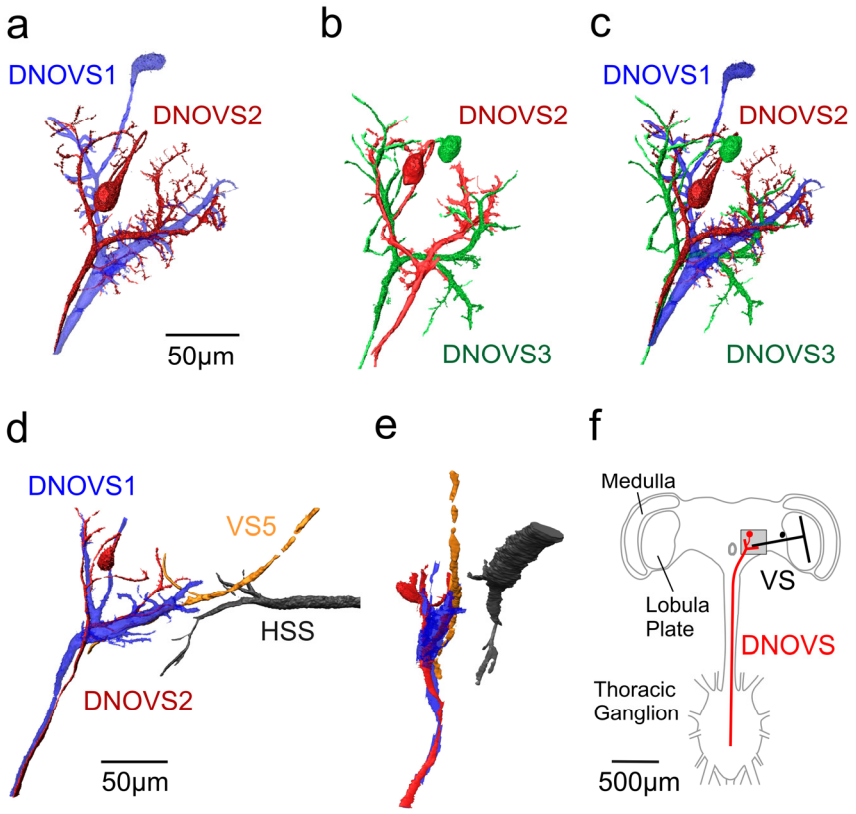

Figure 3.1: Anatomy of DNOVS cells

a) Two-photon imaging of DNOVS1 and DNOVS2. DNOVS1 (blue) was filled with Alexa 568, and DNOVS2 (red) was filled with Alexa 488. b) Two-photon imaging of DNOVS2 and DNOVS3. DNOVS2 (red) was filled with Alexa 568, and DNOVS3 (green) was filled with Alexa 488. c) Reconstruction of all three DNOVS cells. The reconstruction in a,b were superimposed according to the position of DNOVS2. In contrast to DNOVS1, DNOVS2 and DNOVS3 bifurcate in their lateral dentritic branch with numerous short processes. d) x-y projection of DNOVS1 (blue), DNOVS2 (red), VS6 (yellow) and HSS (black). e) Same as in d, but in a y-z projection. The side view shows that the terminal of VS5 and the dendrites of the DNOVS cells are in close vicinity whereas the terminal of the HSS cell lies in different depth. Cells within two-photon image stacks were reconstructed with the AMIRA software package (see Material and Methods). f) Schematic drawing of the fly nervous system showing VS cells within the lobula plate of the fly brain and the DNOVS cells postsynaptically projecting from the brain in the thoracic ganglion. Image stacks from a-e were taken in the highlighted region.

The dendritic branches of all three DNOVS cells are in close vicinity but differ in their arborization pattern. DNOVS2 could be identified in each fly, due to its invariant anatomy (Strausfeld and Bassemir, 1985). Figures 3.1d and e show a stained DNOVS2 (red) and a HSS cell (black), both filled with Alexa 568 and a DNOVS1 (blue) and a VS6

(yellow) both stained with Alexa 488. The axon terminal of the VS5 cell is in close vicinity to the DNOVS cells, whereas the ending of the HSS is in different depth (Fig. 3.1e). The gap between the two cells excludes the existence of direct synaptic contacts between DNOVS2 and HSS.

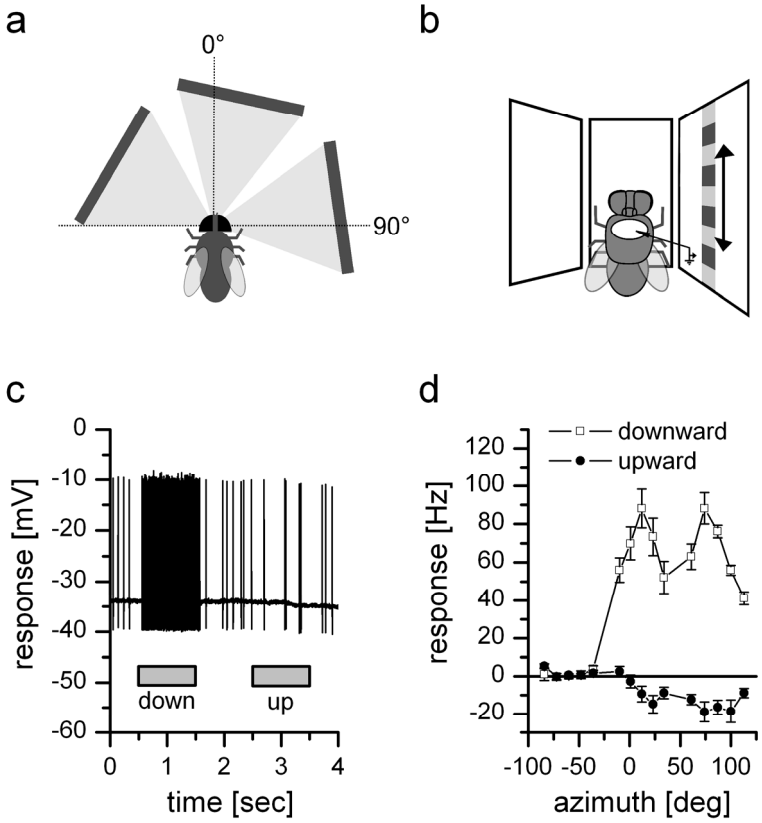

Figure 3.2: Intracellular recording from DNOVS2.

a) top view and b) frontal schematic drawing of the stimulus situation. c) Example response of DNOVS2 to full field down- and upward motion in all three monitors. The cell responds to downward motion with an increase of the spike frequency and to upward motion with a slight decrease of the spike frequency. d) Response of DNOVS2 to vertical motion as a function of the azimuth position. The highest responses to vertical motion are elicited at two positions of the azimuth; at a frontal position (10°) and a lateral position (75°) with downward motion increasing the spike rate and upward motion decreasing the spike rate. The mean firing rate at rest is 5-15 Hz and is increased by 88 Hz at the positions with highest response. In between the response is less with a local minimum at 35° and an increase of the firing rate by 55 Hz. Data represents the mean ± SEM recorded form n = 7 flies.

To measure the sensitivity of DNOVS2 for vertical motion along the azimuth, we presented upward and downward motion at different azimuth positions. Figure 3.2a

shows a top view and Figure 3.2b a frontal schematic drawing of the setup we used. In the following we name the left, middle and right monitor as the contralateral, frontal and ipsilateral monitor, respectively.

The response of DNOVS2 consisted of full blown action potentials with spike amplitudes up to 40 mV. Fluctuations of the membrane potential in response to a visual stimulus were not observed. Presenting motion stimuli, the cell responded either with an increase or a decrease of the firing rate. As an example the response to frontal ipsilateral vertical motion is shown (Fig. 3.2c). The resting frequency of DNOVS2 was between 5-15 Hz. The response to upward and downward motion at different azimuth positions is shown in Figure 3.2d. This stimulus did not elicit any responses of DNOVS2 when presented to the contralateral eye. In the ipsilateral field of view, DNOVS2 responded to downward motion with an increase of firing rate up to 90 Hz. The strongest response was found at two positions of the azimuth at about 10º and 75º. Between these two positions the response only amounted to about 55 Hz. Due to the low resting frequency of the neuron, the responses to upward motion were in general rather small.

To measure the response of DNOVS2 to simultaneous motion stimuli shown at different sectors within the visual field of the fly, we used three monitors at different positions of the visual field (see Material and Methods) presenting combinations of motion stimuli in two of the three monitors (see schematic drawing in Fig. 3.3). We presented simultaneous motion stimuli in the ipsilateral and contralateral field of view. In agreement with the data shown in Figure 3.2d, DNOVS2 responded to ipsilateral downward motion (black, first column) and only slight responses were elicited by contralateral down- or upward motion (column 3 and 4). However, for a combined motion stimulus consisting of contralateral upward and ipsilateral downward motion (penultimate stimulus situation) the measured response is significant stronger than the

arithmetic sum of the individual stimuli ($P<0.05$; Wilcoxon signed- rank test). This supralinear summation might be explained by the spike threshold of DNOVS2. The experiment shows that DNOVS2 responded to a rotational flow field stronger than to a translational one. Furthermore, DNOVS2 was sensitive to contralateral upward motion only in combination with downward motion in the ipsilateral field of view.

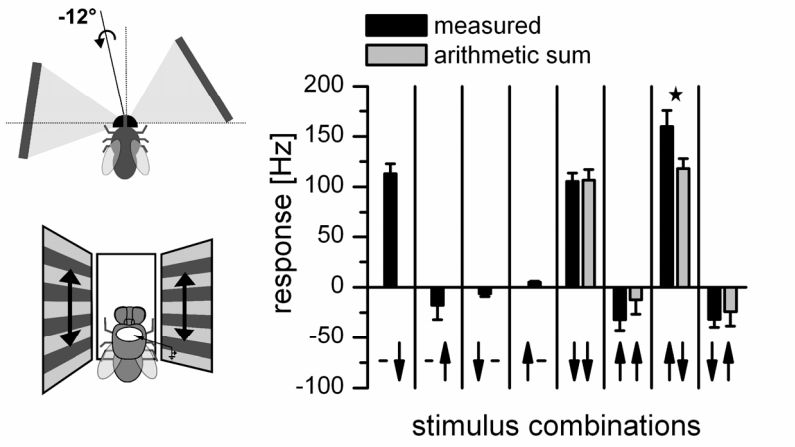

Figure 3.3: Response of DNOVS2 to simultaneous motion in two sectors of the receptive field.

The schematic drawings are indicating the stimulus situation. Black columns show the measured response to simultaneous motion in the ipsi- and contralateral monitor; grey columns indicate the algebraic sum of the responses to individual stimuli. The arrows on the x-axis represent the visual stimulus combination. The left arrow represents contralateral, the right arrow ipsilateral motion. The arrowhead indicates the direction of motion. The neuron responds best to a rotation like stimulus consisting of upward motion in the contralateral and downward motion in the ipsilateral field of view (penultimate stimulus configuration) with an axis of rotation at -12° (indicated in the first drawing). The response to this rotational-like stimulus is stronger than the response to downward motion in both monitors (fifth stimulus situation). This indicates that DNOVS2 responds to a rotational flow field stronger than to a translational one. In addition for the rotational like stimulus the measured response is significant higher than the arithmetic sum of the responses to individual stimuli. Data represents the mean ± SEM from n = 7 flies.

To determine the tuning of DNOVS2 in more detail, we displayed the combined motion stimuli at six other monitor positions, each representing a different axis of

rotation. The combined motion stimulus consisting of an upward motion in one region of the visual field and a downward motion in another region is certainly only a rough approximation of a rotational flow field. However, to avoid circuitous explanation of this stimulus configuration we refer to it in the following as rotational-like stimulus. In Figure 3.4 the responses of DNOVS2 to all 7 rotational-like stimuli are shown. Depending on where the monitors were positioned in the visual field of the fly, downward motion in one and upward motion in the other monitor resulted in different axes of rotation.

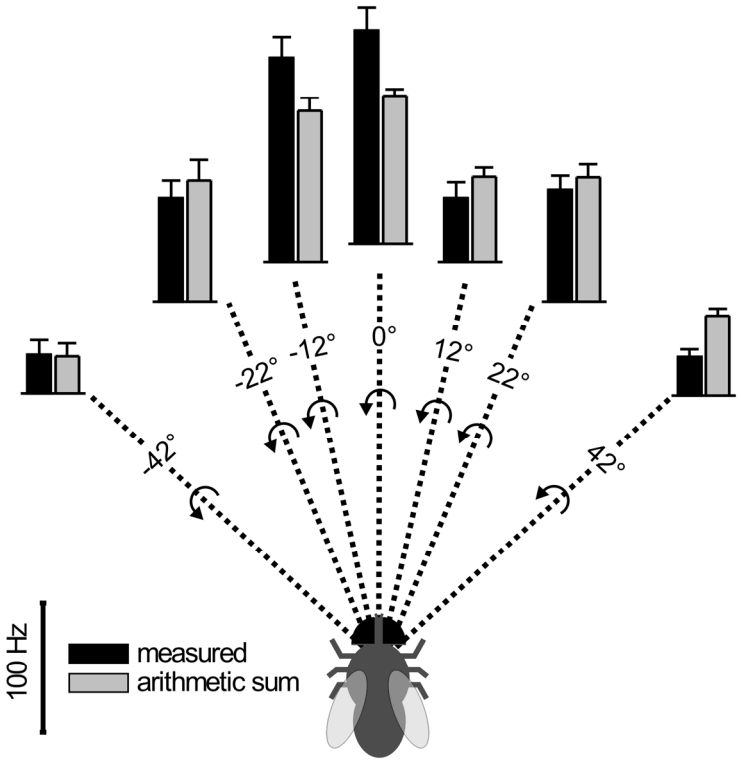

Figure 3.4: Tuning of DNOVS2 to a rotation-like optic flow around a longitudinal body axis.

The responses of DNOVS2 to clockwise rotational-like optic flow at seven different monitor positions, each representing a different axis of rotation, is shown. This results in 7 different axis of rotation, with angular separations from the midline: -42°; -22°; -12°; 0°; 12°; 22°; 42°. Clockwise rotation around a longitudinal axis (0°) elicited the strongest response in DNOVS2. The measured response is significant stronger than the arithmetic sum of the individual components. In contrast, the response to a rotation around an axis at 42° to the right is significant less than the expected one. The clockwise, rotatory stimulus corresponds to a counterclockwise rotation as egomotion (indicated by the arrows). Data represents the mean ± SEM from n = number of fly for each axis as follows: -42° (n= 4); -22° (n= 3); -12° (n= 7); 0° (n= 3); 12° (n= 3); 22° (n= 4); 42° (n= 8).

For example, the position of the monitors in Figure 3.3 corresponded to an axis of rotation at about -12º. A clockwise rotational-like flow field results from a counterclockwise rotation of the fly, which is indicated by the arrows. The strongest response was elicited by a rotational-like flow field around the longitudinal body axis. In this case the response also had the largest non-linear component, i.e. was about 50% higher than expected from the arithmetic sum of the partial flow field. Moving the axis of rotation to either the left or to the right along the azimuth reduced the response of the cell. In addition, the measured responses were in these cases either a linear summation of the individual responses or even less than the arithmetic sum (for example rightmost situation in Fig. 3.4). A sublinear summation might be explained by the response of the cell to null direction stimuli which is limited by the low spontaneous firing rate. Like the measured response strength, the difference between the measured response and the expected ones shifts from sublinear to supralinear depending on the axis of rotation.

As flies have panoramic vision with overlapping frontal visual fields of the eyes (Beersma et al., 1977), we tried to investigate which part of the optic flow is detected by each eye. The binocular overlap in Calliphora is between 10-25° (Beersma et al., 1977) depending on the degree of elevation. Therefore we covered first the ipsilateral eye with aluminum foil and measured the response of DNOVS2 to vertical motion. With the ipsilateral eye covered vertical motion stimuli elicited no response and after uncovering the eye the response of the cell was recovered (data not shown). As expected, a large part of the response arises from the ipsilateral eye. To investigate the influence of the contralateral eye, we covered the contralateral eye and measured the response of the cell to different stimuli. The comparison between the responses of DNOVS2 with both eyes open and the contralateral eye occluded is shown in Figure 3.5. In the first experiment (Fig. 3.5a) we presented simultaneous motion in the ipsilateral and contralateral field of view (same stimulus as in Fig. 3.3). For ipsilateral downward and contralateral upward

motion (first and second stimulus situation) the responses of DNOVS2 with both eyes open (black columns) and the responses with contralateral eye covered (white-striped columns) were similar. However, the responses differed when presenting the combined stimulus (last stimulus situation). Here the response with the contralateral eye covered (white-striped) was less than the response with both eyes open and as high as the arithmetic sum of the individual stimuli (grey amd grey-striped). This suggests that the summation of the individual components is modified in a nonlinear way by visual input from the contralateral eye. By covering the contralateral eye the supralinear summation of the cell disappeared.

To test how the contralateral eye influences the vertical sensitivity of the cell, we measured the response of DNOVS2 to vertical motion along the azimuth, but with the contralateral eye covered (same stimulus as in Fig. 3.2). The comparison of the responses is shown in Figure 3.5b. For lateral stimulus positions greater than 50° from center the measured response for downward motion with the contralateral eye covered matches quite well the response of the cell with both eyes open. For upward motion the responses differ which is probably an effect of the low spontaneous firing rate, which we had during this experiment. However in the frontal part of the visual field the responses for downward motion differ. Here, the response with the contralateral eye covered is less than the response with both eyes open. From this we conclude that part of the neuron's sensitivity to downward motion in the frontal visual field is due to the motion processing of the contralateral eye.

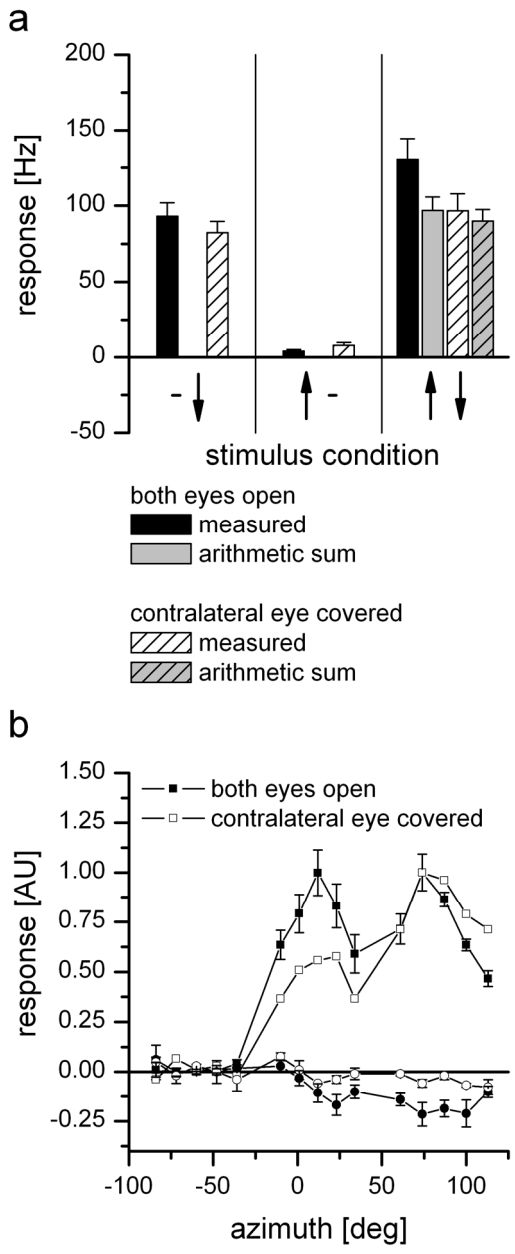

Figure 3.5: Influence of the contralateral eye on DNOVS2.

With the contralateral eye covered, the responses of DNOVS2 to simultaneous motion in two sectors of the visual field (a) and to vertical motion as a function of the azimuth position (b) were measured. The patterns in the graphs refer to the response of the neurons in the following condition: black: both eyes open; white-striped: left eye covered; grey: arithmetic sum of the individual stimuli with both eyes open; grey-striped: arithmetic sum of the individual stimuli with the left eye closed. a) Stimulus presentation in the ipsi- and contralateral field of view. For the individual stimuli (ipsilateral downward and contralateral upward motion) the responses of DNOVS2 with both eyes open and contralateral eye covered are similar. For the combined stimulus (third stimulus situation) the measured response with the contralateral eye covered (white-striped column) is less than the measured response with both eyes open (black column) but as strong as the arithmetic sum of the individual components. Data of for both eyes open are the same as in Figure 3.3 and data for the contralateral eye covered represents the mean. ± SEM from n = 3 flies. b) Response of DNOVS2 to vertical motion as a function of the azimuth position. The responses differ in the frontal field of view, where the response for downward motion with contralateral eye covered (open symbols) is less than the response with both eyes open (solid symbols). Data for the solid symbols are the same as in Figure 3.2 and data for the open symbols are from n = 1 fly.

To determine which tangential cells contribute to the flow field of DNOVS2, we performed double recordings from different VS cells and DNOVS2. In this series of experiments we measured the response of DNOVS2 extracellularly while recording and injecting current in different VS cells intracellularly. DNOVS2 could be identified extracellularly due to its characteristic sensitivity for downward motion along the azimuth (see Fig.3.2d).

As an example Figure 3.6a shows the spike events of DNOVS2 in response to current injection into a VS5 cell. Negative current injection led to a decrease and positive current to an increase of spike frequency in DNOVS2. Thus, current of both polarities was transmitted from VS5 to DNOVS2. We investigated the connectivity of all VS cells (except VS10) and DNOVS2 within one brain hemisphere. The coupling strength between different VS cells and DNOVS2 varied considerably. Current injection into VS1 and VS2 evoked nearly no change in spike frequency in DNOVS2. The strongest coupling could be found between VS5/VS6 and DNOVS2 (Fig.3.6b). In addition, the spike triggered average of the membrane potential of VS5 showed a EPSP-like potential fluctuation whenever a spike occurred in DNOVS2 (Fig.3.6c). Such EPSP-like potential fluctuations were also found in VS6 (data not shown). For other VS cells, no detectable EPSPs could be found.

Multiplying the coupling strength between each VS cell and DNOVS2 with the response of each VS cell to vertical motion along the azimuth (data from Haag et al., 2007) gave us an estimate of the sensitivity profile for a neuron that integrates linearly the output of VS cells. The comparison between this estimated sensitivity and the measured sensitivity for vertical motion is shown in Figure 3.6d. For vertical motion in the ipsilateral field of view the calculated sensitivity matches quite well the measured sensitivity of DNOVS2. Like the measured sensitivity, the calculated one shows a peak

sensitivity of the cell at 75° azimuth position. In contrast, the calculated response for downward motion differs heavily for frontal stimulus positions. DNOVS2 responded with an increase of the firing rate to frontal downward motion and a maximum response was found at 10° azimuth position, whereas the calculated response was much weaker for these azimuth positions.

To provide additional evidence for the proposed connectivity between VS cells and DNOVS2, we injected fluorescein-neurobiotin dyes either into a VS cell (Fig. 3.6e, data from Haag and Borst, 2005) or into DNOVS2 (Fig. 3.6f). The labeled cell was identified under the fluorescence microscope. If the dye was injected into a VS5 cell (Fig.3.6e) DNOVS2 was co-stained (Haag and Borst (2005) identified the cell as a DNOVS3 cell; however from the dendritic anatomy the cell matches quiet well a DNOVS2 cell). Dye injection into DNOVS2 led to a retrograde co-staining of VS6. VS5 was in this case less stained. This indicates an electrical coupling between VS5/VS6 and DNOVS2. The findings are in agreement with a previous experiment by Strausfeld and Bassemir (1985), where they could show anterograde cobalt coupling between VS5 and VS6 onto DNOVS2. Thus, the physiological and anatomical experiments show that DNOVS2 is strongest coupled to VS5 and VS6 members of the VS class.

In order to map the receptive field of the neuron providing contralateral input onto DNOVS2, we recorded from DNOVS2 while presenting ipsilateral downward motion in the full monitor and contralateral upward motion in stripes (width:12°) at different position along the azimuth (Fig. 3.7a). As in previous experiments we calculated the difference between the measured response and the arithmetic sum for the contralateral stimulus at different azimuth positions (Fig. 3.7a). For more lateral stimulus positions the measured response is higher than the arithmetic sum. At about -60° we found a sign reversal and a switch to a sublinear summation of the individual stimuli for

more frontal positions. The highest nonlinearity in the response of DNOVS2 was elicited at -87°, where the difference between the measured response and the arithmetic sum of the individual component is highest. Thus, in the presence of ipsilateral downward motion, DNOVS2 would be most sensitive for contralateral upward motion at -87° azimuth position. This means that in the simplest case one neuron with peak sensitivity for upward motion at this azimuth position conveys motion information from the contralateral eye onto DNOVS2. One candidate that fulfills the requirements would be V2. This neuron has been previously described as a heterolateral spiking neuron connecting both lobula plates with preferred sensitivity for lateral upward motion (Hausen, 1977; Hausen, 1981). Therefore we recorded intra- and extracellularly from V2. We first measured the sensitivity of the cell for vertical motion along the azimuth (Fig. 3.7b). V2 responds with an increase in spike rate to lateral upward motion with a maximum sensitivity at azimuth position of -87°. Lateral downward motion elicited nearly no response in V2, which is probably due to the very low resting frequency of ~1Hz. In addition, V2 is sensitive to frontal downward motion. The shape of V2's sensitivity profile to upward motion along the azimuth is very similar to the nonlinear summation profile in DNOVS2 (Fig. 3.7c). In addition both cells, V2 and DNOVS2, are sensitive to horizontal motion. In Figure 3.7d we show the tuning curves of V2 (red) and DNOVS2 (black) for different motion directions in the frontal monitor. Both cells reveal a similar tuning curve with maximal sensitivity for oblique motion between downward and rightward motion. By filling V2 and VS3 with fluorescent dyes (Alexa 488 and Alexa 568) we reconstructed the cells in AMIRA. The anatomy of V2 shows the en pasant collaterals of the cell projecting to the terminal region of VS3 (Fig. 3.7a, arrow) and therefore to the dendritic region of DNOVS cells. Although the proof of connectivity between V2 and DNOVS2 could not yet be achieved, the physiological response

properties together with the anatomy makes V2 a candidate neuron conveying motion information from the contralateral eye onto DNOVS2.

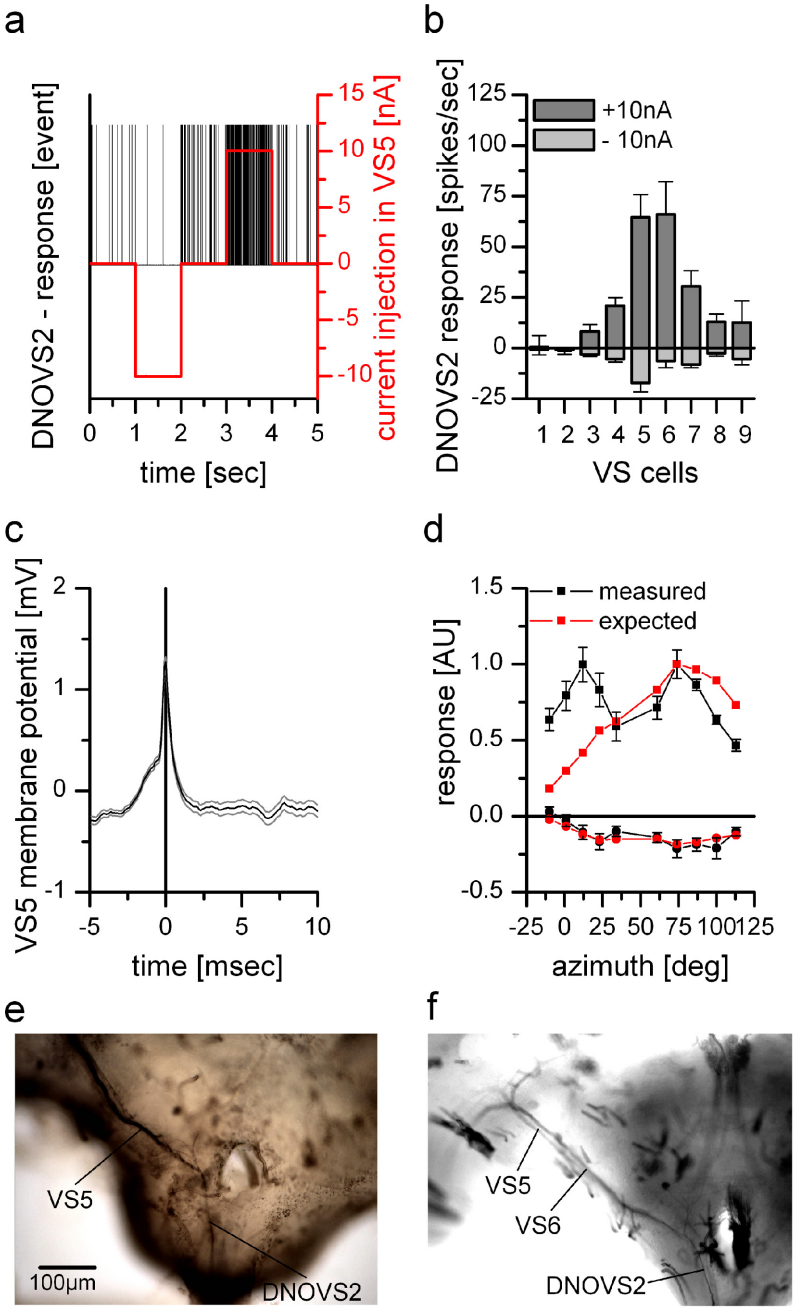

Figure 3.6: Dual recordings and dye-coupling between DNOVS2 and VS cells

a) Current injection of -10 and + 10nA into VS5 led to a decrease and an increase of the spike frequency of DNOVS2, respectively. b) Current injection of -10nA (light grey columns) and +10nA (dark grey columns) in different VS cells elicited different levels of spike frequency decrease and increase of DNOVS2, respectively. Whereas DNOVS2 showed no responses to current injection into VS1 and VS2, it responds when current was injected into VS3-VS9. The strongest response was found for current injection into VS5 and VS6. Data represents the mean ± SEM of VS1 (n=2), VS2 (n=4), VS3 (n=4), VS4 (n=3), VS5 (n=5), VS6 (n=3), VS7 (n=4), VS8 (n=4), VS9 (n=2). c) Spike triggered average (STA) of the membrane potential of a VS5 cell. A spike elicited in DNOVS2 (time point = zero) leads to a slight depolarization of the membrane potential of VS5. This spike induced membrane shift indicates an electrical coupling between VS5 and DNOVS2. Data represents the mean ± SEM of a double recording with n = 1000 detected spike repetitions. d) Expected response of DNOVS2 (red) to vertical motion as a function of the azimuth calculated by the average response of VS1-VS9 to this stimulation (data from Haag et al., 2007)) weighted by their connection strength to DNOVS2 as determined by current injection in (b). The measured (black) and expected (red) response of DNOVS2 differ in the frontal field of view, where the expected response does not show the frontal peak to downward motion. Data for the measured response are the same as in Figure 3.1. e) Neurobiotin staining of VS5. Besides the co-staining of adjacent VS cells, DNOVS2 (or DNOVS3) was found to be labeled, too (data from Haag and Borst, 2005). f) Injection of Neurobiotin into DNOVS2 led to a retrograde staining of VS6 and a weaker stained VS5 cell.

Figure 3.7: Response properties and anatomy of V2. (next page)

a) Nonlinear summation of DNOVS2 as a function of the azimuth (black line). The difference between the measured response and the arithmetic sum of DNOVS2 for ipsilateral downward and contralateral upward motion is calculated for different azimuth positions. The contralateral stimulus was presented in 12° wide stripes at different position along the azimuth. At more lateral positions the measured response of DNOVS2 is higher than the arithmetic sum which indicates a supralinear integration. In contrast, for more frontal positions the response of the cell is less than the arithmetic sum indicating a sublinear integration. The highest nonlinearity was elicited at azimuth position of -87°. Data represents the mean value of recorded from n = 2 flies. b) Response of V2 to vertical motion as a function of the azimuth position. The highest responses to vertical motion is elicited at lateral stimulus positions at about -87° in which upward motion increased the firing rate of the cell. In addition, V2 responds to motion in the frontal part with an inversed preferred direction. Data represents the mean value recorded extracellularly from n = 5 flies. Error bars represent the SEM. c) Overlay of the normalized sensitivity of V2 for upward motion (red) and the normalized nonlinearity profile of DNOVS2 (black) along the azimuth. The curves have a similar shape with a peak at the same azimuth position. d) Orientation tuning of V2 (red) and DNOVS2 (black) in the frontal part of the visual field. The response normalized to the maximum response as a function of the stimulus direction is shown. The tuning curves of DNOVS2 and V2 are almost identical with a response maximum for oblique motion down to the right. Data represents the mean ± SEM of V2 (n=4; extracellular), DNOVS2 (n=3; 1 x intracellular + 2 x extracellular). e) Anatomy of V2. V2 and VS3 cell were filled intracellularly with the fluorescent dye Alexa 488 or Alexa 568, respectively. V2 is a heterolateral neuron projecting from one lobula plate to the other with en passant collateral to the terminal region of VS cells (arrow).

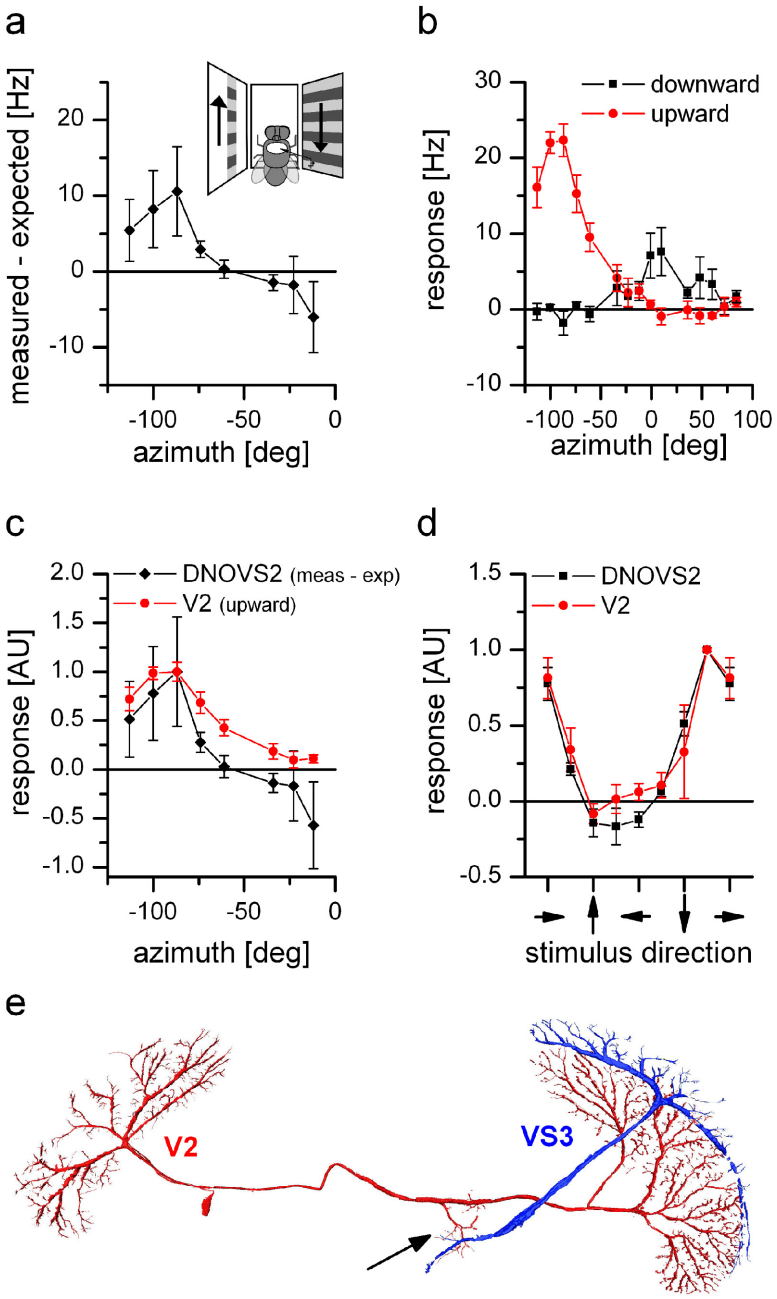

Based on anatomical findings, Strausfeld and Bassemir (1985) suggested that in addition to input from VS-cells, DNOVS2 also receives input from the ocelli via L-neurons. For measuring the responses to the ocellar input, we used an LED to illuminate the ocelli. Figure 3.8 shows the response of DNOVS2 to a 1 sec light pulse emitted by the LED. Turning the LED on and off elicited a fast ON-response and OFF-response in DNOVS2, respectively. Both responses were elicited ~30ms after change of stimulus

condition. Thus, similar to DNOVS1 (Haag et al., 2007), DNOVS2 receives input from the ocelli via L-neurons.

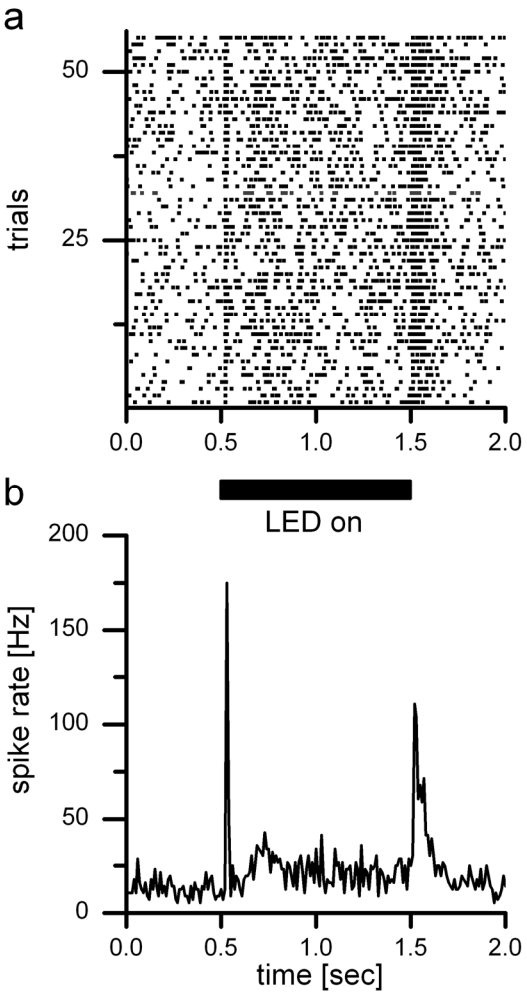

Figure 3.8: Response of DNOVS2 to stimulation of the Ocelli.
Ocelli were stimulated for 1 second with an LED while DNOVS2 was recorded extracellularly. a) Rasterplot of 56 trials is shown. Each dot represents a spike of DNOVS2. b) Spike rate of DNOVS2 with bins of 10 ms. Turning the LED on and off elicited a fast ON-response and OFF-response in DNOVS2, respectively. Both responses were elicited ~30ms after change of stimulus condition. The OFF-response persisted longer than the ON-response. During the stimulation the response was only slightly increased compared to the spontaneous firing rate.

3.4 Discussion

In this study we investigated the flow field selectivity and connectivity of DNOVS2, a prominent descending neuron in the fly visual system that is sensitive to large-field, binocular motion. Our results presented above demonstrate that DNOVS2 is tuned to a flow field that results from rotation of the fly around the longitudinal body

axis. In the presence of ipsilateral downward motion, DNOVS2 is sensitive for contralateral upward motion and increases its spike rate in a nonlinear way (Fig. 3.3). DNOVS2 receives synaptic input from at least two different sources, from a subset of vertical sensitive VS cells on the ipsilateral side as well as from the contralateral eye most likely via V2. Our findings above raise three questions, which we will discuss below: Can the tuning of DNOVS2 be explained by the described connectivity to VS cells and the possible connection to V2? What are the physiological differences between DNOVS2 and DNOVS1? And finally, we compare DNOVS2 with descending neurons of other species and discuss a possible functional implication.

3.4.1 Connectivity to LPTCs

We found that DNOVS2 integrates motion information from both eyes and, by this way, is tuned to rotational optic flow around the longitudinal body axis (Fig. 3.4). Our assumption about the connectivity between DNOVS2 and VS cells is based first on the change of the spike frequency of DNOVS2 in response to current injection into VS cells (Fig. 3.6b) and second on the dye coupling between DNOVS2 and VS5, VS6 (Fig. 3.6e,f). Both types of experiments support the idea that DNOVS2 is connected to VS5 and VS6. The rather weak coupling between DNOVS2 and VS3, VS4, VS7 – VS9 might be attributed to the chain-like coupling of VS cells amongst them (Haag and Borst, 2004). For example, current injection into VS7 leads to a response in VS6, which is transmitted to DNOVS2, and therefore might not indicate a direct coupling between VS7 and DNOVS2. Accordingly, current injection into VS8 leads to an even weaker response in VS6. In addition, EPSP-like fluctuations of the membrane potential were only observable in VS5 and VS6 (Fig. 3.6c), but not in other VS cells. This suggested an

electrical coupling of VS5, VS6 and DNOVS2 which could be confirmed by the dye coupling of neurobiotin between these cells (Fig. 3.6).

Although we could not prove the connectivity between V2 and DNOVS2 experimentally (we tried to perform dual recordings), the physiological response properties of V2 (Fig. 3.7) suggest that motion information from the contralateral eye is conveyed by V2 onto DNOVS2, via its en passant arborization in the posterior ventral protocerebrum. From the coupling of DNOVS2 with VS5 and VS6 alone, the cell would not be able to discriminate between a translational flow field originated by an upward motion of the fly ("lift") and a rotational flow field originated by rotation of the fly around its longitudinal axis ("roll"). However, the additional motion information from the contralateral eye enables DNOVS2 to discriminate between a translational and rotational flow field.

3.4.2 Physiological differences between DNOVS1 and DNOVS2

Another interesting question is how the representation of motion information differs between DNOVS cells. In a previous study we investigated the response properties and connectivity of DNOVS1 (Haag et al., 2007). Like DNOVS2, DNOVS1 projects from the axon terminals of VS cells into the thoracic ganglion and from there onto motor neurons (Strausfeld and Bassemir, 1985; Gronenberg et al., 1995). Both cells receive visual motion input via the VS cells and from the photoreceptors of the ocelli via L-neurons (Strausfeld and Bassemir, 1985; Haag et al., 2007). Similar to DNOVS1, stimulating the ocelli with an LED elicited a short on and off response in DNOVS2 (Fig. 3.8). Both cells have in common that they are tuned to a rotational flow field, but they also exhibit some substantial differences. In contrast to DNOVS2, DNOVS1 responds with a graded shift of the membrane potential to motion stimuli (Haag et al., 2007).

Ipsilateral downward and frontal upward motion elicited the strongest response in DNOVS1, resulting in a tuning to a rotational flow field, in which the pole of rotation is located at 15° azimuth. DNOVS2 is tuned to a rotational flow field with a pole of rotation at 0° azimuth. Thus different axes of rotation are represented by different descending neurons. Whether this is also the case for other descending neurons, like DNOVS3 is still not known. Interestingly, the tuning of the cells is achieved by different kind of synaptic integration. In DNOVS2 the binocular input is integrated in a nonlinear way, whereas in DNOVS1 a linear integration takes place (Haag et al., 2007). As mentioned above, the spike threshold of DNOVS2 is propably responsible for the nonlinear integration. A linear as well as a nonlinear integration of binocular optic flow has been reported for spiking descending neurons of the fly responding best to image expansion (Borst, 1991). This raises the question whether a nonlinear integration is a general feature of spiking neurons only, or whether it could be also achieved in graded potential neurons, but by other mechanisms.

Another difference between DNOVS1 and DNOVS2 is their connectivity pattern with VS cells. Whereas DNOVS2 is coupled most strongly to VS5 and VS6 (Fig. 3.6), current injections and correlation of signals in DNOVS1 and VS cells revealed the strongest coupling of DNOVS1 with VS7 and VS8 (Haag et al., 2007). Lateral VS cells (VS7, VS8) are more sensitive for downward motion at more lateral-caudal positions (Krapp et al., 1998) which is also the case for DNOVS1. Thus different VS cells excite DNOVS1 and DNOVS2 strongest, resulting in different sensitivity profiles for vertical motion along the azimuth.

3.4.3 Functional implication

Descending neurons that are directionally sensitive to wide-field motion have been reported in a number of other insects, for example moths (Collett and Blest, 1966; Rind, 1983), locusts (Kien, 1974; Rowell and Reichert, 1986), dragonflies (Olberg, 1981a,b) and bees (Ibbotson and Goodman, 1990; Ibbotson, 1991). One intensively studied example in locusts is the DCMD (Descending Contralateral Movement Detector), which is connected to the LGMD (Lobula Giant Motion Detector) and might play an important role in collision avoidance (Hatsopoulos et al., 1995; Judge and Rind, 1997; for review see Rind and Simmons, 1999). LGMD/DCMD are sensitive for looming stimuli whereas DNOVS2 was excited strongest by a rotational-like stimulus. Thus, DNOVS2 is probably not involved in avoiding a collision in flies.

In bees, two descending neurons ($DNIV_2$ and $DNIV_4$) were found which share anatomical and physiological similarities with DNOVS2 (Ibbotson and Goodman, 1990). Like DNOVS2, $DNIV_2$ and $DNIV_4$ have their dendritic as well as their axonal arborization confined to the ipsilateral side of the brain and the thoracic ganglion, respectively. $DNIV_2$ and $DNIV_4$ are spiking neurons excited strongest by a movement around the longitudinal body axes. Ibbotson and Goodman (1990) suggested that $DNIV_2$ and $DNIV_4$ are involved in the correction of roll deviation, which could also be the case for DNOVS2.

For both DNOVS cells, it is known that they are dye coupled to neck motor neurons of the frontal nerve (Gronenberg et al., 1995). These frontal nerve neck neurons in turn innervate the large sclerite depressor muscle involved in head roll movements (Strausfeld et al., 1987; Gilbert et al., 1995). Previous studies showed that motor neurons of the frontal nerve are motion sensitive (Milde et al., 1987; Gronenberg et al., 1995; Huston and Krapp, 2003; Krapp and Huston, 2005). Although the number of neck

muscle and motor neurons is manageable (Milde et al., 1987; Strausfeld et al., 1987) the neural circuit as well as the computations underlying these optomotor responses is complex and far from being understood.

However, the connections to neck motor neurons suggest DNOVS1 and DNOVS2 to be involved in the gaze stabilization during flight, which result in an improved condition of vision (Schilstra and van Hateren, 1999; van Hateren and Schilstra, 1999). In free flight, blowflies execute series of saccadic turns with angular velocities of up to several thousand degrees per second; between saccades, the gaze is kept stable (Schilstra and van Hateren, 1998, 1999; van Hateren and Schilstra, 1999). Whereas DNOVS1 ends in the anterior prothoracic ganglion, DNOVS2 extends through pro-, meso- and meatthoracic ganglia (Strausfeld and Bassemir, 1985). Thus, with projections in all three thoracic ganglia, DNOVS2 may participate on one hand in the coordination of gaze stabilization via neck motor neurons; on the other hand DNOVS2 could initiate body saccade. Here again, a further description of the projections is necessary for a complete understanding of the role of DNOVS2 in visually driven behavior.

3.5 Acknowledgements

We are grateful to Renate Gleich and Ursula Weber for excellent technical assistance. This work was supported by the Max-Planck-Society, a grant of the DFG (GRK 1091) to A.W. and by a grant of the BMBF to the Bernstein Center for Computational Neuroscience (BCCN) Munich to A.B.

4 Local and global motion sensitivity in two descending neurons of the fly

This chapter was submitted to the Journal of Neuroscience and is currently under revision.

Authors: Adrian Wertz, Johannes Plett, Juergen Haag and Alexander Borst.

For a moving animal, optic flow is an important source of information about its ego-motion. In flies, the processing of optic flow is performed by motion sensitive tangential cells in the lobula plate. Amongst them, cells of the vertical system (VS cells) have receptive fields with similarities to optic flows generated during rotations around different body axes. Their output signals are further processed by pre-motor descending neurons feeding into the motor circuit of the fly thoracic ganglion.

Here we investigate the local as well as the global motion preferences of two descending neurons called DNOVS1 and DNOVS2. Using an LED arena subtending 240° of azimuth and 95° of elevation, we mapped the receptive fields of DNOVS1 and DNOVS2 as well as those of their presynaptic elements, i.e. VS-cells 1-10 and V2, by measuring locally the cell's motion sensitivity and preferred direction in different parts of the fly's visual field. The receptive field structures of both DNOVS cells can be predicted in detail from the receptive field structure of VS-cells and the V2-cell and the coupling strength of DNOVS with them. We also determined their preferred type of ego-motion using global flow-field stimuli. The results revealed that DNOVS1 and DNOVS2 respond optimally to rotation of the fly around different axes in the horizontal plane. Their preferred axes of rotation result from a match of the optic flow caused by the respective type of ego-motion with their specific receptive field structures.

4.1 Introduction

Optic flow is an important source of information about the ego-motion of an animal (Gibson, 1950). Accordingly, it is used e.g. in humans to control walking (Warren et al., 2001), in hawks to trigger landing (Davies and Green, 1990) and in bees to estimate travel distance (Collett et al., 2006). Flies also rely heavily on optic flow in order to initiate landing when collisions are impending (Borst and Bahde, 1988a; 1988b) and to control course stability during flight (Frye and Dickinson, 2001; Srinivasan and Zhang, 2004; Mronz and Lehmann, 2008).

In the blowfly the processing of optic flow is performed in the lobula plate by a set of about 60 large-field motion-sensitive neurons. These lobula plate tangential cells (LPTCs) can be identified due to their invariant anatomy and characteristic visual response properties (Hausen, 1982a; Hausen, 1982b; Hengstenberg et al., 1982; Borst and Haag, 2002). They have large dendrites and integrate motion signals provided by local, columnar elements (Haag et al., 1992; 1999; 2004; Single and Borst, 1998). In addition to the columnar input, many tangential cells receive input from other tangential cells (Farrow et al., 2003; 2005; 2006; Haag and Borst, 2001; 2002; 2003; 2004; 2005; 2007; 2008; Horstmann et al., 2000; Kalb et al., 2006). Together with the directionally selective input from columnar elements, these lobula plate network interactions are responsible for the tangential cells' tuning to specific flow–fields (Cuntz et al., 2007; Franz and Krapp, 2000; Karmeier et al., 2003; Krapp et al., 1998; Krapp and Hengstenberg, 1996). Two LPTC subgroups, the ten VS cells (vertical system (Hengstenberg, 1982)) and the three HS cells (horizontal system (Hausen, 1982a)), on either side of the brain are the major output elements of the lobula plate (Strausfeld, 1976). In two previous studies (Haag et al., 2007; Wertz et al., 2008)., we found that VS

cells are electrically coupled, to a group of Y-shaped descending neurons called DNOVS (for Descending Neurons of the Ocellar and Vertical System) feeding into the motor circuit of the fly thoracic ganglion (Strausfeld and Bassemir, 1985). In particular, DNOVS1 and DNOVS2 turned out to be connected to different subsets of VS-cells suggesting a preference of both DNOVS for rotational flow-fields around different body axes (Haag et al., 2007; Wertz et al., 2008). However, a precise comparison of the receptive fields of pre- (VS- and V2-cells) and postsynaptic elements (DNOVS1 and 2) was not possible due to limitations of the stimulus device used previously.

Stimulating the cells by means of a custom built LED arena subtending 240° of azimuth and 95° of elevation, we first measured the receptive fields of DNOVS1 and DNOVS2 using local stimuli. In the second set of experiments the preferred type of ego-motion was determined using global flow-field stimuli. By comparing the results with the expectation given through the known connectivity of DNOVS with VS cells, we investigated the transformation of motion information from VS onto DNOVS cells.

4.2 Materials and Methods

4.2.1 Preparation and Setup

Three – to ten days old female blowflies (*Calliphora vicina*) were briefly anesthetized with CO_2 and mounted ventral side up with wax on a small preparation platform. The head capsule was opened from behind; the trachea and air sacs that cover the lobula plate were removed. To eliminate movements of the brain caused by peristaltic contractions of the esophagus, the proboscis of the animal was cut away and the gut was pulled out. This allowed stable intracellular recordings of up to 45 min. After alignment of the fly with

reference to their deep pseudopupil (Franceschini and Kirschfeld, 1971), it was mounted on a heavy recording table facing the LED-Arena (Fig. 1). For recordings of DNOVS2, the following additional dissection steps were taken. First, the thorax was opened from behind to get access to the connective. Then, the large direct flight muscles and intestinal organs were pulled out. To minimize movements of the connective, the legs were cut away and the abdominal region was waxed. To stabilize the recordings, the connective was lifted up by a hook. The brain and the connective were viewed from behind through a fluorescence stereo microscope (MZ FLIII; Leica, Bensheim, Germany).

4.2.2 Electrical Recordings

For intracellular recordings, glass electrodes were pulled on a Flaming/Brown micropipette puller (model P-97; Sutter Instrument, Novato, CA), using thin-walled glass capillaries with an outer diameter of 1 mm (GC100F-10; Science Products GMBH, Hofheim, Germany). The tip of the electrode was filled with either 10 mM Alexa Fluor 488 hydrazide (Alexa 488) or 10 mM Alexa Fluor 594 hydrazide (Alexa 594, both Invitrogen, Carlsbad, CA). Alexa 488 and Alexa 594 fluoresce as green and red, respectively, allowing us to identify more than one cell at a time. The shaft of the electrode was filled with 2 M KAc plus 0.5 M KCl. The electrodes had resistances between 25 and 50 MΩ. Recorded signals were amplified using an SEL10 amplifier (NPI Electronic, Tamm, Germany). The output signals of the amplifier were fed to a personal computer (PC) via an analog-to-digital converter (PCI-DAS6025, Measurement Computing, Massachusetts, USA) with Matlab (MathWorks, Natick, MA) at a sampling rate of 10 kHz. For recording from DNOVS1, a VS cell was filled with Alexa and visualized under fluorescence light (Fig. 1c). The VS cell then served as a landmark for finding the DNOVS1 neuron. All of the recordings were made from the dendritic region

of DNOVS1 and from the axons of the VS cells. After the recording, several images of each Alexa-filled VS-cell were taken by a CCD camera (Leica DC 320). These images allowed anatomical identification of the recorded cell on the basis of their characteristic branching patterns and the relative position of their ventral dendrite within the lobula-plate (Farrow, 2005). The V2-cell was recorded intra- and extracellularly from its axonal arborization and could be identified due to its invariant anatomy (Hausen and Egelhaaf, 1989) and its sensitivity for vertical motion along the azimuth (Wertz et al., 2008). Extracellular recordings of DNOVS2 were made in the connective near the thoracic ganglion. Standard tungsten electrodes with an impedance of 1MΩ were used. DNOVS2 was identified based on the position of the tungsten electrode within the connective together with the cell's strong response to downward motion and the specific sensitivity profile along the azimuth (Wertz et al., 2008). Extracellular signals were amplified; band-pass filtered and subsequently processed by a threshold device delivering a 100-mV pulse of 1 ms duration each time a spike was detected (workshop of Max-Planck-Institute for Biological Cybernetics, Tübingen, Germany). The output signals of the threshold device were fed to the same PC that was also used to control the stimulus.

4.2.3 Visual stimulation

For visual stimulation an LED arena was custom built based on the open-source information of the Dickinson Laboratory (http://www.dickinson.caltech.edu /PanelsPage). Our arena consists of 30 by 16 TA08-81GWA dot matrix displays (Kingbright, California, USA), each harboring 8 by 8 individual green (568 nm) LEDs, covering 240° in azimuth and 95° in elevation of the fly's visual field with an angular resolution better than 1° between adjacent LEDs. This angular resolution is sufficient

hence, in *Calliphora*, the highest spatial resolution was found in the frontal visual field and amounts to 1.2° (Petrowitz et al., 2000).

The arena is capable of frame rates above 600 fps with 16 intensity levels. Each dot matrix display is controlled by an ATmega644 microcontroller (Atmel, California, USA) that obtains pattern information from one central ATmega128 based main controller board, which in turn reads in pattern information from a compact flash (CF) memory card. For achieving high frame rates with a system of this size each panel controller was equipped with an external AT45DB041B flash memory chip for local pattern buffering. Matlab was used for programming and generation of the patterns as well as for sending the serial command sequences via RS-232 to the main controller board and local buffering. The luminance range of the stimuli was 0 – 80 cd/m2.

4.2.4 Mapping of the receptive field

Data were acquired and analyzed with the data acquisition and analysis toolboxes of Matlab. To determine the receptive field of a cell, a bar of 15° length and a Gaussian cross-section of □ = 2° was moved at 120°/sec and a frame rate of 450 fps horizontally leftwards across the arena and then rightwards at 6 different elevation positions from -37.5° to 37.5° in steps of 15° (Fig. 4.1a). Afterwards the bar was moved vertically down- and upwards at 16 different azimuth positions from -112.5° to 112.5° in steps of 15°. For these resulting 96 positions, we calculated the horizontal and vertical sensitivities (Fig. 4.1b) by averaging 100 ms of the response of a cell at the given time point minus the resting potential (or spike frequency in rest) before stimulus onset. From both these measurements, a vector field was calculated using the horizontal and vertical sensitivities as x- and y-components of the respective vector. In this vector field the angle of an arrow indicates the local preferred direction, while the length of an arrow indicates the

cell's local sensitivity. All sensitivities were normalized to the maximal local sensitivity of the vector field. In control experiments, the cell's local preferred direction was determined using gratings which moved in various directions at one given location. The control experiments were performed at different positions and with different cells. Both types of measurements lead to the same result (data not shown).

To compare two receptive fields (a and b) with each other, we defined a difference index (DI) by calculating the average vector length of the difference between the two vector fields (a, b):

$$DI = \frac{1}{n} \sum_{i=1}^{n=96} \sqrt{\left(a_{x,i} - b_{x,i}\right)^2 + \left(a_{y,i} - b_{y,i}\right)^2}$$

With each of the vector field being normalized to maximum vector length = 1, the DI can range between 0 (identical vector fields) and 2 (two homogenous and opposite vector fields).

To compare the receptive fields of DNOVS cells with the output from VS cells we calculated an expected receptive field. The receptive field for a given VS-cell was multiplied with the measured coupling strength to DNOVS cell (Fig. 3a, d) and integrated over all VS-cells. The coupling strengths for DNOVS1 were obtained from Haag et al. (2007) and for DNOVS2 from Wertz et al. (2008). This integration gave us a linear expected receptive field from the output of VS-cells (Fig. 3). To include V2 in the expectation for DNOVS (Fig. 4) we incorporated the receptive field of V2 in a nonlinear way. If the expectation from VS cells at a given point within the receptive field reached a certain threshold, we added the sensitivity of V2 at this point. Since the connection strength between DNOVS2 and V2 is not yet clear, we varied the threshold and the strength of the sensitivity of V2. This resulted in different expected receptive fields which were quantified by calculating the DI. The lowest DI of 0.154 was found for a

threshold of 40% of the maximum response and a three times stronger input of V2 than the input from VS cells.

4.2.5 Measuring the preferred ego - motion

In order to measure the preferred ego-motion of a cell, we programmed a virtual cage with regularly tiled walls, ceiling and floor, in which a virtual fly could be moved according to the six degrees of freedom as well as rotating it around 36 different axes in the horizontal plane. At every point in time, we projected the environment onto the virtual fly's eye and used the resulting movies subsequently as stimuli displayed to a real fly in the LED arena while recording from the neurons. All movies consisted of 360 frames and were displayed for one second. To measure the preferred movement according to the six degrees of freedom we presented the six movies as follows: lift, sideslip, thrust, yaw, pitch and roll. All six movies were presented forward and backward representing the opposite movements along or around an axis.

To measure the preferred axis of rotation we generated 18 movies of rotations around axes within the horizontal plane. The axes had an interval of 10° and were played forward and backwards resulting in 36 counterclockwise rotations. In the following, a rotation around an axis at 0° represents a counterclockwise rotation around the fly's longitudinal axis (roll movement). Nose-down pitch was assigned as 90° and nose-up pitch as -90°, respectively.

For both set of experiments, the mean responses of DNOVS1 were calculated by averaging the membrane potential over 200 ms, starting 100 ms after stimulus onset minus the mean membrane potential within 200 ms before stimulus onset. For DNOVS2, responses were calculated by adding the spikes in the same time intervals as indicated above. The exact axis of rotation was determined by fitting a sine function to

the responses of a cell to the different axis of rotation (Fig. 6c, see also Karmeier et al. (2005)). The fits were based on the following free parameters: phaseshift (y_0), amplitude (w), and offset (A). From the fits we obtained the preferred axis of rotation by determining the azimuth position at which the fitted tuning curve had its maximum. In addition, we defined the width of the tuning curve by its width at half-maximum height of the fit. For DNOVS2 we fitted a truncated sine function to the responses to account for the fact that the cell's firing frequency cannot become negative.

4.2.6 Predicting the preferred ego – motion from local motion preferences

In order to estimate the preferred ego-motion from the measured receptive field, we compared the receptive field of a cell with flow fields generated by various kinds of ego-motion. To do so, we fed each image sequence as perceived by the virtual fly through a two-dimensional array of local motion detectors of the Reichardt type (Reichardt, 1969). The resulting time-dependent vector fields were time-averaged over the stimulus period. To quantify the match between the receptive field of the cell and the flow fields resulting from a particular flight maneuver, each of the two vector fields was first normalized with respect to the maximum vector length. The match between both vector fields was then determined by projecting the flow field onto the receptive field of the neuron, i.e. by filtering the flow-field by the receptive field of the cell. Accordingly, the matching index MI was determined by averaging the scalar products between all the vectors of the flow field (a) and the receptive field (b) at any given spot.

$$MI = \frac{1}{n}\sum_{i=1}^{n=96}\left(a_{x,i}b_{x,i} + a_{y,i}b_{y,i}\right)$$

4.3 Results

4.3.1 Receptive fields determined from local motion sensitivity

In the first set of experiments we measured the local motion sensitivities and local preferred direction of DNOVS and VS cells at 96 positions within the visual field. A small vertical bar was moved horizontally along the azimuth while recording from DNOVS1 and VS cells intracellularly or DNOVS2 extracellularly. The response of the cell at each point in time was used as an indication for its sensitivity to horizontal motion at each particular position of the bar. In the same way, the cell's sensitivity for vertical motion was probed using vertically moving bars at different elevations (Fig. 4.1a). From these measurements, a vector field was calculated using the horizontal and vertical sensitivities as x- and y- components of the respective vector (Fig. 4.1b). In the following this vector field is called the receptive field of a cell. Cells were measured intracellularly and filled with a fluorescent dye (Fig 4.1c). The characteristic dendritic anatomy of DNOVS1 allowed us to identify the cell (red labeled cell in Fig. 4.1c). VS cells were unambiguously identified by a method described by Farrow (2005). In this method, not only the characteristic anatomy of the cell was taken into account, but also the relative position of their ventral dendrite within the lobula-plate (see green cells in Fig 4.1c). The local motion sensitivities were measured from -120° to 120° along the azimuth and from -45° to 45° in elevation. However, as DNOVS cells did not reveal any sensitivity to local motion in front of the contralateral eye, receptive fields are shown from -30° to 120° along the azimuth only.

The receptive field of DNOVS1 shows a rotational structure with a mix of upward and front-to-back motion in the dorso - frontal part and downward motion in the lateral part (Fig. 4.1d). DNOVS2 responds broadly to downward motion and to front–to–back

motion in the frontal part (Fig. 4.1e). Similar to the receptive fields of VS cells (Krapp et al., 1998), the receptive fields of DNOVS cells suggest that both cells should respond best to rotational flow fields, but with different axes of rotation.

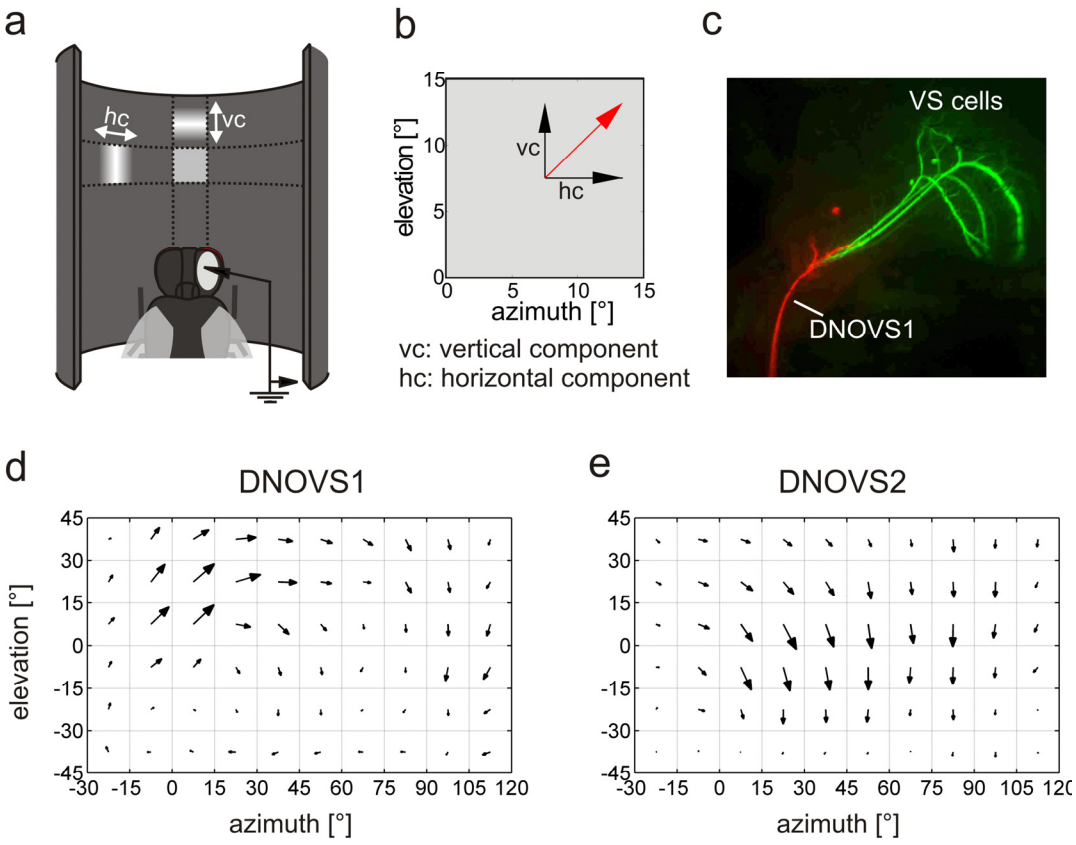

Figure 4.1 Receptive fields of DNOVS1 and DNOVS2.

For mapping the receptive field of a cell a small bar was moved first horizontally and then vertically while recording from the cell (a). The response of each cell at each point in time was used as an indication for its sensitivity for horizontal or vertical motion at each particular position, respectively. From the resulting horizontal (hc) and vertical response component (vc), a vector (red arrow) was calculated (b). Recorded cells were filled with a fluorescent dye (c) allowing us to identify the VS cells (green) and DNOVS (red) anatomically (see Materials and Methods). In d and e the receptive field of DNOVS1 and DNOVS2 is shown, respectively. As both cells did not respond to local motion in front of the contralateral eye, receptive fields are shown from -30° to 120° in azimuth only. DNOVS1 responded frontally to upward motion and laterally to downward motion with a dorsally front-to-back motion in between. DNOVS2 responded over a broad range to downward motion and frontally to horizontal motion. The receptive fields of DNOVS1 and DNOVS2 are similar to rotational flow fields resulting from rotations around particular body axes. Data represent the mean responses recorded from n = 4 flies for DNOVS1 and n=3 flies for DNOVS2.

Both DNOVS cells are electrical coupled to VS cells (Haag et al., 2007; Wertz et al., 2008). In order to investigate which part of the local motion properties can be derived from this coupling, we measured the receptive fields of all 10 VS cells using the same stimuli as described above (Fig. 4.2). All VS cells were sensitive for downward motion and the sensitivity shifts along the azimuth according to the location of the cells dendrite in the lobula plate (Krapp et al., 1998; Haag et al., 2007). In addition, VS7 – VS10 responded to upward motion in the frontal visual field. All VS cells responded to horizontal motion, too. Whereas VS1 responded dorsally to back-to-front motion, VS2 to VS10 responded to front-to-back motion. Moreover, VS7 to VS10 responded ventrally slightly to back-to-front motion. The receptive fields described here are quite similar to the receptive fields measured by Krapp et al. (1998) using a locally rotating dot. Both stimuli, the locally rotating dot and our vertically and horizontally moving bar, produced, in general, similar receptive fields that seemed to be tailored to sense rotational optic flow. Noticeable differences between the receptive fields as determined by the two studies were only observable for VS4 and VS7 to VS10. To quantify the similarity between the receptive fields measured by Krapp and colleagues (Krapp et al., 1998) and receptive field determined in this study, we calculated a difference index (DI) for each VS cell (Table 4.1). In agreement with the visual inspection, the difference turned out to be rather small for many VS-cells. However, larger DI's were found for VS4 and VS7 to VS10.

VS cell	DI
VS1	0.122
VS2	0.125
VS3	0.138
VS4	0.241
VS5	0.165
VS6	0.199
VS7	0.204
VS8	0.207
VS9	0.236
VS10	0.286

Table 4.1 Difference index (DI) for the ten VS cell.

The differences between the receptive fields of VS cells measured by Krapp et al. (1998) and our measured receptive fields were calculated as the mean vector length of the difference vector field (for details, see Material and Methods).

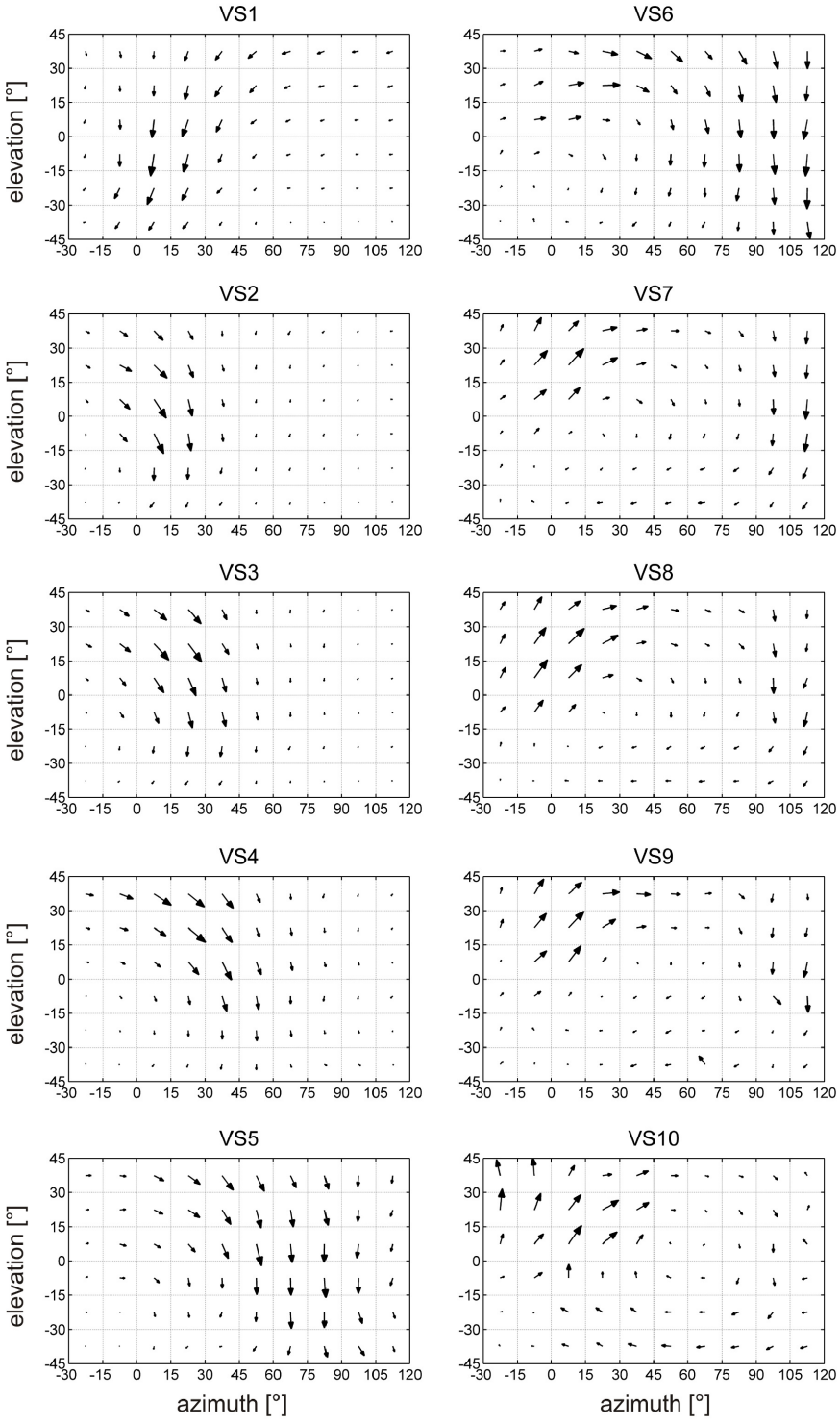

Figure 4.2 Receptive fields of VS cells.

The receptive fields of VS1 to VS10 were measured in the same way as for the DNOVS cells (Fig.4.1). The sensitivity for downward motion shifted along the azimuth from VS1 to VS10. All VS cells have receptive fields with similarities to optic flows generated during rotations about different body axes. Data represent the mean responses recorded from n number of flies for VS1 (n=7), VS2 (n=8), VS3 (n=10), VS4 (n=8), VS5 (n=5), VS6 (n=6), VS7 (n=10), VS8 (n=6), VS9 (n=3), VS10 (n=2).

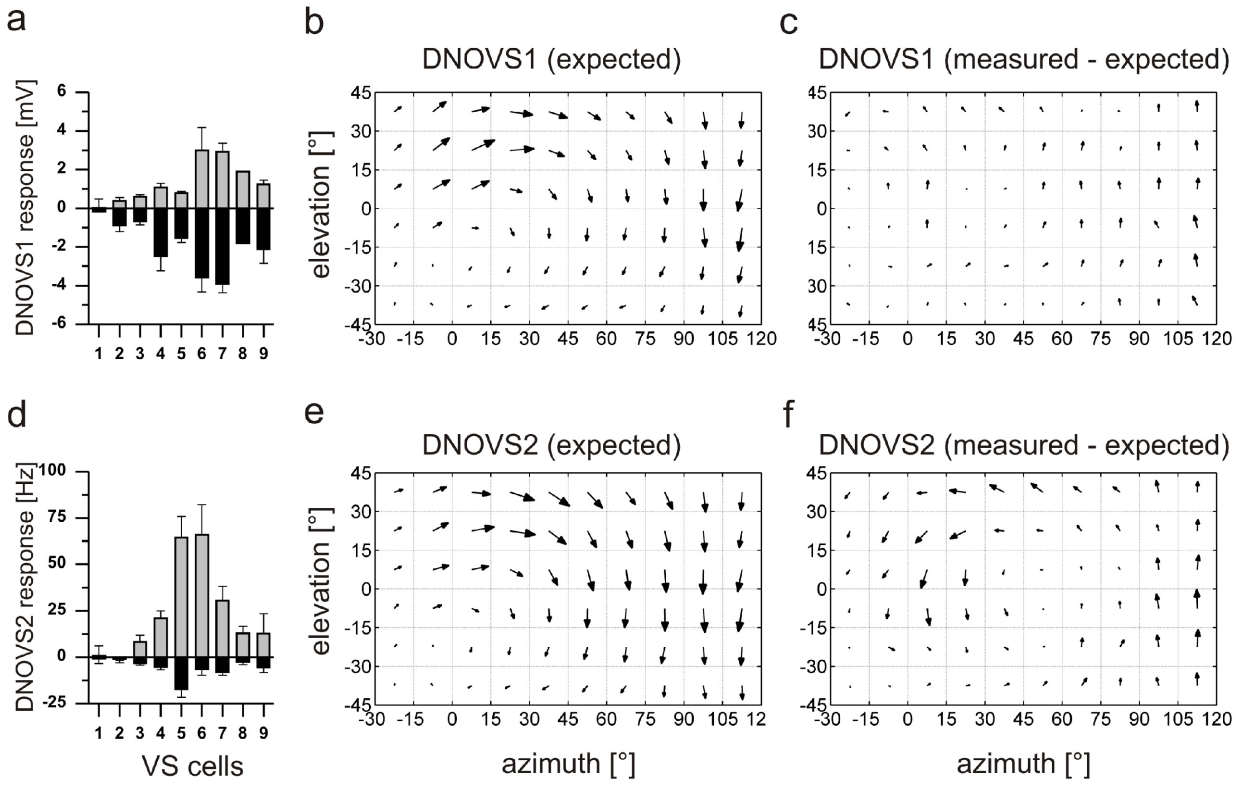

Figure 4.3 Receptive fields of DNOVS1 and DNOVS2 as expected from their coupling with VS cells.

a, d) Coupling strength between DNOVS1 or DNOVS2 and different VS cells as determined by current injection (data in a from Haag et al., 2007, in d from Wertz et al., 2008). With the given connectivity the expected receptive fields of DNOVS1 (b) and DNOVS2 (e) and the differences between the measured and expected receptive field (c, f) were calculated. For DNOVS1, the measured and expected receptive field matched quite well whereas the expected receptive field of DNOVS2 differed remarkably from the measured one.

With the known receptive fields of VS cells and the connectivity pattern of each DNOVS cell with VS cells (Fig. 4.3a,d data from Haag et al., 2007 and Wertz et al., 2008) we calculated the expected receptive fields for both descending neurons (Fig. 4.3b, e, see Material and Methods for details of the calculation). To point out the differences we subtracted the expected receptive field from the measured one (Fig. 4.3c, f). We then quantified the differences between the measured and expected receptive fields by calculating a difference index DI. A DI of 0.179 for DNOVS1 indicates that the expected receptive field of DNOVS1 matched the measured one quite well. Slight

differences were only observed in the lateral part where one would expect DNOVS1 to be more sensitive for downward motion and in the frontal part of the visual field where DNOVS1 responded stronger to upward motion than expected. In contrast to DNOVS1, the DI for DNOVS2 was higher with a value of 0.250. Thus, the expected receptive field of DNOVS2 differed remarkably from the measured one, especially in the frontal part of the visual field (Fig. 4.3d). There, DNOVS2 responded much stronger to downward motion than expected. Laterally, the cell responded less to downward motion, similar to DNOVS1. In addition, from the connectivity with VS cells alone, one would expect DNOVS2 to be more sensitive to front-to-back motion.

In addition to the input from VS cells, DNOVS2 integrates motion information from the contralateral eye in a nonlinear way, probably via the heterolateral spiking neuron V2 (Wertz et. al, 2008). In order to estimate the influence of V2 on the receptive field of DNOVS2, we mapped the receptive field of V2 (Fig. 4.4a). V2 is sensitive to upward motion in the lateral field and to downward motion in the frontal field. In addition, V2 is sensitive to horizontal back-to-front motion. In a first approximation we adjusted the expected receptive field of DNOVS2 with the receptive field of V2, by a linear summation. However, the resulting receptive field indicated a strong upward sensitivity from the contralateral eye (data not shown) which was not observable for DNOVS2. As a nonlinear summation of V2 output occurs in DNOVS2 (Wertz et. al, 2008), we adjusted the receptive field of DNOVS2 by incorporating nonlinearly the sensitivity of V2 (see Materials and Methods). These settings produced the lowest DI of 0.154 between the receptive field of DNOVS2 and the nonlinear expected receptive field. In Figure 4.4b, c the resulting nonlinear, expected receptive field and the difference between the measured receptive field of DNOVS2 and the expected one by incorporating the local motion properties of V2 are shown. The differences between the measured and nonlinear, expected receptive field of DNOVS2 now was rather small (DI

= 0.154). Thus, by adding the receptive field of V2 the differences between the expectation and the measured results became smaller indicating an influence of V2 on the local motion properties of DNOVS2.

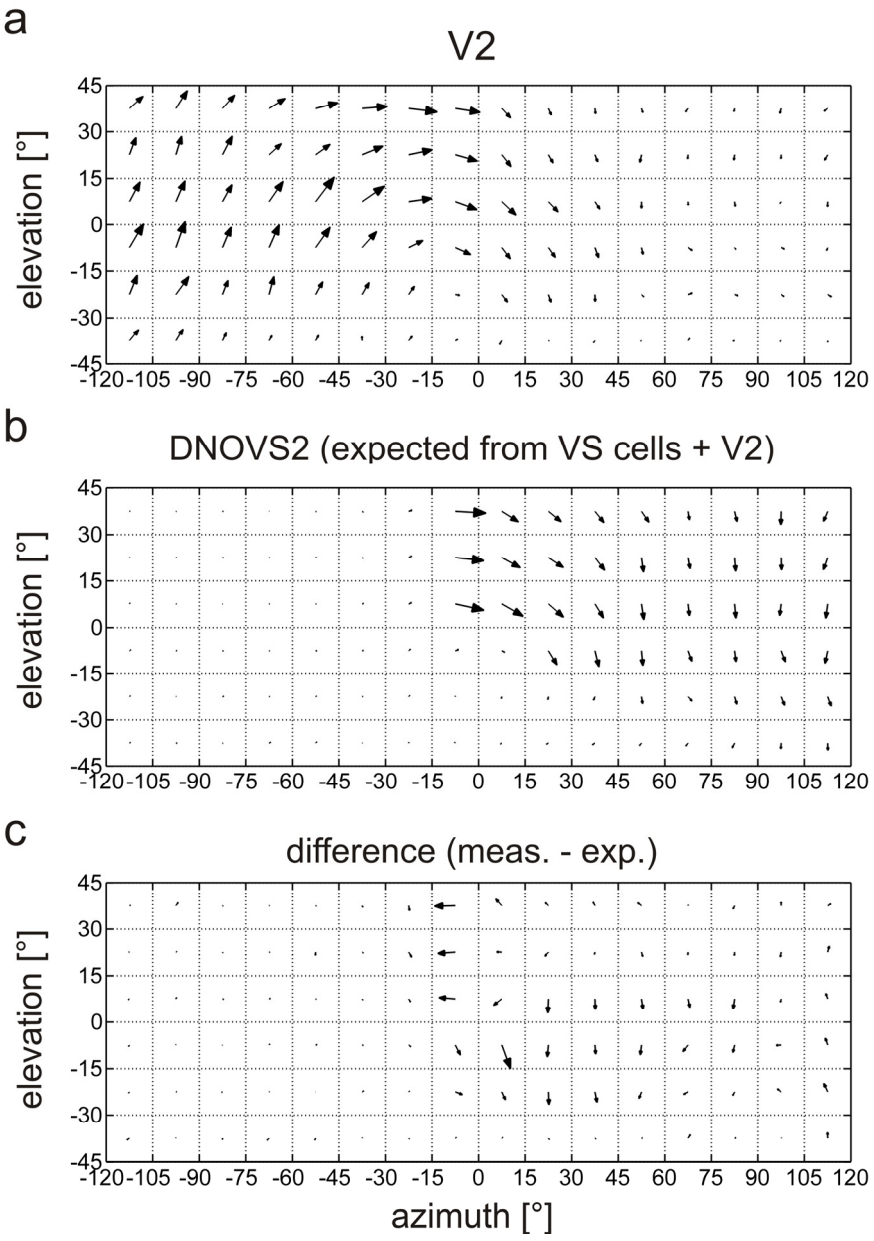

Figure 4.4 Expected receptive field of DNOVS2 taking into account the additional input from V2.

a) Receptive field of V2. Data represent the mean results obtained from n = 4 flies. **b**) Expected receptive field of DNOVS2. The receptive field of V2 was incorporated to the expected receptive field of DNOVS2 (Fig. 4.3e) in a nonlinear way. **c**) Difference between the expected receptive field of DNOVS2 and the measured one. Only slight differences were found, indicating a significant influence of V2 on the local motion sensitivity of DNOVS2 (compare to Fig.3f).

4.3.2 Global motion sensitivity

The receptive fields of DNOVS cells described so far demonstrate that DNOVS1 and DNOVS2 have local motion properties potentially tuned to encode rotational optic flow. In previous studies, in which we used uniform grating motion presented on two monitors (Haag et al., 2007; Wertz et al., 2008), we could show that both cells responded strongest to a shearing stimulus, consisting of upward motion in one part of the visual field and downward motion in another part. However, the previous stimulus device did not allow for presentation of more complex stimuli.

In order to measure the preferred global flow field of a cell, we programmed a virtual cage with regularly tiled walls, ceiling and floor, in which a virtual fly was moved according to the six degrees of freedom. At every point in time, we projected the environment onto the virtual fly's eye and used the resulting movies subsequently as stimuli displayed to a real fly in the LED arena while recording from descending neurons or VS cells. In the following all responses are shown as if the fly were performing this movement. In Figure 5 the average response of one DNOVS1 to the three translational (Fig. 4.5a) and the three rotational movements (Fig. 4.5b) is shown. All movies were shown forward and backward, resulting in movements first in one direction (black traces) followed by the opposite direction (red traces). To all kinds of movements, DNOVS1 depolarized in one direction and hyperpolarized in the opposite direction. On average, DNOVS1 (Fig. 4.5c) responded maximally to nose-down pitch or counterclockwise roll movements of the fly. As expected from the receptive field of DNOVS1 (Fig. 4.1d) the three translational movements elicited a weaker response than the three rotational ones.

The spike rate of DNOVS2 was maximally increased for counterclockwise roll movements (Fig. 4.5d). Nose-up pitch and yaw elicited a weaker response. Whereas DNOVS2 responded only with a slight increase to sideslip and thrust, the cell responded

strongly to an upward lift. From the receptive field of DNOVS2 (Fig. 4.1e) one would expect the sensitivity to lift movements but not the strong response for pitch movements. Both DNOVS cells revealed strong response to both rotations in the horizontal plane, i.e. pitch and roll, indicating their preferred axis of rotation in between.

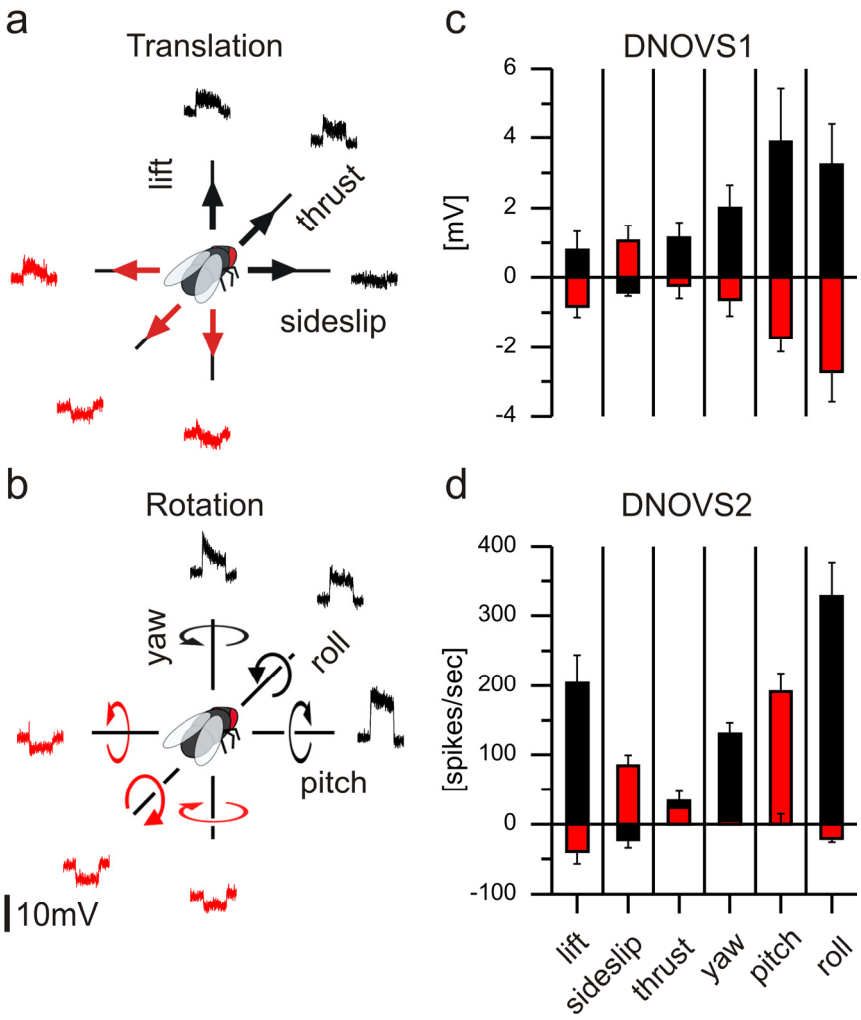

Figure 4.5 Response of DNOVS1 and DNOVS2 to movements according to the six degrees of freedom.

a,b) Example response of DNOVS1 to the three translations (lift, sideslip, thrust) and to the three rotations (yaw, pitch, roll). Results are shown as movements by the fly with different direction indicated by the black and red color. The mean responses of DNOVS1 (n=6) and DNOVS2 (n=4) are shown in c and d. Data represents the mean ± SEM.

In the same way, we measured the preferred movement according to the six degrees of freedom of all VS cells and V2 (Fig. 4.6). The responses of each cell to all six movements were normalized to the maximum response and then averaged over flies. Whereas sideslip and thrust movements elicited only weak responses, VS1 - VS6 depolarized strongly to upward lift movement (black bars in Fig. 4.6a) and hyperpolarized to downward lift movement (red bars). VS7 - VS9 showed a weaker response to lift and VS10 depolarized to a downward lift movement. All VS cells showed their strongest response to rotational movements (Fig. 4.6b). VS1 - VS3 responded strongest to nose-up pitch, VS4 - VS7 to counterclockwise roll and VS8 - VS10 to nose-down pitch movements. In the opposite direction the cells hyperpolarized strongest. Unexpected from horizontal translations (sideslip and thrust), VS cells responded remarkably to yaw. Except VS1 and VS6, all VS cells depolarized to a leftward yaw movement. VS1 depolarized to rightward yaw, whereas VS6 did not respond to yaw. As expected from their receptive fields and previous global motion stimulations (Karmeier et al., 2005), rotations in the horizontal plane elicited the strongest response in VS cells.

An intracellular example response of V2 to the three rotational movements is shown in Figure 4.6c. The average of translational and rotational movements of three extracellular and one intracellular measurement are shown in Fig. 4.6d. As expected from the receptive field of the cell (Fig. 4.4a), V2 responded strongest to counterclockwise roll with a strong depolarization superimposed with a high frequency of action potentials. Clockwise roll elicited a hyperpolarization. Whereas sideslip, thrust, yaw and pitch elicited a weaker response, V2 increased its firing rate remarkably to downward lift. The receptive field as well as the global stimuli indicates a tuning of the cell approximately around the roll axis.

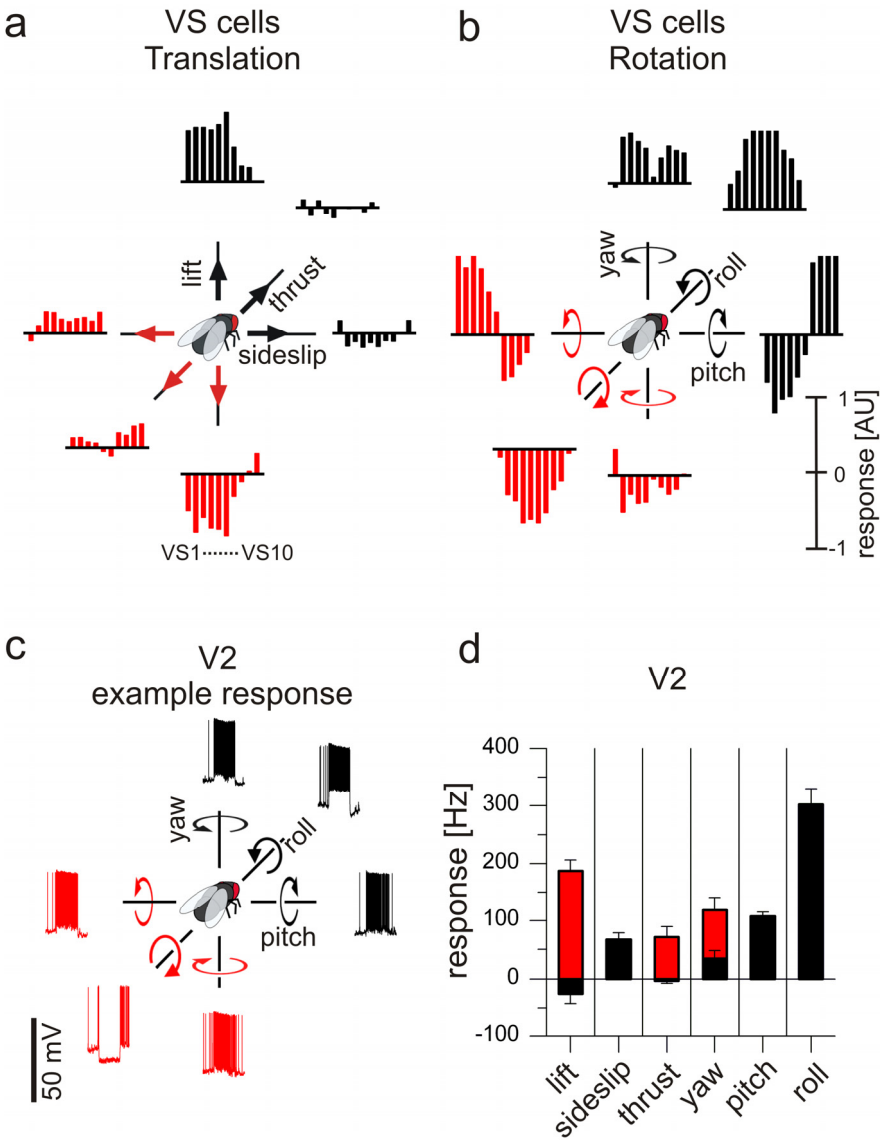

Figure 4.6 Response of VS cells and V2 to movements according to the six degrees of freedom.

In a and b the mean responses of the 10 VS cells to the three translations (lift, sideslip, thrust) and the three rotations (yaw, pitch, roll) are shown. Before averaging, the responses of each cell to all translations and all rotations were normalized to the maximum response. Each bar represents the mean response of one VS cell, with VS1 to VS10 from left to right. Data represent the mean of n=number of flies: VS1 (n=6), VS2 (n=2), VS3 (n=4), VS4 (n=6), VS5 (n=3), VS6 (n=5), VS7 (n = 7), VS8 (n = 5), VS9 (n = 2), VS10 (n = 1). c) Example response of V2 to the three rotations. d) Average responses of n = 4 V2 cells to the same global motion stimuli used in a and b.

VS cells have receptive fields with similarities to optic flow fields generated during rotations about different body axes (see Fig. 4.2 and Krapp et al. (1998)). Karmeier et al. (2003; 2005) showed that the preferred axis of rotation axis estimated from VS receptive fields is in agreement with the one obtained from global wide-field stimulation of the same neurons. Thus, to determine the exact axis of rotation of DNOVS1 and DNOVS2, we rotated the virtual fly around 36 axes of rotation within the horizontal plane. The resulting stimulus movies were presented to the real fly while we recorded from the neurons of interest. In Figure 4.7a an example response of DNOVS1 to 12 rotations in the horizontal plane, separated by 30°, is shown. As the tuning curve showed a sinusoidal response characteristic, the exact axis of rotation was determined by fitting sine functions to the responses (Fig. 4.7b). Rotations eliciting an increase of the spike frequency in DNOVS2 followed nicely the sinusoidal response characteristics, too. For DNOVS2 we fitted a truncated sine function to the responses as the hyperpolarization of the cell is limited to the firing frequency. These sine functions allowed a determination of the response maximum of both DNOVS cells. The mean responses of DNOVS1 and DNOVS2 to all 36 rotations together with the maxima are shown in Figure 4.7c. Red represents a depolarization of DNOVS1 or an increase of the firing rate of DNOVS2 and blue a hyperpolarization of DNOVS1. The maxima are shown with black stripes. In the following the counterclockwise roll movement around the longitudinal body axis is defined as a rotation with a pole at 0°, nose down pitch with a pole at +90° and nose-up pitch with a pole at -90°. DNOVS1 depolarized to counterclockwise rotations around poles from +100° to -20°. The opposite movements elicited a hyperpolarization in DNOVS1. DNOVS2 increased its firing rate for counterclockwise roll movements around poles from -90° to 50°. DNOVS1 responded maximally to a counterclockwise rotation around an axis at azimuth position 32° ± 3° and DNOVS2 to a rotation around an axis at azimuth position at -25° ± 3°.

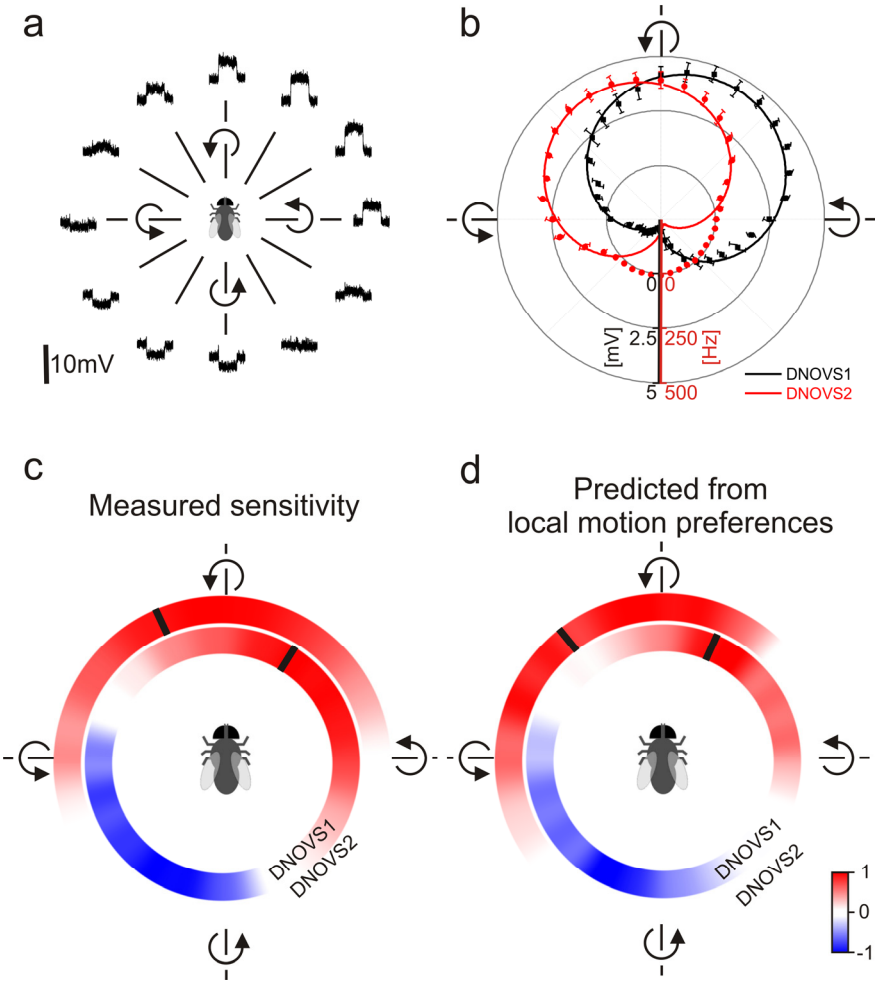

Figure 4.7 Preferred axis of rotation of DNOVS1 and DNOVS2.

a) An example response of DNOVS1 to 12 different axes of rotation is shown. **b**) Polar plot of responses. Using a sine function fitted to the responses of a cell (solid line) the maximum response was calculated and is indicated with a black tick in (c). **c**) Mean responses for all 36 rotations of DNOVS1 (n = 3 flies) and DNOVS2 (n = 3 flies), shown in color-code. Red represents a depolarization of DNOVS1 or an increase of the firing rate of DNOVS2, blue a hyperpolarization. DNOVS1 responded maximally to a counterclockwise rotation of the fly around an axis at 32 ± 5°, DNOVS2 to a counterclockwise rotation around an axis at -15° ± 3°. **d**) Predicted responses to rotations in the horizontal plane calculated from the local motion preferences of DNOVS cells (see Fig. 4.1).

To compare the rotation tuning of DNOVS cells with their receptive fields, we determined the optic flow for each stimulus movie. The matching index (MI) obtained by projecting the respective optic flow onto the receptive field of the neuron indicates the similarity between both vector fields. MIs for all rotations are shown color-coded in Figure 4.7d together with the calculated preferred axis of rotation indicated by a black tick. Although the preferred axis of rotation of both cells are slightly shifted compared to the measured ones, the tuning curve expected from the receptive fields matched quite well the measured tuning curve.

To compare the tuning of DNOVS cells with the tuning of VS cells we measured the response of VS cells to the same set of stimuli (Fig. 4.8a). Again, red represents a depolarization and blue a hyperpolarization of the cell. Compared to DNOVS1, VS cells responded on average with larger graded potential up to 20mV. In Figure 8a the mean response of all 10 VS cells to the 36 rotations is shown beginning with VS1 plotted in the innermost circle and VS10 in the outermost one. The axes of rotation depolarizing a cell shifted along the azimuth, from VS1 - VS10. VS1 depolarized to nose-up pitch and nearby axes of rotation. VS6, instead, responded with a depolarization to counterclockwise rotation around the longitudinal body axis with a pole of rotation approximately at 0° (roll movement of the fly). VS10 was most sensitive to rotations related to nose-down pitch. By comparing the flow fields produced by the stimulus movies with the receptive fields of VS cells, we calculated the MIs for each VS cell to the different rotations. The results are shown color coded in Figure 8b. Like for DNOVS cells, the prediction from local motion preferences is quite similar to the measured tuning curve.

With the same set of stimuli we measured the responses of V2 to different rotations (Fig. 4.8c). Here, red represents an increase of the spike frequency. V2

responded to rotations from nose-down pitch to nose-up pitch with the strongest response approximately for counterclockwise roll. The preferred axis of rotation is indicated by a black bar and was calculated by fitting a truncated sine function to the tuning curve of V2. From the receptive field, the prediction for the tuning curve of V2 was calculated (Fig. 4.8d). Again, the prediction from the receptive field matched the measured tuning curve rather well.

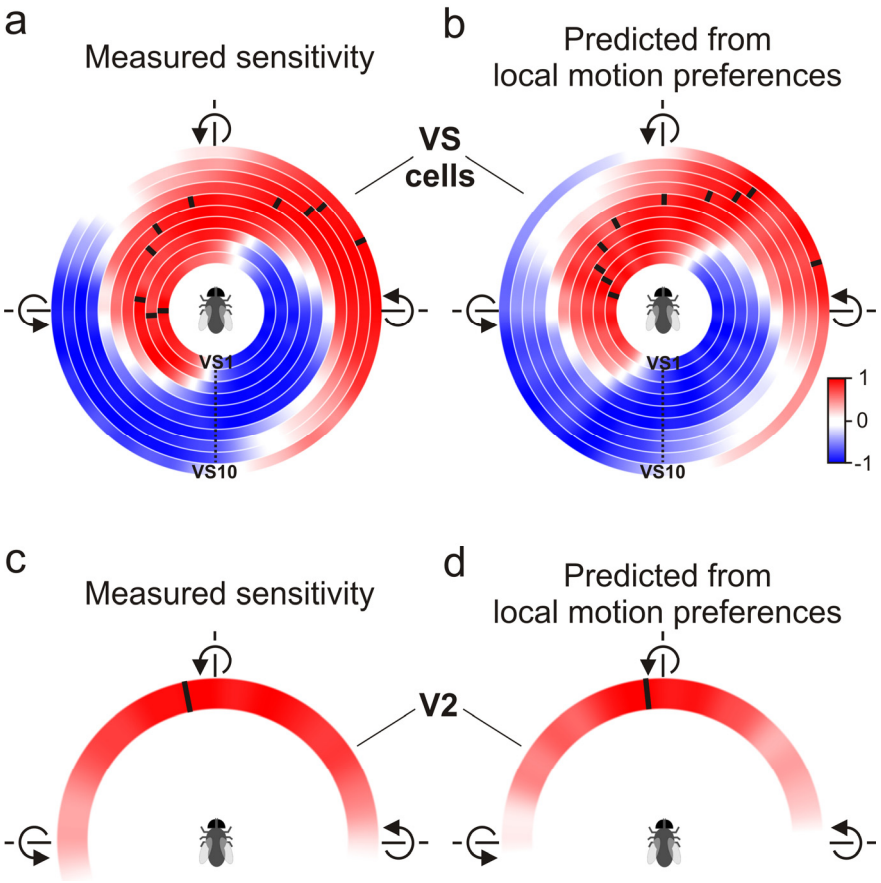

Figure 4.8 Preferred axis of rotation of 10 VS cells and V2.

a) Mean responses of 10 VS cells are shown color coded with red representing a depolarization and blue a hyperpolarization. The preferred axis of rotation (black ticks) shifts along the azimuth with increasing VS-cell number. Data represents the mean of n number of flies for VS1 (n = 5), VS2 (n = 2), VS3 (n = 4), VS4 (n = 6), VS5 (n = 3), VS6 (n = 5), VS7 (n = 4), VS8 (n = 4), VS9 (n = 2), VS10 (n = 1). b) Sensitivities as predicted from local motion properties. c) Mean responses of n = 3 V2 cells to global motion stimuli as occurring during rotation around different axes are shown. **d**). Sensitivity of V2 to global motion stimuli as predicted from its local motion sensitivities.

By fitting a sinusoidal function to the response curves of each VS cell, we determined the preferred axis of rotation for each cell (see Fig. 4.7, Fig. 4.8). The preferred axes of all VS-cells are shown in Fig. 4.9 together with the ones of the V2-cell and both DNOVS-cells. The preferred axis of rotation of DNOVS1 was next to the preferred axis of VS7. Both receptive fields are very similar. Unexpected from the receptive field of DNOVS2, the cell's preferred axis of rotation was found to be next to the preferred axis of VS6, although the receptive fields of both cells differed remarkably. To investigate if DNOVS cells are more specifically tuned to their preferred axis of rotation, we calculated the tuning width for VS-, V2- and DNOVS-cells (Fig. 4.9b). As the tuning width, we defined the part of the sine eliciting over 50% of the maximum response of a cell. The tuning widths of VS cells increased slightly from VS1 to VS10. DNOVS1 was found to be strongest coupled to VS6 and VS7 (Haag et al., 2007) and its tuning width was similar to the tuning width of both cells. The tuning width of DNOVS2 was also similar to the tuning width of VS cells, strongest coupled to DNOVS2 (Wertz et al., 2008). In addition, the tuning width of V2 and DNOVS2 were nearly the same. Thus, DNOVS cells are not tuned more specifically to an axis of rotation than are VS cells or V2.

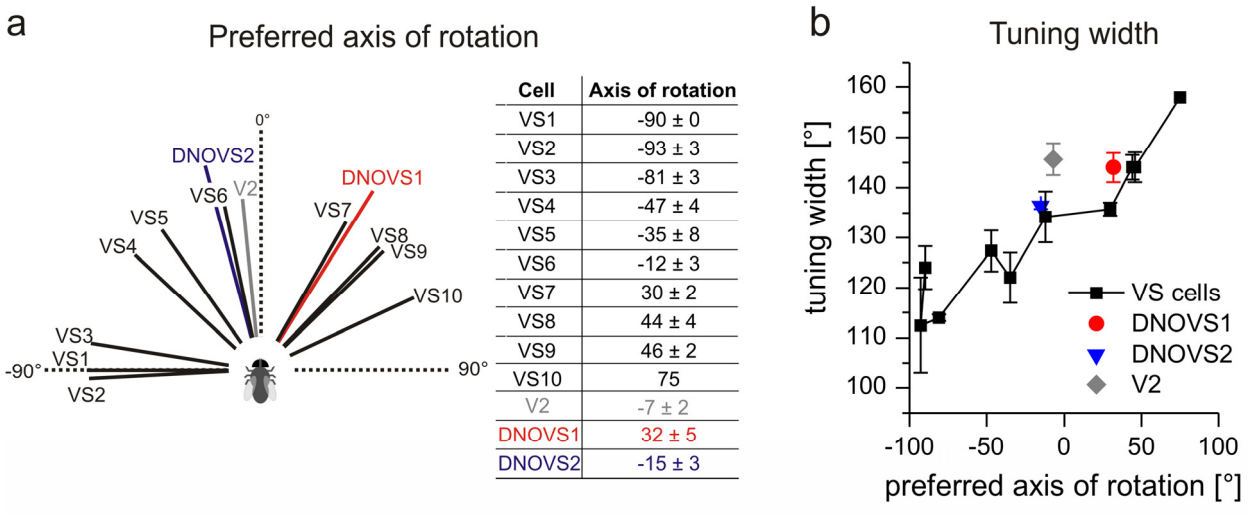

Cell	Axis of rotation
VS1	-90 ± 0
VS2	-93 ± 3
VS3	-81 ± 3
VS4	-47 ± 4
VS5	-35 ± 8
VS6	-12 ± 3
VS7	30 ± 2
VS8	44 ± 4
VS9	46 ± 2
VS10	75
V2	-7 ± 2
DNOVS1	32 ± 5
DNOVS2	-15 ± 3

Figure 4.9 Preferred axes of rotation and tuning width of all cells examined in this study.
a) Preferred axis of rotation of DNOVS1 and 2, VS-cells 1-10 and V2. b) Tuning width of DNOVS, VS and V2 defined as the part of the sine function eliciting 50% of the maximum response of a cell.

4.4 Discussion

In this study, we characterized the receptive fields and global motion sensitivities of two descending neurons in the fly called DNOVS1 and DNOVS2, as well as of their presynaptic elements in the lobula plate. The receptive fields of both DNOVS-cells have similarities to optic flows generated by rotations of the animal around different body axes (Fig. 4.1). Presenting global stimulus movies, we also measured the tuning curve of each cell to all the six principle types of ego-motions (Fig. 4.5) as well as to rotations around different axes within the horizontal plane (Fig. 4.7). Both cells turned out to be tuned to rotations around different body axes. By filtering the optic flow generated by each particular type of ego-motion with the receptive field of the cell, we received similar tuning curves for rotations as the measured ones. Thus, the sensitivity of the cells to different global motion patterns can be well predicted from their receptive fields based

on measurements of their local motion preferences. Both measurements reveal a tuning of DNOVS cells to optic flows arising from self-rotation of the fly. DNOVS1 responds best to a counterclockwise rotation around an axis in the horizontal plane at 32° azimuth, and DNOVS2 to an axis of rotation at -15° azimuth (Fig. 4.9).

After describing the methodological considerations and comparing our measurements of VS cell receptive fields with previously published ones, we will discuss the local and global motion tuning of DNOVS cells and what we can conclude from the tuning to understand the transmission of motion information from VS cells onto descending neurons.

4.4.1 Methodological considerations and VS cell receptive fields.

The main difference between our stimulus device and previously described LED-based stimulators for investigating fly visual motion processing (Joesch et al., 2008; Lindemann et al., 2003; Reiser and Dickinson, 2008) is the better spatial resolution, combined with a high temporal resolution and a fairly large coverage of the fly's visual field. With less than 1° spatial resolution and refresh rates of over 600 fps, the new panel-based display system described here has been designed as a stimulus source matching the requirements for experiments on *Calliphora* vision. However, covering only 95° in elevation, the extension in elevation is one limitation of the arena. The LED-based stimulator FliMax (Lindemann et al., 2003) extends over a broader range, especially in ventral parts of the visual field. The locally rotating dot used by Krapp et al. (1997) allows measurement of interpolated receptive field extending from –75 to +75 deg in elevation. However, our arena combines the possibility of presenting both local as well as global stimuli with a spatial and temporal resolution sufficient for *Calliphora*.

The receptive fields of VS cells determined here were in general similar to those published earlier (Krapp et al., 1998). In contrast to Krapp et al. (1998), however, we found the sensitivity for vertical motion of VS4 to be shifted towards frontal parts of the visual field. In addition, with our stimulus, VS4 did not respond to dorso-lateral back-to-front motion. In fact, the receptive field structure of VS4 measured by Krapp et al. (1998) has a large resemblance to the receptive field structure of VS5 as determined in both studies. The DI between the receptive field of VS4 measured by Krapp et al. (1998) and the receptive field of VS5 was 0.163, lower than the DI for VS4 with 0.241. Furthermore, VS4 was more frontally sensitive for vertical motion along the azimuth (Haag et al., 2007) than expected from the receptive field of the cell described by Krapp et al. (1998). Thus, as a reasonable explanation, the VS4 cell in Krapp et al (1998) seems to be a misidentified VS5-cell. In addition, VS7 to VS10 are stronger sensitive to upward motion in frontal parts of the receptive field than described by Krapp et al. (1998). The highest difference was found for VS10. A reason for this difference might be that Krapp et al. (1998) restricted the visual input to the ipsilateral eye by occluding the contralateral eye. Thus, the stronger response to upward motion might be due to motion information from the contralateral eye via heterolateral neurons like Vi (Haag and Borst, 2007).

4.4.2 Local and global motion tuning of DNOVS-cells

To investigate the transmission of motion information from VS cells to descending neurons, we calculated the expected responses for both DNOVS cells from their connectivity pattern with VS cells (Haag et al., 2007; Wertz et al., 2008), and compared these expectations with the measured ones. The receptive field of DNOVS1 can be explained by a linear weighted summation of VS cell output signals (Fig. 4.3). In order to explain the receptive field of DNOVS2, the linear weighted sum of VS cell

output signals together with the nonlinear effect of V2 have both be taken into account (Fig. 4.4). These findings are in agreement with the previously described binocular, nonlinear integration of DNOVS2 (Wertz et al., 2008) in contrast to the monocular, linear integration of motion signals in DNOVS1 (Haag et al., 2007).

We also measured the responses of DNOVS-cells and their presynaptic lobula plate cells to global motion stimuli, comprising all principles patterns according to the 6 degrees of freedom (Figs 4.5 and 4.6) as well as 36 patterns arising from rotations around different axes within the horizontal plane of the fly (Figs 4.7 and 4.8). When comparing these responses with the optic flow of the stimulus pattern filtered through the receptive field, we found a surprisingly good match, for all the cells, between the measured responses and the prediction from local motion preferences (Figs 4.7 and 4.8). This says that all cells basically perform a linear integration of their presynaptic signals. Apart from some sublinear saturation characteristics (Haag et al., 1992), spatial integration of VS cells has been found to be fairly linear (Haag and Borst, 2007). However, this has never been observed with stimuli covering basically the whole receptive field of most of the cells. Thus, VS-cells can indeed be regarded as matched filters for the fly's rotation around different axes within the horizontal plane, as proposed by Franz and Krapp (2000).

Given the linearity of spatial integration found in both DNOVS cells, one expects no increase in response selectivity at this level as compared to the presynaptic neurons. As is shown in Fig. 4.9, this is what indeed is found: The tuning width in both DNOVS-cells is in the range of the VS- and the V2-cell. Therefore, response selectivity does not seem to increase when going from lobula plate tangential cells to the level of descending neurons. What then is changing in the representation of optic flow? Here, we can only speculate at present. Maybe, differences in the robustness of coding become evident when using naturalistic stimuli with irregular contrast distributions, instead of

homogeneous and regular high-contrast patterns. An increased response selectivity might also be observable when reducing the mean luminance and/or contrast of the stimuli.

4.4.3 Visuomotor transformation in DNOVS cells

DNOVS1 and DNOVS2 project to the thoracic ganglion and there inter alia onto neck motor neurons of the frontal nerve (FNMN), (Gronenberg et al., 1995; Strausfeld and Bassemir, 1985). 21 paired of neck motor neurons were identified, which are organized on each side into four neck muscle nerves innervating 21 neck muscles (Strausfeld and Seyan 1985; Strausfeld et al. 1987). FNMNs innervate a variety of different neck muscles that, based on their anatomy (Strausfeld et al., 1986) could potentially be involved in nose-up pitch, nose-down pitch, yaw and roll. In addition, FNMNs are motion sensitive (Milde et al., 1987), and have receptive fields reminiscent of specific optic flow fields generated during pitch, a combination of pitch and roll and almost pure roll rotation (Huston and Krapp, 2008). DNOVS1 is tuned to a combination of pitch and roll and DNOVS2 is tuned nearly to roll rotation. Thus, the synaptic connection between lobula plate tangential cells and descending neurons might be regarded as a coordinate transformation where, from the full set of preferred axes of rotations represented within the lobula plate, those ones become transmitted to the motor centers that are appropriate for the muscles they finally innervate.

Neck motor neurons are sensitive to visual motion presented on either eye and are therefore more selective to rotation than lobula plate tangential cells. (Huston and Krapp, 2008). Although DNOVS2 is binocular (Wertz et al., 2008), neither DNOVS2 nor DNOVS1 were sensitive to local motion presented to the contralateral eye (Fig. 4.1). Thus, to achieve binocular receptive fields found for FNMNs (Huston and Krapp, 2008), different descending neurons should converge onto FNMNs. Strausfeld et al.

(1995) proposed a heterolateral connection in the thoracic ganglion. With lesion experiments, Strausfeld et al. (1995) showed that motion information from the contralateral DNOVS1 projects via a heterolateral neuron in the prothoracic ganglion onto the ipsilateral FNMN-8. Whether this is also the case for the contralateral DNOVS2 is not yet clear. However, the binocular integration of the ipsi- and contralateral DNOVS1 in the prothoracic ganglion would lead to binocular receptive field like it was found for "FN NMN A" by Huston and Krapp (2008). Thus, the binocular integration at the level of descending neurons, like it was found for DNOVS2 (Wertz et al., 2008) or at the level of the prothoracic ganglion (Strausfeld et al., 1995) are at least to pathways to achieve a higher binocularity in FNMNs.

4.5 Acknowledgements

We are grateful to Renate Gleich for excellent technical assistance, Maximilian Joesch and Franz Weber for help on stimulus generation. This work was supported by the Max-Planck-Society, a grant of the DFG (GRK 1091) and by a grant of the BMBF to the Bernstein Center for Computational Neuroscience (BCCN) Munich.

5 General discussion

A series of electrophysiological and neuroanatomical experiments was conducted during the research for this thesis to analyze the processing of optic flow information in premotor neurons of the fly. Specifically, the focus of this thesis lay on the descending neurons DNOVS1 and DNOVS2. Research on these two neurons is justified for at least two reasons: First, while lobula plate tangential cells (LPTCs) have been studied extensively with respect to their visual response properties and their connectivity amongst them, little is known about premotor descending neurons postsynaptic to LPTCs supplying motor neurons in the thoracic ganglion. Second, by characterizing the motion sensitivity and connectivity of DNOVS1 and DNOVS2 with VS cells, the circuit for motion processing can be extended. Adding premotor or motor neurons to the established lobula plate circuit (for review see Borst and Haag, 2007) is necessary to understand how neuronal activity generates behavior. In this chapter the processing of optic flow, the multisensory integration as well as the behavioral relevance of both DNOVS cells will be discussed.

5.1 Optic flow processing in DNOVS cells

Both DNOVS cells are electrically coupled to a subset of VS cells. Whereas DNOVS2 is coupled most strongly to VS5 and VS6 (Fig. 3.6), current injections in DNOVS1 and VS cells revealed the strongest coupling of DNOVS1 with VS6 and VS7 (Fig. 2.4). In addition, DNOVS2 receives input from the contralateral eye, probably via V2. The connectivity patterns are summarized in Figure 5.1a. Does the integration of different LPTC output lead to different sensitivity profiles? The determination of the tuning of DNOVS1 and DNOVS2 by measuring the local and global motion sensitivities (chapter 4) revealed that both cells are tuned to rotations around particular body axes (Fig. 5.1b). DNOVS1 responded maximally to a counterclockwise rotation around an axis at azimuth position at 32° and DNOVS2 to a rotation around an axis at azimuth position at -25°. In addition, their preferred axes of rotation result from a match of the optic flow caused by the respective type of ego-motion with their specific receptive field structures (Fig. 4.7). This is similar to VS cells. VS cells have receptive fields tailor suited to sense rotatory optic flow, each VS cell for a distinct axis of rotation (Krapp et al., 1998 and Fig. 4.2). The measurement of their global motion sensitivity (Fig. 4.8) revealed that these cells are indeed tuned to rotations around particular body axes. To investigate the processing of optic flow from VS cells to descending neurons, we calculated the expected responses for both DNOVS cells from their connectivity pattern with VS cells. The receptive field structures of both DNOVS cells can be predicted in detail from the receptive field structure of VS-cells and the V2-cell together with the coupling strength of DNOVS with them. This linearity of spatial integration found in both DNOVS cells leads to a tuning width which is in the range of the VS- and the V2-cell. The response selectivity does not seem to increase when going from lobula plate tangential cells to the level of descending neurons (Fig. 4.9). But why do the DNOVS cells collect motion

information from various VS cells? One explanation could be that this particular wiring performs a linear interpolation between the output signals of VS cells. This would lead to a more robust representation of the axis of rotation in DNOVS than in VS cells. In a simulation study, Cuntz et al. (2007) showed that a robust coding is achieved by the electrical axo-axonal coupling between VS cells. The hypothesis that rotations are encoded more robustly at the next processing level than in VS cells is actually one project in the lab of Alexander Borst.

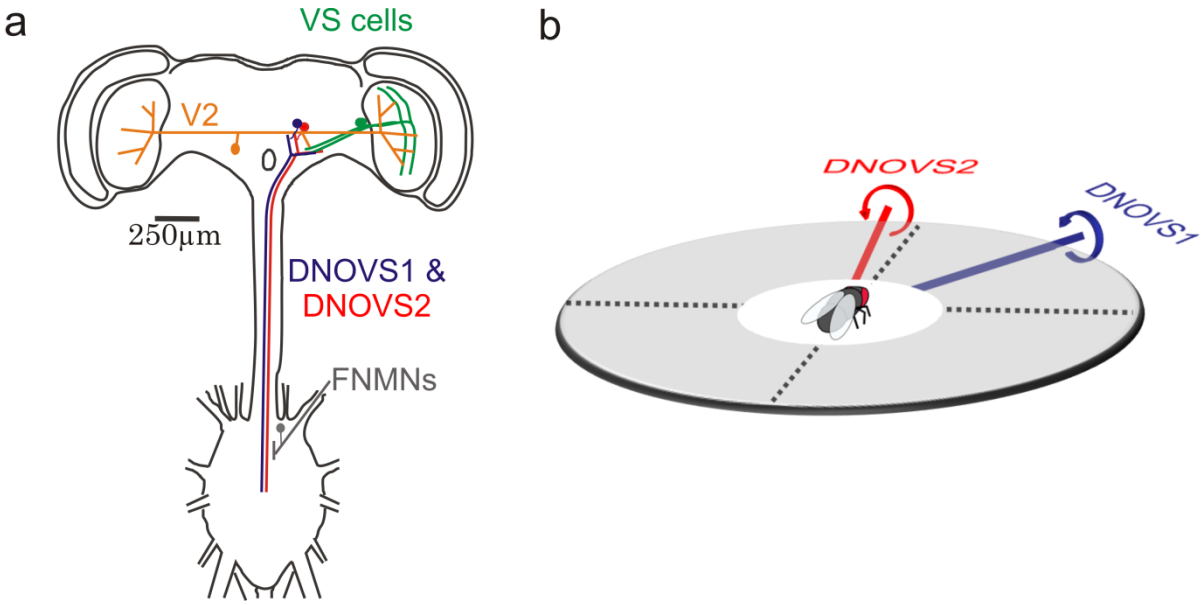

Figure 5.1 Neural network summary and preferred axis of rotation.

a) Schematic of the nervous system of the fly. DNOVS cells (blue and red) are electrically coupled with a different subset of VS cells (green). Probably V2 (orange) conveys motion information from the contralateral eye onto DNOVS2. Both DNOVS cells are dye coupled to neck motor neurons of the frontal nerve (FNMNs, black). b) Preferred axis of rotation of DNOVS1 (blue) and DNOVS2 (red) in the horizontal plane (grey).

5.2 Multisensory integration

The results presented in chapter 2 and chapter 3 demonstrate that both DNOVS cells receive synaptic input from at least two different sources, from a subset of large-field motion sensitive VS-cells as well as from the ocelli via ocellar interneurons. The three ocelli are light sensitive organs and form a triangle on the dorsal surface of the head. Stimulating the ocelli with a LED elicited a short on and off response in DNOVS1 (Fig. 2.7) as well as in DNOVS2 (Fig. 3.8). In dragonflies (Stange, 1981) as well as in locusts (Taylor, 1981a, 1981b), the ocelli are very effective rotation detectors, crucial to proper gaze and flight stabilization. In contrast to locusts where ocelli play a role in optomotor behavior of the animal (Taylor, 1981) it has been shown in the blowfly that the ocellar dorsal light response has only little influence on the optomotor response (Hengstenberg, 1993; Schuppe and Hengstenberg, 1993). However in a recent study Parson and colleagues (2006) found that the ocellar component of V1's response appears to be tuned to rotation, similar to that shown for the compound eye component (Karmeier et al., 2003). DNOVS cells are tuned to rotation via the compound eyes. Whether the ocellar component of DNOVS responses is tuned to rotation is not yet clear. To measure the responses of DNOVS cells to subsequent stimulation of the ocelli, mimicking a role movement, is necessary to investigate the possible interplay between ocellar and motion input.

In addition to visual motion and stimulation of the ocelli, DNOVS cells respond to antennal air currents (Gronenberg et al., 1995). Thus at the level of descending neurons like DNOVS cells, at least three sensory modalities are integrated. DNOVS cell are dye coupled to FNMNs which in turn receive input from two additional sensory modalities, the halteres and the prosternal organ (Gronenberg et al., 1995). Dye coupling

between FNMN 8 to the contralateral haltere interneuron (Gronenberg, 1995) suggests that this motor neuron is also driven by the halteres to provide head rotation in response to body roll (see Nalbach and Hengstenberg, 1994). The prosternal organ is a head posture proprioceptor at the base of the neck (Peters, 1962; Preuss and Hengstenberg, 1992). Electrical stimulation of the prosternal organ afferences elicits head movement around the roll (and pitch) axes via activity in FNMNs (Gilbert et al., 1995). Thus, from LPTCs to FNMNs different sensory modalities are integrated. Whether and how the integration occurs in DNOVS cells is still an open question.

5.3 Behavioral Relevance

The connections to neck motor neurons suggest that DNOVS1 and DNOVS2 are involved in the gaze stabilization during flight, which results in an improved condition of vision (Schilstra and van Hateren, 1999; van Hateren and Schilstra, 1999). The fly turns its head around all three body axes while flying or walking. Such movements occur either spontaneously or in response to an unexpected change of the flight attitude, for example by turbulence (Hengstenberg et al. 1986). Yaw turns are ultimately directed towards objects of interest, whereas roll- and pitch movements are made to stay aligned with the horizontal plane, and are closely associated with the fly's equilibrium control. The compound eyes are part of the head capsule and are thus moved in rigid conjunction with the head. The neck joint is formed by the articulated sclerites and soft folds of the neck cuticle. Head movements are effected by 21 pairs of neck muscles, with a single motor neuron innervating each muscle (Strausfeld and Seyan 1985; Strausfeld et al. 1987). In the blowfly Calliphora, the range of head turns is ± 20° both horizontally (yaw) and vertically (pitch), and ± 90° for rotations around the longitudinal body axis (roll). Here, head movements are interpreted exclusively as eye movements.

DNOVS cells are coupled to FNMNs, which in turn are suggested to be cardinal elements in head rotation (Gronenberg et al., 1995). This is supported by the results of frontal nerve microablation (Gilbert et al., 1995). In addition, FNMNs have receptive fields reminiscent of specific optic flow fields generated during pitch, a combination of pitch and roll and almost pure roll rotation (Huston and Krapp, 2008). Thus, the synaptic connection between lobula plate tangential cells and descending neurons might be regarded as a coordinate transformation. From the full set of preferred axes of rotations represented within the lobula plate, those ones become transmitted to the motor centers that are appropriate for the muscles they finally innervate. One robust approach to clarify this computation is to add the neck motor neurons into the established network. The physiology together with the precise connectivity will provide insights on how the underlying computation occurs at a single cell level mechanistically and functionally.

To conclude, by connecting the sensory brain with the motor brain (thoracic ganglion), this thesis offers electrophysiological data on the sensory-motor transformation in flies and thus contributes to the field of systemic neuroscience by investigating visually guided behavior in flies at the neuronal level.

References

Bausenwein B, Dittrich APM, Fischbach KF (1992) The optic lobe of Drosophila melanogaster. II. Sorting of retinotopic pathways in the medulla. Cell Tissue Res 267: 17-28.

Bausenwein B, Fischbach KF (1992) Activity labeling patterns in the medulla of Drosophila melanogaster caused by motion stimuli. Cell Tissue Res 270: 25-35.

Beersma DGM, Stavenga DG, Kuiper JW (1977) Retinal lattice, visual field and binocularities in flies. J Comp Physiol A 119: 207-220.

Borst (1991) Fly visual interneurons responsive to image expansion. Zool Jb Physiol 95: 305-313.

Borst A, Bahde S (1988a) Spatio-temporal integration of motion - A simple strategy for safe landing in flies. Naturwiss 75: 265-267.

Borst A, Bahde S (1988b) Visual information processing in the fly's landing system. J Comp Physiol A 163: 167-173.

Borst A, Dickinson M (2003) Visual course control in flies. In: The Handbook of Brain Theory and Neural Networks, pp 1205-1210. MIT Press..

Borst A, Egelhaaf M (1992) In vivo imaging of calcium accumulation in fly interneurons as elicited by visual motion stimulation. Proc Natl Acad Sci USA 89: 4139-4143.

Borst A, Egelhaaf M (1993) Detecting visual motion: Theory and models. In: Visual motion and its role in the stabilization of gaze (Miles FA, Wallman J, eds), pp 3-27. Amsterdam, London, New York, Tokyo: Elsevier.

Borst A, Haag J (1996) The intrinsic electrophysiological characteristics of fly lobula plate tangential cells: I. Passive membrane properties. J Computat Neurosci 3: 313-336.

Borst A, Haag J (2002) Neural networks in the cockpit of the fly. J Comp Physiol 188: 419-437.

Buchner E, Buchner S, Bülthoff I (1984) Deoxyglucose mapping of nervous activity induced in Drosophila brain by visual movement. J Comp Physiol A 155: 471-483.

Buchner E, Götz KG, Straub C (1978) Elementary detectors for vertical movement in the visual system of Drosophila. Biol Cybern 31: 235-242.

Card G. and Dickinson MH (2008). Visually mediated motor planning in the escape response of Drosophila. Curr Biol 18: 1300-1307.

Chan WP, Prete F, Dickinson MH (1998) Visual input to the efferent control system of a fly's "gyroscope". Science 280: 289-292.

Clifford CW, Ibbotsen MR (2003) Fundamental mechanisms of visual motion detection: models, cells and functions. Prog Neurobiol 68: 409-437.

Coggshall JC, Boschek CB, Buchner SM (1973) Preliminary investigations on a pair of giant fibers in the central nervous system of dipteran flies. Z Naturforsch 28c: 783-784.

Collett TS, Blest AD (1966) Binocular, directionally-selective neurons, possibly involved in the optomotor response of insects. Nature 212: 1330 – 1333.

Collett M, Collett TS, Srinivasan MV (2006) Insect navigation: measuring travel distance across ground and through air. Curr Biol 16: R887-R890.

Collett TS, Land MF (1975) Visual control of flight behavior in the hoverfly. Journal of Comparative Physiology A-Neuroethology Sensory Neural and Behavioral Physiology 99: 1-66.

Cuntz H, Haag J, Borst A (2003) Neural image processing by dendritic networks. Proc Natl Acad Sci USA 100: 11082-11085.

Cuntz H, Haag J, Fortsner F, Segev I, Borst A (2007) Robust coding of flow-field parameters by axo-axonal gap junctions between fly visual interneurons. Proc Natl Acad Sci USA 104: 10229-10233.

Davies MNO, Green PR (1990) Optic flow-field variables trigger landing in hawk but not in pigeons. Naturwiss 77: 142-144.

Denk W, Strickler JH, Webb WW (1990) Two-photon laser scanning fluorescence microscopy. Science 248: 73-76.

Denk W, Horstmann H (2004) Serial block-face scanning electron microscopy to reconstruct three-dimensional tissue nanostructure. PLoS Biol 2:1900-1909.

Dubs A (1982) The spatial integration of signals in the retina and lamina of the fly compound eye under different conditions of luminance. J Comp Physiol A- 146: 321-343.

Dürr V, Egelhaaf M (1999) In vivo calcium accumulation in presynaptic and postsynaptic dendrites of visual interneurons. J Neurophysiol 82: 3327-3338.

Eckert H (1973) Optomotorische Untersuchungen am visuellen System der Stubenfliege *Musca domestica* L. Kybernetik 14: 1-23.

Eckert H (1980) Functional properties of the H1-neurone in the third optic ganglion of the blowfly, *Phaenicia*. J Comp Physiol 135: 29-39.

Eckert H (1982) The vertical-horizontal neurone (VH) in the lobula plate of the blowfly, *Phaenicia*. J Comp Physiol 149: 195-205.

Eckert H, Dvorak DR (1983) The centrifugal horizontal cells in the lobula plate of the blowfly *Phaenicia sericata*. J Insect Physiol 29: 547-560.

Egelhaaf M, Borst A (1993) A look into the cockpit of the fly: visual orientation,algorithms and identified neurons. J Neurosci 13: 4563-4574.

Egelhaaf M, Borst A, Reichardt W (1989) Computational structure of a biological motion detection-detection system as revealed by local detector analysis in the fly`s nervous system. J Opt Soc Am A 6: 1070-1087.

Egelhaaf M, Borst A, Warzecha AK, Flecks S, Wildemann A (1993) Neural circuit tuning fly visual neurons to motion of small objects II. Input organization of inhibitory circuit elements revealed by electrophysiological and optical recording techniques. J Neurophysiol 69: 340-351.

Elyada et al. (submitted) Different receptive fields in axon terminals and dendrites underlie robust population coding in blowfly visual interneurons.

Exner S (1868) Über die zu einer Gesichtswahrnehmung nöthige Zeit. Sitzungsberichte der kaiserlichen Akademie, Math Naturw Classe 58: 601-631.

Exner S (1875) Experimentelle Untersuchung der einfachsten psychischen Prozesse. Pflüger's Archiv f Physiologie 11: 27-432.

Farrow, K (2005) Lateral interactions and receptive field structure of lobula plate tangential cells in the blowfly. Doctoral Thesis, Muenchen.

Farrow K, Haag J, Borst A (2003) Input organization of multifunctional motion sensitive neurons in the blowfly. J Neurosci 23: 9805-9811.

Farrow K, Borst A, Haag J (2005) Sharing receptive fields with your neighbors: Tuning the vertical system cells to wide field motion. J Neurosci 25: 3985-3993.

Farrow K, Haag J, Borst A (2006) Nonlinear, binocular interactions underlying flow field selectivity of a motion-sensitive neuron. Nat Neurosci 9**:** 1312-1320.

Fermi G, Reichardt W (1963) Optomotorische Reaktionen der Fliege *Musca domestica.* Abhängigkeit der Reaktion von der Wellenlänge, der Geschwindigkeit, dem Kontrast und der mittleren Leuchtdichte bewegter periodischer Muster. Kybernetik 2: 15-28.

Franceschini, N. and Kirschfeld, K. (1971). Les phénomènes de pseuopupille dans l'oeil composé de *Drosophila*. 159-182.

Franz MO, Krapp HG (2000) Wide-field, motion-sensitive neurons and matched filters for optic flow fields. Biol Cybern 83: 185-197.

Frye MA, Dickinson MH (2001) Fly flight: a model for the neural control of complex behavior. Neuron 32: 385-388.

Gauck V, Egelhaaf M, Borst A (1997) Synapse distribution on VCH, an inhibitory, motion-sensitive interneuron in the fly visual system. J Comp Neurol 381: 489-499.

Geiger G, Nässel DR (1981) Visual orientation behaviour of flies after selective laser beam ablation of interneurones. Nature 293: 398-399.

Geiger G, Nässel DR (1982). Visual processing of moving single objects and wide-field patterns in flies: behavioural analysis after laser-surgical removal of interneurons. Biol Cybern 44: 141-149.

Gibson JJ (1950) Perception of the Visual World. Mifflin, Houghton.

Gilbert C, Gronenberg W, Strausfeld NJ (1995) Oculomotor control in calliphorid flies: head movements during activation and inhibition of neck motor neurons corroborate neuroanatomical predictions. J Comp Neurol 361: 285-297.

Götz KG (1964) Optomoter studies of the visual system of several eye mutants of the fruit fly *Drosophila*. Kybernetik 2: 77-92.

Gronenberg W, Milde JJ, Strausfeld NJ (1995) Oculomotor control in calliphorid flies: organization of descending neurons to neck motor neurons responding to visual stimuli. J Comp Neurol 361: 267-284.

Gronenberg W, Strausfeld NJ (1990) Descending neurons supplying the neck and flight motor of diptera: Physiological and anatomical characteristics. J Comp Neurol 302: 973-991.

Gronenberg W, Strausfeld NJ (1991) Descending pathways connecting the male-specific visual system of flies to the neck and flight motor. J Comp Physiol A 169: 413-426.

Haag J (1994) Aktive und passive Membraneigenschaften bewegungsempfindlicher Interneurone der Schmeissfliege *Calliphora erythrocephala*. Doctoral Thesis, Tuebingen.

Haag J, Borst A (2001) Recurrent network interactions underlying flow-field selectivity of visual interneurons. J Neurosci 21: 5685-5692.

Haag J, Borst A (2002) Dendro-dendritic interactions between motion-sensitive large-field neurons in the fly. J Neurosci 22: 3227-3233.

Haag J, Borst A (2003) Orientation tuning of motion-sensitive neurons shaped by vertical-horizontal network interactions. J Comp Physiol A 189: 363-370.

Haag J, Borst A (2004) Neural mechanism underlying complex receptive field properties of motion-sensitive interneurons. Nat Neurosci 7: 628-634.

Haag J, Borst A (2005) Dye-coupling visualizes networks of large-field motion-sensitive neurons in the fly. J Comp Physiol A 191: 445-454.

Haag J, Borst A (2007) Reciprocal inhibitory connections within a neural network for rotational optic-flow processing. Frontiers Neurosci 1.

Haag J, Borst A (2008): Electrical coupling of lobula plate tangential cells to a heterolateral motion-sensitive neuron in the fly. J Neurosci 28: 14435-14442.

Haag J, Denk W, Borst A (2004) Fly motion vision is based on Reichardt detectors regardless of the signal-to-noise ratio. Proc Natl Acad Sci 101: 16333-16338.

Haag J, Egelhaaf M, Borst A (1992) Dendritic integration of motion information in visual interneurons of the blowfly. Neurosci Lett 140: 173-176.

Haag J, Vermeulen A, Borst A (1999) The intrinsic electrophysiological characteristics of fly lobula plate tangential cells: III. Visual response properties. J Computat Neurosci 7: 213-234.

Haag J, Wertz A, Borst A (2007) Integration of lobula plate output signals by DNOVS1, an identified premotor descending neuron. J Neurosci 27: 1992-2000.

Hardie RC (1984) Functional organization of the fly retina. In: Progress in Sensory Physiology 5 (Autrum H, Ottoson D, Perl ER, Schmidt RF, Shimazu H, Willis WD, eds), pp 1-79. Berlin, Heidelberg, New York, Tokyo: Springer-Verlag.

Hassenstein B, Reichardt W (1956). Systemtheoretische Analyse der Zeit-,Reihenfolgen- und Vorzeichenauswertung bei der Bewegungsperzeption des Rüsselkäfers Chlorophanus. Z. Naturforsch. 11b, 513-524.

Hatsopoulos N, Gabbiani F, Laurent G (1995) Elementary computation of object approach by a wide-field visual neuron. Science 270: 1000–1003.

Hausen, K. (unpublished) The neural architecture of the lobula plate of the blowfly, *Calliphora erythrocephala*.

Hausen K (1976) Functional characterization and anatomical identification of motion sensitive neurons in the lobula plate of the blowfly *Calliphora erythrocephala*. Z Naturforsch 31c: 629-633.

Hausen K (1977) Struktur, Funktion und Konnektivität bewegungsempfindlicher Interneurone im dritten optischen Neuropil der Schmeissfliege *Calliphora erythrocephala*. Doctoral Thesis, Tuebingen.

Hausen K (1981) Monocular and binocular computation of motion in the lobula plate of the fly. Verh Dtsch Zool Ges 74: 49-70.

Hausen K (1982a) Motion sensitive interneurons in the optomotor system of the fly. I. The Horizontal Cells: Structure and signals. Biol Cybern 45: 143-156.

Hausen K (1982b) Motion sensitive interneurons in the optomotor system of the fly. II. The Horizontal Cells: Receptive field organization and response characteristics. Biol Cybern 46: 67-79.

Hausen K (1984) The lobula-complex of the fly: Structure, function and significance in visual behaviour. In: Photoreception and vision in invertebrates, (Ali MA, ed). pp 523-559. New York, London: Plenum Press.

Hausen K, Egelhaaf M (1989) Neural mechanisms of visual course control in insects. In: Facets of vision (Stavenga DG, Hardie RC, eds), pp 391-424. Berlin, Heidelberg, New York, London, Paris, Tokyo: Springer.

Hausen K, Wehrhahn C (1983) Microsurgical lesion of horizontal cells changes optomotor yaw response in the blowfly *Calliphora erythocephala*. Proc R Soc Lond B 219: 211-216.

Hausen K, Wehrhahn C (1990) Neural circuits mediating visual flight control in flies. II. Separation of two control systems by microsurgical brain lesions. J Neurosci 10: 351-360.

Hausen K, Wolburg-Buchholz K, Ribi WA (1980) The synaptic organization of visual interneurons in the lobula complex of flies. Cell Tissue Res 208: 371-387.

Heisenberg M (1972) Comparative behavioral studies on two visual mutants of *Drosophila*. J Comp Physiol 80: 119-136.

Heisenberg M, Wonneberger R, Wolf R (1978) Optomotor-blind (H31) -a *Drosophila* mutant of the lobula plate giant neurons. J Comp Physiol 124: 287-296.

Hengstenberg R (1977). Spike response of "non-spiking" visual interneurone. Nature 270: 338-340.

Hengstenberg R (1982) Common visual response properties of giant vertical cells in the lobula plate of the blowfly *Calliphora*. J Comp Physiol A 149: 179-193.

Hengstenberg R (1984) Roll-stabilization during flight of the blowfly's head and body mechanical and visual cues. In: Localization and orientation in biology and engineering (Varju D, Schnitzler H, eds), pp 121-134. Berlin, Heidelberg: Springer-Verlag.

Hengstenberg R (1988) Mechanosensory control of compensatory head roll during flight in the blowfly *Calliphora erythrocephala meig*. J Comp Physiol A 163: 151-165.

Hengstenberg R (1991) Gaze control in the blowfly *Calliphora*: a multisensory, two-stage integration process. Semin Neurosci 3: 19-29.

Hengstenberg R (1993) Multisensory control in insect oculomotor systems. Rev Oculomot Res 5:285-298.

Hengstenberg R, Hausen K, Hengstenberg B (1982) The number and structure of giant vertical cells (VS) in the lobula plate of the blowfly *Calliphora erytrocephala*. J Comp Physiol A 149: 163-177.

Hengstenberg R, Sandeman DC, Hengstenberg B (1986) Compensatory head roll in the blowfly Calliphora during flight. Proc R Soc Lond B 227: 455-482.

Horstmann W, Egelhaaf M, Warzecha AK (2000) Synaptic interactions increase optic flow specificity. Eur J Neurosci 12: 2157-2165.

Huston SJ, Krapp HG (2008) Visuomotor transformation in the fly gaze stabilization system. PLoS Biology 6: e173.

Ibbotson MR (1991) A motion-sensitive visual descending neurone in *Apis mellifera* monitoring translatory flow-fields in the horizontal plane. J Exp Biol 157: 573–577.

Ibbotson MR, Goodman LJ (1990) Response chracteristics of four wide-field motion-sensitive descending interneurones in *Apis mellifera*. J Exp Biol 148: 255-279.

Järvilehto M, Zettler F (1973) Electrophysiological-histological studies on some functional properties of visual cells and second order neurons of an insect retina. Z Zellforsch 136: 291-306.

Joesch M, Plett J, Borst A, Reiff DF (2008) Response properties of motion-sensitive visual interneurons in the lobula plate of *Drosophila melanogaster*. Curr Biol 18: 368-374.

Judge S, Rind FC (1997) The locust DCMD neuron, a movement-detecting neurone tightly tuned to collision trajectories. J Exp Biol 200: 2209–2216.

Kalb J, Egelhaaf M, Kurtz R (2006) Robust integration of motion information in the fly visual system revealed by single cell photoablation. J Neurosci 26: 7898-7906.

Karmeier K, Krapp HG, Egelhaaf M. (2003) Robustness of the tuning of fly visual interneurons to rotatory optic flow. J Neurophysiol 90: 1626-1634.

Karmeier K, Krapp HG, Egelhaaf M (2005) Population coding of self-motion: Applying bayesian analysis to a population of visual interneurons in the fly. J Neurophysiol 94: 2182-2194.

Kien J (1974) Sensory integration in the locust optomotor system.- II: Direction selective neurons in the circumoesophageal connectives and the optic lobe. Vision Res 14: 1255-1268.

Kimpo RR, Theunissen FE, Doupe AJ (2003) Propagation of correlated activity through multiple stages of a neural circuit. J Neurosci 23: 5750–5761.

Kirschfeld K. (1967). Die Projektion der optischen Umwelt auf das Raster der Rhabdomere im Komplexauge von *Musca*. Exp. Brain Res. 3: 248-270.

Krapp HG, Hengstenberg R (1996) Estimation of self - motion by optic flow processing in single visual interneurons. Nature 384**:** 463-466.

Krapp HG, Hengstenberg R (1997) A fast stimulus procedure to determine local receptive field properties of motion-sensitive visual interneurons. Vision Res 37: 225-234.

Krapp HG, Hengstenberg B, Hengstenberg R (1998) Dendritic structure and receptive-field organization of optic flow processing interneurons in the fly. J Neurophysiol 79: 1902-1917.

Kunze P (1961) Untersuchung des Bewegungssehens fixiert fliegender Bienen. Z vergl Physiol 44: 656-684.

Land MF (1997) Visual acuity in insects. Annu Rev Entomol 42: 147-177.

Land MF, Eckert H (1985) Maps of the acute zones of fly eyes. J Comp Physiol A 156: 525-538.

Laughlin S (1981) Neural principles in the peripheral visual system. In: Handbook of sensory physiology VII/6B (Autrum H, ed), pp 133-280. Berlin, Heidelberg, New York: Springer

Lindemann JP, Kern R, Michaelis C, Meyer P, van Hateren JH, Egelhaaf M (2003) FliMax, a novel stimulus device for panoramic and highspeed presentation of behaviourally generated optic flow. Vision Res 43: 779-791.

Milde JJ (1984) Ocellar interneurons in the honeybee Structure and signals of L-neurons. J Comp Physiol 154:683-693.

Milde JJ, Homberg U (1984) Ocellar interneurons in the honeybee: characteristics of spiking L-neurons. J Comp Physiol 155: 151-160.

Milde JJ, Strausfeld NJ (1986) Visuo-motor pathways in arthropods. Naturwissenschaften 73: 151-154.

Milde JJ, Seyan HS, Strausfeld NJ (1987) The neck motor system of the fly *Calliphora erythrocephala*. 2. Sensory organisation. J Comp Physiol A 160: 225-238.

Mizutani A, Chahl JS, Srinivasan MV (2003) Insect behaviour: Motion camouflage in dragonflies. Nature 423: 604.

Mronz M, Lehmann FO (2008). The free-flight response of *Drosophila* to motion of the visual environment. J Exp Biol 211: 2026-45.

Nalbach G., Hengstenberg R (1994) The halteres of the blowfly *Calliphora*. II. Three-dimensional organization of compensatory reactions to real and simulated rotations. J. Comp. Physiol. A 175: 695-708,

Olberg RM (1981a) Object and self movement detectors in the ventral nerve cord of the dragonfly. J Comp Physiol A 141: 327-334.

Olberg RM (1981b) Parallel encoding of direction of wind, head, abdomen and visual pattern movement by single interneurons in the dragonfly. J Comp Physiol A 142: 27-41.

Parsons MM, Krapp HG, Laughlin SB (2006) A motion-sensitive neurone responds to signals from the two visual systems of the blowfly, the compound eyes and ocelli J Exp Biol 209: 4464-4474.

Peters W (1962). Die propriorezeptiven Organe am Prosternum und an den Labellen von *Calliphora erythrocephala* Mg. Z. Morph. Ökol. Tiere 51: 211 -226

Petrowitz R, Dahmen H, Egelhaaf M, Krapp HG (2000) Arrangement of optical axes and spatial resolution in the compound eye of the female blowfly *Calliphora*. J Comp Physiol 168: 737-746.

Pierantoni R (1976) A look into the cock-pit of the fly. Cell Tissue Res 171: 101-122.

Poggio T, Reichardt W (1976) Visual control of orientation behaviour in the fly II. Towards the underlying neural interactions. Quart Rev Biophys 9: 377-438.

Reichardt, W (1969) Movement perception in insects. In: Processing of optical data by organisms and machines. New York: Academic 465-493.

Reichardt W, Poggio T (1976) Visual control of orientation behaviour in the fly I. A quantitative analysis. Quart Rev Biophys 9: 311-375.

Reiser MB, Dickinson MH (2008) A modular display system for insect behavioral neuroscience. J Neurosci Methods 167: 127-139.

Rind FC (1983) A directionally selective motion-detection neuron in the brain of a moth. J Exp Biol 102: 253-271.

Rind FC, Simmons PJ (1999). Seeing what is coming: Building collision-sensitive neurones. Trends Neurosci 22: 215–220.

Rister J, Pauls D, Schnell B, Ting CY, Lee CH, Sinakevitch I, Morante J, Strausfeld NJ, Ito K, Heisenberg M (2007) Dissection of the peripheral motion channel in the visual system of *Drosophila melanogaster*. Neuron 56: 155-170.

Rowell CHF, Reichert M (1986). Three descending interneurons reporting deviation from course in the locust. II Physiology J Comp Physiol A 158: 775-794.

Schilstra C, van Hateren JH (1998). Stabilizing gaze in flying blowflies. Nature 395: 654.

Schilstra C, van Hateren JH (1999). Blowfly flight and optic flow. I. Thorax kinematics and flight dynamics. J Exp Biol 202: 1481-1490.

Schuppe H, Hengstenberg R (1993) Optical properties of the ocelli of *Calliphora erythrocephala* and their role in the dorsal light response. J Comp Physiol A 173: 143-149.

Simmons PJ, Jian S, Rind FC (1994) Characterisation of large second-order ocellar neurons of the blowfly *Calliphora erythrocephala*. J Exp Biol 191: 231-245.

Single S, Borst A (1998) Dendritic integration and its role in computing image velocity. Science 281: 1848-1850.

Srinivasan MV, Zhang S (2004) Visual motor computations in insects. Ann Rev Neurosci 27: 679-696.

Stange G (1981). The ocellar component of flight equilibrium control in dragonflies. J. Comp. Physiol. 141: 335 -347.

Strausfeld NJ (1976) Atlas of an insect brain, Springer.

Strausfeld NJ (1989) Beneath the compound eye: Neuroanatomical analysis and physiological correlates in the study of insect vision. In: Facets of Vision (Stavenga DG, Hardie RC, eds), pp 317-359.

Strausfeld NJ, Bassemir UK (1985a) Lobula plate and ocellar interneurons converge onto a cluster of descending neurons leading to neck and leg motor neuropil in *Calliphora erythrocephala*. Cell Tissue Res 240: 617-640.

Strausfeld NJ, Bassemir UK (1985b) The organization of giant horizontal-motion-sensitive neurons and their synaptic relartionships in the lateral deutocerebrum of *Calliphora erythrocephala* and *Musca domestica*. Cell Tissue Res 242: 531-550.

Strausfeld NJ, Gronenberg W (1990) Descending neurons supplying the neck and flight motor of diptera: Organization and neuroanatomical relationships with visual pathways. J Comp Neurol 302: 954-972.

Strausfeld NJ, Lee JK (1991) Neuronal basis for parallel visual processing in the fly. Vis Neurosci 7: 13-33.

Strausfeld NJ, Kong A, Milde JJ, Gilbert C, Ramaiah L (1995) Oculomotor control in calliphorid flies: GABAergic organization in heterolateral inhibitory pathways. J Comp Neurol 361: 298-320.

Strausfeld NJ, Seyan HS (1985) Convergence of visual, haltere, and prosternal inputs at neck motor neurons of *Calliphora erythrocephala*. Cell Tissue Res 240: 601-615.

Strausfeld NJ, Seyan HS, Milde JJ (1987) The neck motor system of the fly *Calliphora erythrocephala*. J Comp Physiol A 160:205-224.

Takemura SY, Lu Z, Meinertzhagen IA (2008) Synaptic circuits of the *Drosophila* optic lobe: the input terminals to the medulla. J Comp Neurol 509: 493-513.

Tanouye,M.A. and Wyman,R.J. (1980). Motor outputs of giant nerve fiber in *Drosophila*. J. Neurophysiol. 44: 405-421.

Taylor CP (1981a). Contribution of compound eyes and ocelli to steering of locusts in flight. I. Behavioral analysis. J. Exp. Biol. 93: 1 -18

Taylor CP (1981b) Contribution of compound eyes and ocelli to steering of locusts in flight: II. Timing changes in flight motor units. J Exp Biol 93: 19-31.

Toh Y, Kuwabara M (1975) Synaptic organization of the fleshfly ocellus. J Neurocytol 4: 271-87.

Van Hateren JH, Schilstra C (1999). Blowfly flight and optic flow. II. Head movements during flight. J Exp Biol 202: 1491-1500

Warren WH, Kay BA, Zosh WD, Duchon AP, Sahuc S (2001) Optic flow is used to control human walking. Nat Neurosci 4: 213-216.

Warzecha AK, Egelhaaf M, Borst A (1993) Neural circuit tuning fly visual interneurons to motion of small objects. I. Dissection of the circuit by pharmacological and photoinactivation techniques. J Neurophysiol 69: 329-339.

Wertz A, Borst A, Haag J (2008) Nonlinear integration of binocular optic flow by DNOVS2, a descending neuron of the fly. J Neurosci 28: 3131-3140.

Weber F, Eichner H, Cuntz H, Borst A (2008) Eigenanalysis of a neural network for optic flow processing. New Journal of Physics 10: 1:21.

Acknowledgements

This thesis would not have been accomplished without the encouragement, advice and assistance of a number of people. First of all, let me thank Alexander Borst who gave me the opportunity to work in his lab. I appreciate his intensive support and excellent guidance throughout my entire time in his lab. Special thanks go to my second supervisor Juergen Haag for all the helpful discussion and for sharing all his practical experience with me. He always assisted me with my work through his advice as well as his actions. Both, Axel and Bulle, are providing a great environment and it is a pleasure to work with them.

I owe thanks to Mark Hübener for helpful advice and being part of my thesis committee. Thanks to Renate who often supported me with delicious cake and who cared for the flies, always keeping them alive. I am also grateful to the Histo group, in particular Ursula Weber and Marianne Braun for their help with the neurobiotin stainings, and Werner Heilmann and Helmut Wintersberger from the workshop for help- and skillful constructions at my setup.

Additionally, I gratefully acknowledge the doctoral fellowship (2005-2008) of the DFG which gave me the possibility to realize my dissertation within the Graduate College: "Orientation and Motion in Space".

I would like to thank all the present and former members of the Borst lab for an extremely warm and kind working atmosphere. Especially, I want to name Yishai, Franz and Friedrich for teaching and help with Matlab; Jones for constructing such a nice

LED-arena and the “big fly group” & Max, Dierck and Bettina for fruitful discussions about the amazing capabilities of flies. In addition I want to thank Alex, Nina, Marco, Martina, Max, Jones, Marcel, Steph and Yishai for important discussions about life, future plans or just the latest football results.

Furthermore, I want to express my gratitude to all the people I did not mention by name but who exerted influence on my work during the last three years in any way.

I am grateful to my parents, my sister and my brother for their encouragement and help throughout my student life, despite the fact that I always failed to explain what I was actually doing and where all this will finally end.

The ultimate thank goes to my little family Anja, Lino and Lilli for their ability to make me laugh and feel good at any time reminding me that there is a life beside science.

Curriculum Vitae

Adrian Wertz

Education

Since 2005	**Ph.D. Thesis:** Max-Planck-Institute of Neurobiology, Martinsried, Germany. Department of Systems and Computational Neurobiology. "Optic flow processing in premotor descending neurons of the fly" Supervised by Prof. Dr. Alexander Borst and Dr. Juergen Haag supported by DFG (GRK1091).
2004 – 2005	**Diploma thesis** Julius-Maximilians University Würzburg, Germany. Department of Behavioral Physiology and Sociobiology "Neuroanatomy and neurophysiology of the rhinophore of *Aplysia punctata*." Supervised by Prof. Dr. Wolfgang Rössler (University of Würzburg) and Dr. Ulf Bickmeyer (Alfred-Wegener Institute for Polar and Marine Research).
2003 – 2004	**Research Trainee, Scientific Park (Parc Científic) of Barcelona, Spain** Title of assignment: "Stability of DNA and RNA-triple helices, a molecular dynamic approach." Supervised by: Prof. Dr. Modesto Orozco (MMB-PCB).
2000 - 2005	**Undergraduate studies of Biology** Majors in neurobiology, bioinformatics, behavioral biology and sociobiology at the Julius-Maximilians University, Würzburg, Germany.
1998 – 2000	**Undergraduate Studies of Physics** Studies of physics at the Julius-Maximilians University, Würzburg, Germany.
1997 – 1998	**Civil Service, Gustav-Werner-Foundation (Bruderhaus-Diakonie), Reutlingen, Germany**
1997	**High School Graduation (Abitur)** Johannes-Kepler Gymnasium Reutlingen, Baden-Württemberg, Germany..

Publications

Wertz A, Plett J, Haag J, Borst A (submitted): Local and global motion sensitivities in two descending neurons of the fly.

Wertz A, Borst A, Haag J (2008): Nonlinear integration of binocular optic flow by DNOVS2, a descending neuron of the fly. J Neurosci 28: 3131-3140.

Haag J, **Wertz A**, Borst A (2007): Integration of lobula plate output signals by DNOVS1, an identified premotor descending neuron. J Neurosci 27: 1992-2000.

Wertz A, Rössler W, Obermayer M, Bickmeyer U. (2007) Functional neuroanatomy of the rhinophore of Archidoris pseudoargus. Helgoland Marine Research 61:135-142

Wertz A, Rössler W, Obermayer M, Bickmeyer U (2006) Functional neuroanatomy of the rhinophore of Aplysia punctata. Frontiers in Zoology 3: 6

Versicherung

Ehrenwörtliche Versicherung

Ich versichere hiermit ehrenwörtlich, dass die vorgelegte Dissertation von mir selbständig und ohne unerlaubte Hilfe angefertigt ist.

Martinsried, den…….

Erklärung

Hiermit erkläre ich, dass die Dissertation nicht ganz oder in wesentlichen Teilen einer anderen Prüfungskommission vorgelegt worden ist und dass ich mich anderweitig einer Doktorprüfung ohne Erfolg nicht unterzogen habe.

Martinsried, den…….